# γ-Titanium Aluminide Manufactured by Electron Beam Melting

An Investigation of Microstructural Behavior and Related Mechanical Properties for Aerospace Applications

by

Sanna Fager Franzén
Joakim Karlsson

**Diploma work No. 37/2010**

at Department of Materials and Manufacturing Technology
CHALMERS UNIVERSITY OF TECHNOLOGY
Gothenburg, Sweden

Diploma work in the Master programme Advanced Engineering Material

**Performed at**: Arcam AB
Krokslätts Fabriker 27A
437 37 MÖLNDAL

**Supervisor(s):** PhD Ulf Ackelid
Arcam AB
Krokslätts Fabriker 27A
437 37 MÖLNDAL

**Examiner:** Professor Maria Knutson Wedel
Department of Materials and Manufacturing Technology
Chalmers University of Technology, SE-412 96 Göteborg

**γ-Titanium Aluminide Manufactured by Electron Beam Melting**
An Investigation of Microstructural Behavior and Related Mechanical Properties
SANNA FAGER FRANZÉN, JOAKIM KARLSSON



Diploma work no 37/2010
Department of Materials and Manufacturing Technology
Chalmers University of Technology
SE-412 96 Göteborg
Sweden
Telephone + 46 (0)31-772 1000

Reproservice
Gothenburg, Sweden 2010

γ-Titanium Aluminide Manufactured by Electron Beam Melting
An Investigation of Microstructural Behavior and Related Mechanical Properties
SANNA FAGER FRANZÉN, JOAKIM KARLSSON
Department of Materials and Manufacturing Technology
Chalmers University of Technology

SUMMARY

Gamma titanium aluminides (γ-TiAl) have been recognized for decades to be suitable for aerospace applications due to their low density and high strength at elevated temperatures. However, TiAl is limited in application due to difficulties during machining which arise from the inherent brittle nature associated with intermetallic phases. Electron Beam Melting (EBM) has recently been proven as a processing method to produce complex, near net shape γ-TiAl parts with short lead times.

In this report the resulting microstructure from the as-EBM built material is presented. The as-EBM-built material is treated through Hot Isostatic Pressing (HIP) and thoroughly investigated using optical microscope, SEM and FIB-SEM technologies. From the as-HIPed material different heat treatments were applied to achieve the theoretical available microstructures. The heat treated material was evaluated using SEM and grain size measurements. By using tensile testing the mechanical properties of all different treatments were evaluated.

The results from investigations conclude that EBM is a feasible way to produce γ-TiAl material. Different microstructures are achievable with applicable heat treatments and process parameters from the EBM machine. By using the EBM technology γ-TiAl produced material will experience unique microstructural features with very small grain size.

Keywords: near gamma titanium aluminide, Electron Beam Melting, microstructure, FIB-SEM, tensile

## Acknowledgement

We would first like to acknowledge Ulf Ackelid at Arcam AB. Ulf has been our supervisor through this project and provided us with his guidance, knowledge and inspiration.

To our examiner at Chalmers Maria Knutson Wedel we would like to say a special thanks. You helped us with all our complicated questions that have come up along the project.

We would like to say thank you to PhD Ryan Dehoff at Oak Ridge National Laboratory. You helped us with all our materials investigations and arrangement for our stay at Oak Ridge National Laboratory. Even though we knew you were busy you took your precious time to help us.

At Oak Ridge National Laboratory we would also like to say thank you to the Materials processing group director William Peters, who arranged us all the funding for our project, PhD Orlando Rios who helped us with all our strange microstructures, Chad Parisch, for your excellent work with the FIB-SEM investigation. We would also like to acknowledge all the guys in the high bay lab at the Materials processing group, you helped us out on our tight schedule. A big thank you to all other at Oak Ridge National Laboratory who helped us out during our stay

Thanks to Joseph, Diego, Brian, Jesse, Auirley and the rest from the Early Career Professionals group who made our nights and weekends memorable.

A special thanks we would like to send to all Arcam personnel who have helped us during our project.

THANK YOU!

Sanna & Joakim

Göteborg 2010-08-27



A Portion of this research was conducted at the SHaRE User Facility, which is sponsored by the Division of Scientific User Facilities, Office of Basic Energy Sciences, U.S. Department of Energy.

TABLE OF CONTENTS

# 1 Introduction

Titanium Aluminide (TiAl) is a member of the material group of ordered intermetallics, which are characterized by unique mechanical properties due to their long-range ordered crystal structure (1). TiAl has high strength, good high-temperature properties and low density (2). These properties make the material attractive for aerospace applications (3), especially as a substitution for nickel-based superalloys used in the low pressure turbine in an aircraft engine (4). As an example, the alloy Ti-48Al-2Cr-2Nb is a certified alloy by GE and tested for use in commercial turbofan engines (5).

As TiAl has a high strength the ductility of the material is low and the material experience severe brittleness and low fracture toughness at ambient temperature (6). Research has been conducted on TiAl for about 20 years and during the last years the main focus has been to tailor the material by alloying in order to increase the room temperature ductility (7).

TiAl used for structural applications contains two phases, γ-TiAl as the base and $\alpha_2$-$Ti_3Al$ distributed in different ways depending on the type of microstructure obtained. The microstructure of the material is important for its mechanical properties and there is a trade-off between the different properties. This must be considered when the material is designed for structural applications. However, the dependency of microstructure makes it possible to tailor the material to fit the contemplated application. This can be done by conventional metallurgical processing, as for example designing of heat treatment cycles (8).

TiAl has a density half of the density of nickel-based superalloys (1), high strength and good thermal stability (9). Despite this TiAl is not a material used in a wide range of structural applications. A reason for this is believed to be TiAl's brittleness which makes it hard to process with conventional manufacturing methods. Manufacturing methods like casting and forging have been applied but they are accompanied with problems and limitations (10). Due to the low fracture toughness post-processing and machining is also challenging without fracture the material (2). For example to replace nickel-based superalloys with TiAl in low pressure turbines the material must be able to be manufactured to a blade with complex shape. Production is not easy and limits a cost-effective use of TiAl (4).

Electron Beam Melting (EBM) is a technique, developed by Arcam AB in Sweden, which produces net-near shape products by additive manufacturing (11). An electron beam melts powder on a powder bed according to a computer-made 3D-drawing and the structure is built up layer by layer (3). Recent research has shown that EBM is a feasible way to manufacture TiAl (3), (12). The material waste is low, time from drawing to production is short and complex structures can be obtained with minimal requirements of post-manufacturing (11).

## 1.1 Aim of the study

The aim of this study is to investigate the material properties of γ-TiAl (Ti-48Al-2Cr-2Nb) material manufactured by EBM for aerospace applications.

As the obtained microstructure is important for the mechanical properties HIP and heat treatment cycles shall be investigated in order to present cycles that gives the most ideal microstructure and enhanced mechanical properties. For the HIP cycle, parameters such as temperature, pressure and time must be determined. For heat treatment; temperature, time and cooling rate are the determining properties. Different heat treatment paths are also to be investigated as there exists a trade-off between different microstructure and properties. To evaluate the obtained microstructure micro hardness and tensile tests at ambient and elevated temperature are to be performed.

EBM is a new and unique manufacturing method for TiAl and in order to tailor a proper HIP and heat treatment cycle the as-built material must be studied, together with literature in the relevant area of TiAl. Literature is also gathered in order to increase the company's knowledge of the material. As it is a new and different manufacturing technique the comparability to conventional manufacturing techniques, regarding microstructure and mechanical properties, shall also be investigated.

# 2 Aircraft Engine

The development of the aircraft engines is a continuously ongoing process as new aircrafts are developed and fuel prices are rising. The size of the aircrafts has increased lately. One example is the Boeing 777 which is a twin engine aircraft (powered by only two engines)with a length of nearly 70 m (13). Powering the Boeing 777 are two GE90 engines. This engine type is the largest commercial engine used today with a diameter of up to 3.5 meters (14).

The function of an aircraft engine can easily be said to be a gas turbine cycle. Air is compressed and combusted with fuel under high pressure. The thrust producing mechanism is the increased momentum created through the engine (15). A picture of the GE90 engine and its vital parts can be found in Figure 1.

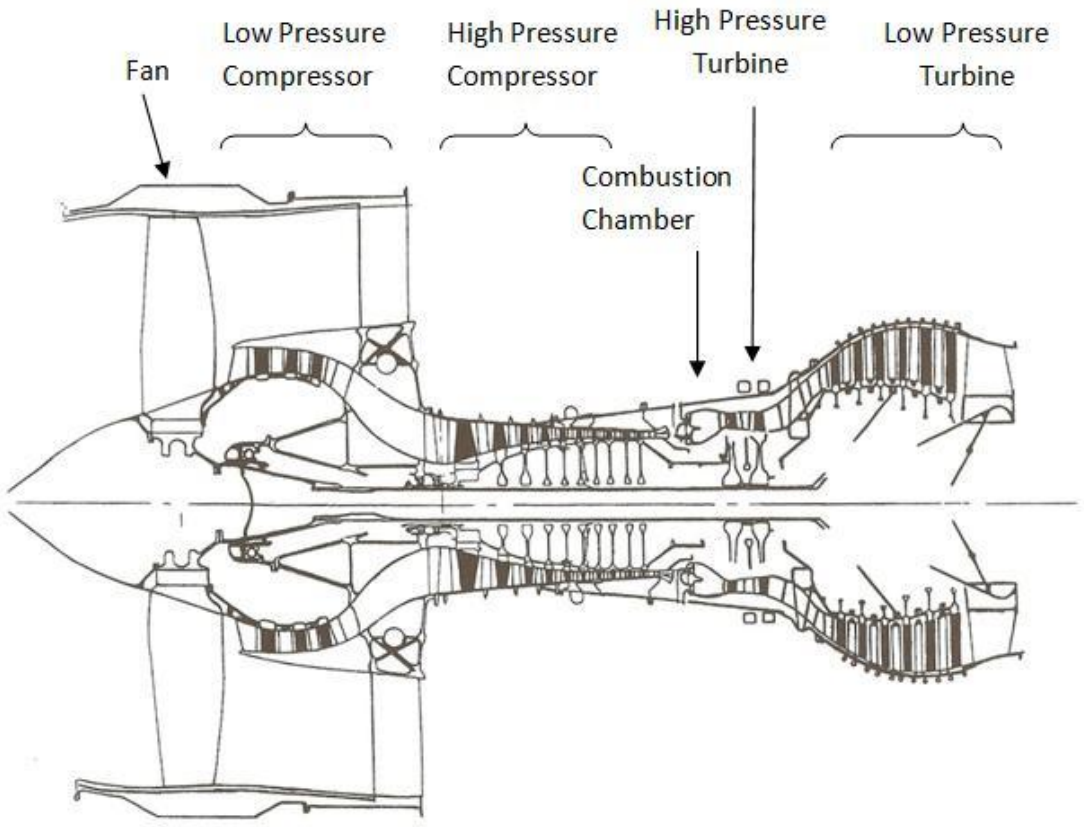


**Figure 1** *GE90 aircraft engine with important areas marked out. Picture based on* **(15)**

The air is sucked into the engine by the fan which also works as a barrier for debris (14). The air is then compressed in the Low Pressure Compressor (LPC) and High Pressure Compressor (HPC). After the air is compressed it will enter the combustion chamber were it is combusted together with fuel. Behind the combustion chamber the High Pressure Turbine (HPT) and Low Pressure Turbine (LPT) is located. The turbines drive the compressors but also provide essential power to the aircraft by generating electric power, hydraulic power, and pneumatic power (15).

With all applications in the aerospace industry weight is an important issue (16). With engines of the size of the GE90 with all the equipment mentioned above the weight becomes very high. To decrease

the weight innovative materials have to be used. Recent studies have focused on replacing the superalloy LPT blades with lighter ones made of TiAl (4). The inlet temperature into the turbine stages is usually in the range between 1430 and 1180°C (15). This temperature is well beyond the operating temperature of TiAl (17). However, the temperature in the turbine decreases as the combusted air progress through the turbine stages (15), (18). Therefore TiAl is considered to be used in the LPT stages as the temperature is lower. Also the HPC blades and engine casings have been considered to be changed to TiAl (4), (19), (2). Even if the blades are able to be lighter with TiAl, compared to the superalloys used today with twice the density (19), the largest weight savings will be in the turbine disk (20). As the turbine blades will become lighter the forces acting on the blades will be lower and the structures supporting the blades can be diminished (20).

When considering new materials for jet engine applications some specific properties of the material must be considered. Most important are the strength, stiffness, maximum service temperature and ductility of the material (19), (2). In Table 1 the properties of γ-TiAl and nickel-based superalloys are compared.

**Table 1.** *Comparison between Cast γ TiAl and Cast nickel-based superalloy* **(19)**

| | **Cast γ-TiAl** | **Cast Nickel-Based Superalloys** |
|---|---|---|
| **Density (g/cm$^3$)** | 3.9 | 8.3 |
| **Yield Strength (MPa)** | 275 - 380 | 850 |
| **Ultimate Tensile Strength (MPa)** | 360 – 500 | 1,000 |
| **Ductility (%)** | 1 – 3 | 3 – 5 |
| **Modulus of elasticity (GPa)** | 160 – 175 | 206 |
| **Poisson's Ratio** | 0.27 | 0.29 |
| **Coefficient of Thermal Expansion ($10^{-6}$/°C)** | 10.8 | 14.8 |
| **Thermal Conductivity (W/m*K)** | 22 | 11 |
| **Maximum Use Temperature (°C)** | 800 | 1,000 |

The nickel-based superalloys are the material commonly used in jet engines for high temperature applications. As can be seen in the table the nickel-based superalloys have superior properties compared to the γ-TiAl. However, as the density for the γ-TiAl is much lower than the nickel-based superalloys, the specific properties such as specific strength and specific ultimate tensile strength will be considerably higher for the γ-TiAl (19).

Other properties that is important for jet engine design is the fatigue-, crack-growth-, creep- and creep-fracture properties. These properties are used to decide the final design and operating conditions for the component and its material (19). Comparison of the rupture strength after 1,000 hours of operation at a temperature of 705 °C between γ-TiAl and nickel-based superalloys shows that the rupture strength is lower for TiAl material. Once again, since the TiAl has a much lower density it will have an advantage (19). Creep and crack growth resistance may be the most important properties in jet engine design and TiAl has been reported to fit these requirement well (19).

# 3 Intermetallics

Ordered intermetallics are a unique material group that forms long-range ordered crystal structure below the critical ordering temperature ($T_c$). Due to this order they have unique properties, including increasing yield strength with increasing temperature. Depending on the strength, the material also suffers from severe brittleness at ambient temperature and low fracture toughness (1).

The intermetallics often exist in specific, fairly narrow, composition ranges and have simple stoichiometric ratio. Most of them are ordered until the melting temperature, while others pass through different ordered structures before disordering. When the composition deviates from the stoichiometric ratio the structure may become less ordered. By introducing vacancies or by placing atoms between ordinary places in the sub-lattice the ordered structure can be maintained (1).

As mentioned above, intermetallics suffer from brittleness, most often due to low density of gliding dislocations or immobile dislocations. The lack of dislocation mobility prohibits the specimen to match the superimposed strain rate and it cracks (2).

Combinations of materials that forms intermetallics were first found in the early 1900s and since then mechanical properties of these compounds have been studied (21). At first the studies were more theoretical to understand how the compounds affect the materials, since they often were found as second phases in structural materials (21). In time the ordered intermetallics were studied as a possible structural material (1), but the interest was subsided during late 1960s because of their embrittleness and the difficulty to manufacture to structural components. However, the interest rose again during the late 1970s due to the discovery that intermetallics could be made more ductile with help of different alloying elements (1). The ductility and thereby the formability can be improved by microalloying with different elements. For example $Co_3V$ alloyed with iron shows an increase in ductility by changing the crystal structure from hexagonal to cubic. In $Ni_3Al$ microalloyed with boron, the boron forms carbides in the grain boundaries and thereby suppresses intergranular fracture (1).

Recent research for new high-temperature structural material has again increased the interest for intermetallics, as they exhibit good high-temperature properties due to their long-range order. The ordered structure lowers the dislocation mobility and prevents diffusion processes more effectively at elevated temperatures (1).

As recent research has shown, a usable material can be formed and tailored by use of alloy design work. Research has also shown that simple structures, such as fcc, bcc and hcp structures, with simple crystalline structure and high symmetry have the best ductility (22). As a result, nickel (Ni), iron (Fe) and titanium (Ti) have been discovered as having good properties, such as good mechanical properties and oxidation resistance at high temperatures, combined with low density and relatively high melting point (1). Much of the contemporary research is therefore concentrated to these materials.

# 4 Titanium Aluminide

TiAl has good thermo-physical properties; such as high melting point, low density, high elastic modulus and good structural stability. The primary reason for these properties is the ordered nature, the strong bonding of the compounds and the high critical ordering temperature ($T_c$) of the material (2). For γ-TiAl alloys, the material does not become disordered until the melting temperature of around 1440 °C (8).The expected service temperature is in a range between 600 to 760 °C (4).

Even compared to conventional Ti alloys the density of TiAl is lower and due to the high Al content the corrosion resistance is improved (2). The diffusion rate in TiAl is also lower than conventional Ti alloys, which increases the high temperature stability of the material and thereby the high temperature properties (9).

Contrary, the ordered nature also leads to some negative properties. As mentioned above intermetallics are hard but the hardness also leads to brittleness and low fracture toughness at room temperature. This also applies for TiAl and is one challenge when using them as structural materials. Another challenge is due to the hardness of the material as it becomes hard to process with conventional manufacturing methods (6).

## 4.1 The intermetallic compounds

The phase diagram (see Figure 2) of TiAl contains many different intermetallic compounds, such as $Ti_3Al$, TiAl, $TiAl_2$ and $TiAl_3$ (23). However, the research for structural materials has been concentrated to materials with two different bases; either γ-TiAl or $\alpha_2$-$Ti_3Al$, as they have shown to have the potential to meet the design requirements needed for the intended applications (2). A third compound has lately been developed, orthorhombic intermetallics with $Ti_2AlNb$ as the base (4).

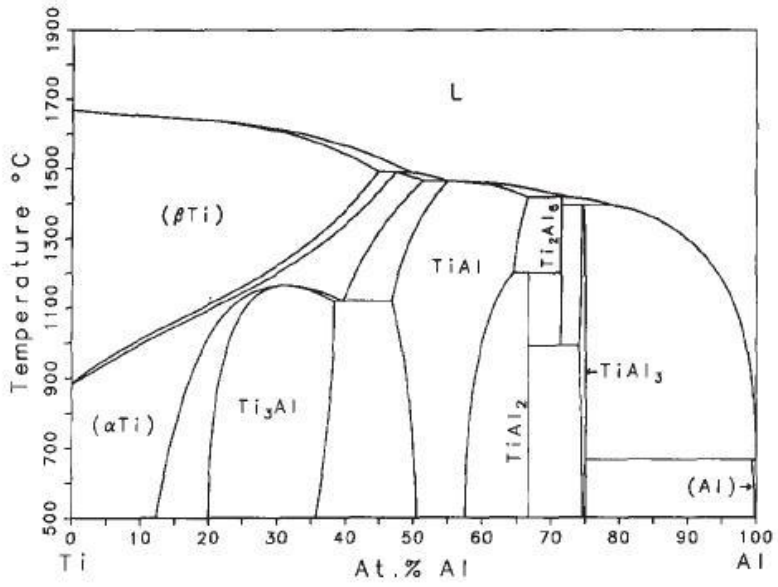


**Figure 2** *Binary phase diagram Titanium and Aluminum* **(24)**

### 4.1.1 $\alpha_2$-$Ti_3Al$

The $\alpha_2$ phase has a hexagonal ordered $D0_{19}$ crystal structure (see Figure 3), the stacking sequence is ABAB… and the stoichiometric composition is $Ti_3Al$. The (0002) planes are closed packed (23) and in

total the structure contains three independent slip systems (9). Dislocation motions can occur on the {0001} basal, the {1010} prism and the {0221} pyramidal planes. The lattice parameter of the structure has been shown to be a=0.577 nm and c=0.420 nm (9); giving the lattice parameters a (c/a) ratio of 0.8 (23).

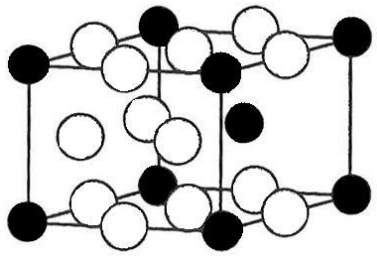

**Figure 3** *Crystal structure for $\alpha_2$ structure. Picture based on* **(23)**

The $\alpha_2$ phase exist between 22-39 at.% aluminum (Al) (23) and the structure stays ordered until a temperature of 1180 °C and Al content of 32 at.%, before it transform to a disordered hcp structure (25). The structural $\alpha_2$ based alloys developed up to now are two phased, consisting of $\alpha_2$ and β phase (9). β phase is a disordered body centered cubic Ti phase (25) with a Ti content of between 0 to 47.5 at.% Al (23). These two phase alloys have approximately two times the strength of single phase $\alpha_2$ (9).

To create the two phases a β stabilizing element in addition to niobium (Nb), for example molybdenum (Mo), chromium (Cr) or tantalum (Ta) (2), is often present and the alloys also contains around 11 to 18 at.% Nb. The Nb, with retained Al concentration, enhances most of the material properties, but could in too high concentrations increase the creep sensibility. Other alloying elements can be added to improve this performance and tailor the material properties. However, the most important thing is to maintain control of the microstructure (9).

### 4.1.2 γ-TiAl

The γ phase has a face-centered tetragonal (fcc) $L1_0$ structure (see Figure 4) and the stoichiometric composition is TiAl (8). The tetragonality is small, with c/a ratio being only around 1.02, but with increasing Al content the tetragonality increases up to c/a=1.03 (9). With a decreased Al content the c/a ratio becomes around 1 and the structure becomes ordered fcc (3).The lattice parameters have been measured to be a=0.39985 nm and c=0.40796 nm for a stoichiometric composition. The stacking sequence is ABCABC…, composed of close-packed {111} planes (23). The Ti and the Al is successively arranged on the (002) plane (9).

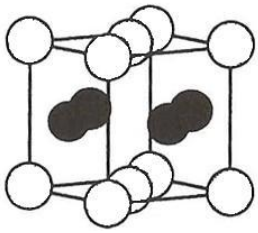

**Figure 4** *Crystal structure for γ- TiAl. Picture based on* **(23)**

The successive arrangement imply that two types of dislocations occur in γ-TiAl; both ordinary and super dislocation with the ½<110> Burgers vector type (9). As in fcc, the lowest energy slip plane is the {111} plane and the ordinary dislocation movement occurs in the three ½ <110> directions (25). However, due to the alternating layer of Ti and Al in the c-direction, the ordinary movement in the {111} plane requires more energy in that direction, leading to only two easily activated slip systems in that plane (23). The superdislocation, higher energy dislocations (8) , occur in the <011>=½<011> + ½<011> direction and the superdislocation movement leaves the superlattice undisturbed. However, the superdislocation can move further to other more energetic favorable partial dislocations; like stacking fault and anti phase boundaries (9). This dislocation movement is equivalent to <101>, but not to <110> due to the tetragonality and ordering of the structure. Other slip systems, involving planes not as close-packed as {111}, are only activated at higher temperatures (25). At ambient temperature ordinary dislocations and mechanical twinning are the most important deformation paths. Mechanical twinning is done by twinning shear around the ⅙ <11$\bar{2}$> direction. Ordered γ-phase has only this twinning direction that doesn't change the structure (2).The twinning is associated with a 180 degree rotation about the {111} plane. Apart from the true twinning a pseudo-twinning can occur in the γ-phase, around 1/6 <1$\bar{2}$1] or 1/6<$\bar{2}$11] on the {111} plane. This twinning is a rotation of 60° or 120° and it alters the structure, which introduces a misfit of 1-2%. This misfit leads to misfit dislocations at the interface. Due to the crystal structure twinning and superdislocations are not activated in the same grains, i.e. in grains with high density of superdislocations the density of twinning system is low and vice versa (23).

It is the strong bond between Ti and Al that makes the deformation hard and the material brittle. However, at elevated temperatures the strong bond helps retaining the strength and creep resistance. In high temperatures the diffusion rate controls the resistance to creep and because of the strong bond the activation energy for diffusion is high. This high energy barrier gives the material a high stiffness over a wide temperature range (8).

The γ phase exists between 48 and 69.5 at.% Al (23) and when the composition is off-stoichometric the excess Ti or Al atoms are placed as anti-site atoms without creation of vacancies. There are two different kinds of structural γ alloys that have been developed during the years; single-phase γ or two phase γ+$\alpha_2$ (9). For engineering applications the material is always two-phase, containing a fraction of up to 20 % $\alpha_2$, and the Al content is around 45-48 at.% (2). The alloys introduced also contain between 1 and 10 at.% of at least one other metal; vanadium, chromium, manganese, niobium, tantalum, tungsten or molybdenum. By appropriate alloying and microstructure design the material can be tailored to obtain desired mechanical properties. Especially the ductility and strength is dependent on the alloying composition and the thermo-mechanical processing conditions (9).

The interest in TiAl springs from, as mentioned above, an interest to increase the thrust-to-weight ratio of high-performance aircraft engines. This must be done by decreasing the weight of the component, but at the same time increase the high temperature properties. The interest for γ-TiAl started around 1950, but it took some time before practical design problem was solved, like ambient temperature ductility (8). Among γ and $\alpha_2$ Ti alloys the interest has the past two decades strongly been focused on γ-based alloys (2). Considerable efforts have been focused on research and development of γ alloys useable for engineering purposes. The most promising composition is Ti-(34-49)Al-(5-10)Nb-(2-5)Cr for high-temperature and long-term operation applications (3).

## 4.2 γ-Titanium Aluminide Microstructure

In γ- TiAl with an Al concentration of between 46-52 at.% the microstructure generally consists of either a single phase microstructure of pure γ phase or a two-phase system containing a mixture between γ phase and $\alpha_2$ phase (21). These single and two phase systems combine to build up different characteristic microstructures available in the material. The different microstructures that appear in γ-TiAl are lamellar, near lamellar, duplex, pseudo-duplex and equiaxed (see Figure 5) (2), and is dependent of the heat treatments applied to the material and the cooling rate (2) (23).

The equiaxed microstructure only contains single phase γ TiAl of equal amounts of Ti and Al. One controlling parameter of the obtained microstructure is the Al content. Large amount of Al (above 52 at.%) will give the equiaxed plain γ structure as it is the stable phase in the phase diagram as seen in Figure 2 (8). For materials with Al amount between 46 and 50 at.% combined microstructures can form depending on heat treatment. This is because of that the compound will be in the two-phase region of the phase diagram (8). For lower amount of Al plain $\alpha_2$, α and β may be obtained (2). In addition, alloying elements changing the phase equilibriums will have an effect on the microstructure.

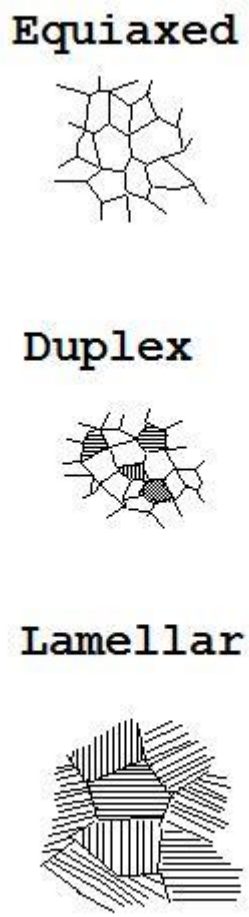


**Figure 5** *The apparent microstructures in γ Titanium Aluminide*

### 4.2.1 Eqiuaxed

The equiaxed microstructure consists of single γ phase and is seen as the top microstructure in Figure 5. The microstructure is built up of smaller equiaxed grains (8). Its mechanical advantages are that γ-TiAl has a high elastic modulus and improved high temperature properties while still having a low density. The disadvantages are its poor room-temperature properties such as fracture toughness and ductility (21). This microstructure is very brittle and therefore not desired in structural applications.

### 4.2.2 Lamellar

A lamellar microstructure is seen as the bottom microstructure of Figure 5. This microstructure consists of alternating γ and $\alpha_2$ plates stacking up into lamellas and creating zebra-looking grains. The lamellar structure is believed to be more ductile than the equiaxed which arises from the spacing created between the lamella plates. In the interfaces of the lamellas twinning and dislocations are built up (2). The twinning and dislocations enhance the high temperature strength, fracture toughness and creep resistance. The lamellar structure suffers from poor ductility at low and ambient temperatures. However its low temperature properties are still superior compared to equiaxed TiAl (2). A lamellar microstructure with very small grains has been reported to give excellent mechanical properties. The grain size must be in the range of 10-30 µm to give the sufficient ductility (26).

### 4.2.3 Duplex

The two microstructures above are in their pure form very brittle at lower temperatures and therefore not desirable in structural applications. To enhance this property a more ductile microstructure must be achieved which is obtained by the formation of the duplex microstructure. The duplex structure is a mixture of equiaxed γ grains and lamellar colonies, the above mentioned microstructures (8). A TiAl containing both equiaxed and lamellar microstructure is influenced by the mechanical properties of both of the microstructures. Properties such as lamellar spacing, thickness of the lamellas, volume fraction of microstructures and grain sizes will influence the mechanical properties (6). A duplex structure is therefore preferred for structural applications (8).

The duplex microstructure is not formed directly from the as-cast material. Firstly, the right amount of Al must be present in the material as duplex microstructure contains both γ and $\gamma+\alpha_2$ phases. These two phases only coexists in Al amounts of 45 – 51 at.% in the phase diagram. Secondly, the material must be sufficiently heat treated.

By introducing lamellar microstructure in between fine γ grains the ductility of the microstructure will be increased (21). The ductility will be improved by the interfaces between the lamellar and equiaxed structure that is obtained in the duplex structure (8). As ductility is improved other properties such as creep resistance, fractures toughness and high temperature strength can be enhanced with addition of lamellar microstructure (2). To combine these properties an amount of about 30 vol.% of added lamellar structure to the equiaxed is believed to be most desirable (21).

### 4.2.4 Pseudo Duplex

Pseudo-duplex structure consists just like regular duplex of both γ grains and $\gamma+\alpha_2$ lamellas but with a larger amount of γ phase. The structure is characterized by the diffuse interfaces between the lamellas and γ grains (23). This arises as the γ grains and γ phase in the lamellas have identical crystallographic orientation (27). The pseudo diplex structure can be seen in Figure 6.

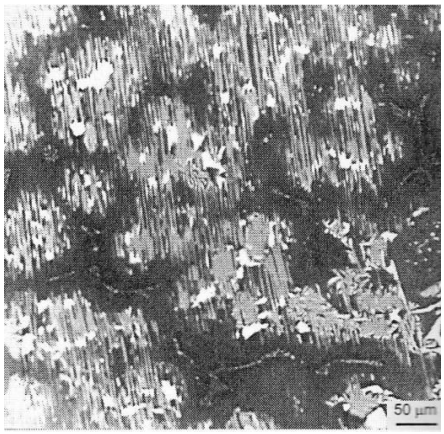


**Figure 6** *Optical micrograph of the pseudo duplex microstructure* **(23)**

# 5 Design of Microstructure

The microstructure obtained in the as-produced materials is dependent on the manufacturing method (8). As the material cools down from liquid to room temperature it passes through different phases in the phase diagram. Depending on the manufacturing method the material will cool differently and thereby have a different path through the phase fields. The resulting microstructure will in the end therefore become different depending on manufacturing method and cooling rate (28).

Often the quality or the type of microstructure achieved in the as-produced material will not be the one desired. To alter and change the microstructure of the material it can be subjected to different kinds of treatments. Hot Isostatic Preassuring (HIP), Heat Treatment and Hot working are some examples (28), (21), (8), (29).

## 5.1 Hot Isostatic Pressing

Hot Isostatic Pressing (HIP) is a processing or post processing method where both heat and high pressure is applied. Both loose powder and already manufactured parts are possible to HIP (21), (30). By HIP powder feedstock the objective is to produce a near net shape material of full density (31). Contrary, HIPing an already produced component the objective is to reduce the amount of porosity within the component (32), (30). Another objective is to produce a homogeneous microstructure and remove the anisotropy within the material (33). During HIP processing the component is placed within a gas tight oven. If the component is to be produced from powder it is sealed into a container. This container is usually of glass, steel or Ti and should soften as temperature and pressure are applied (21). Heat is then applied followed by an inert gas, for example argon or nitrogen. This gas is applied to raise the pressure and conduct the heat within the oven (21). A schematic of the HIP process and equipment is seen in Figure 7. The physical processes acting during HIP are plastic yielding, creep and diffusion (34), (30).

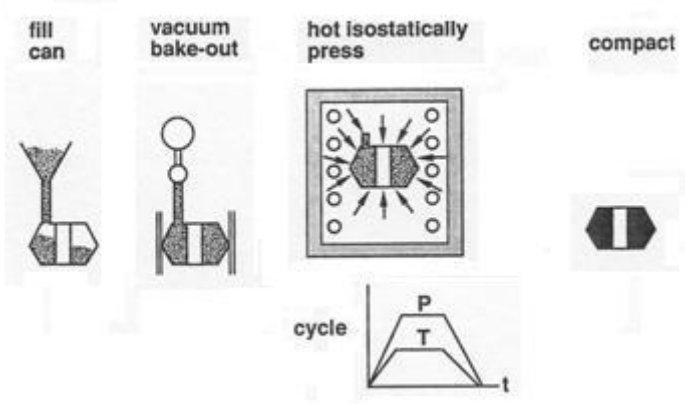


**Figure 7** *Schematic of a HIP cycle. Picture based on* **(21)**

While HIPing already produced TiAl components the temperature needs to be raised into the two-phase field for the diffusion of the voids to occur (35). As the voids are pressed and diffused out of the sample strain and plastic energy are built up around the former pores. These energies decrease with distance from a pore. However if the stresses are high enough they will cause recrystallization to relieve stresses (30). As a drawback, the recrystallization will make the microstructure in the HIPed material inhomogeneous. Other microstructure changes that occur during HIP are grain growth and

phase transformations (36), (37). Since the HIP cycles usually are carried out in temperatures in the two phase fields of the TiAl phase diagram, grain growth will occur similar to transformations occurring during heat treatment, which are described below (30), (34). Depending on the alloy, material and manufacturing principle the resulting microstructure after HIP will differ (38), (37). Multiple papers have reported that the ductility of the material will increase together with increasing HIP temperature, which is a good feature for the usually brittle TiAl material (39), (10). It has also been shown that closing of the pores are made if the temperature is above 1100˚C, but in order to increase the ductility a HIP temperature over 1200˚C is required (37).

## 5.2 Heat treatment

With different manufacturing technologies different as-produced microstructures will appear. For example, cast materials will usually be slowly cooled, especially in the centre of the part. The as-cast material tends to become segregated as cooling occurs differently in the material and peritectic reactions take place (8). By instead using powder metallurgy manufacturing the microstructure will be less segregated as the size of the melt becomes smaller (8). It is believed that EBM gives less segregation as the melting occurs in small areas where cooling is sufficient (3).

As TiAl, with the composition of 48 at.% Al, cools down from liquid it can be seen from the phase diagram that three primary solidification phases and two peritectic reactions are possible (8). The sequence during the whole cooling process is as follows (40):

$$L \rightarrow \beta + L \rightarrow \beta + L + \alpha \rightarrow L + \alpha \rightarrow \alpha \rightarrow \alpha + \gamma \rightarrow \alpha_2 + \gamma$$

For Ti-48Al-2Cr-2Nb small amounts of β phase may formed during cooling as especially Cr helps stabilizing and forming the β phase (40). From Figure 8 preliminary temperatures and obtained microstructures is shown (41). Depending on cooling rate, holding time and alloy these temperatures may vary.

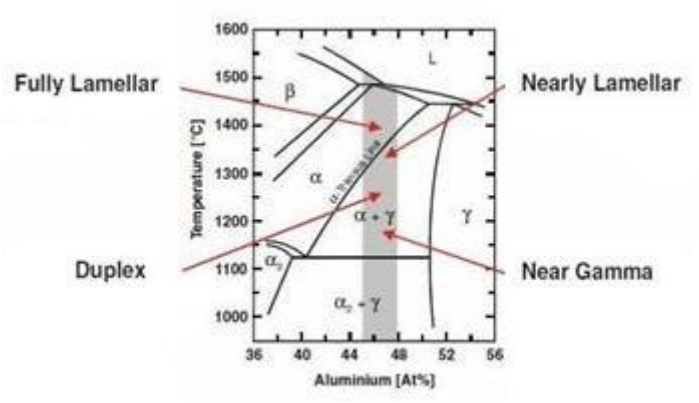


**Figure 8** *Temperature dependence to receive different microstructures during heat treatment. For micrographs, see* **(41)**

### 5.2.1 Transformations from α phase field

When material is heated above the α transus temperature, which is at 1365°C for Ti-48Al-2Nb-2Cr (40), up into the single α phase region the Al becomes completely soluted in the hexagonal-closed-packed Ti. From here the microstructure is possible to be "reset" (29).

If the preexisting microstructure is γ-phase segregated with α, the dendritic segregation will dissolve and the microstructure will become completely homogenized (32). However, heating in this area induce grain growth of the α grains created as the γ grains dissolves (32). It is found that the γ grains dissolve through diffusion-controlled dissolution (42). As these γ grains dissolve the newly created α grains will start to grow according to diffusion-controlled growth, as can be seen in Equation 1 .

$$\frac{dD_\alpha}{dt} = k^* \left[ \left( \frac{1}{D_\alpha} \right) - \left( \frac{1}{D_\alpha^L} \right) \right]^{p-1}$$

**Equation 1** *Diffusion-controlled grain growth* **(42)**

where $D_\alpha$ denotes grain size of the α grains as a function time, k* denotes the rate constant, $D_\alpha^L$ denotes the α grain size limit and p denotes the grain growth exponent. If the pre-existing material consist mainly of lamellas homogenization will be more complicated (32), (43).

Grain growth is an issue at this temperature (33) and should it occur recrystallization is needed. Recrystallization can be obtained by either hot working or re-nucleation. The re-nucleation is a function of the $\alpha_2+\gamma \rightarrow \alpha$ reaction as the γ dissolves and new grains might be nucleated (44). If lamellas are present and hot working applied, there will be new sites for nucleation where the lamellas are distorted (32).

#### *5.2.1.1 Massive Transformation*

If a high cooling rate is applied, i.e. water quenching, the existing α phase will massively transform into γ structure (2), (29), (45). The cooling rate for massive transformation has to be fast enough to hinder the formation of Widmanstätten and primary lamellar structure (46). The resulting microstructure is fine grained and feathery. For micrographs see e.g. (46). Here the γ grains start to transform from the existing α grain boundaries and propagate into the α grain. The α → γ transfer will be complete if the grain is small, otherwise some α will be retained (33). In the transformation no orientation relationship will exist between the transforming γ grain and the α grain being consumed, although there will be orientation relationships between the γ grains transforming alongside each other (33). The ordering of γ from α phase is believed to be either atom transfer, as some atoms switch places in the lattice and end up in wrong positions, or by an intermediate fcc structure followed by ordering to $L1_0$ as the created anti-phase boundaries grow together (33).

The structure is transformed from disordered α phase to an ordered γ phase. It has been reported that the diffusion needed takes place before the actual transformation. The massive transformation nucleates below the α transus temperature in the two phase field (47). At this point the Gibbs free energy of both α and γ is the same (46), (29). As the massive transformation is nucleated it grows until the temperature drops below 1125 °C where diffusion and reordering cannot take place (29).This short time of complicated transformation induces dislocation and stacking faults in the {111} planes as well as numbers of anti phase domains into the microstructure (43), (46). The stacking fault hinders the normal massive transformation path, where disordered α massively forms

disordered fcc followed by ordering of the fcc to γ $L1_0$. Instead a direct transformation from disordered α to ordered γ is more likely to occur (46).

#### *5.2.1.2 Widmanstätten formation*

For heat treatment in the single α phase field with an intermediate cooling applied to the material the cooling will be slow enough to avoid massive transformation (29). The diffusion rate and time at elevated temperature is however lower than the one needed to form fully lamellar structure and the resulting microstructure will consist of some lamellas with Widmanstätten colonies appearing. (43), (45). The typical microstructure of this cooling rate consists of a fine lamellar structure with Widmanstätten needles in random directions. Widmanstätten colonies are formed inside lamellar grains with small spacing. Depending on the amount of Al in the material the amount of formed Widmanstätten colonies will change (33). The formation of Widmanstätten colonies is not yet fully understood. It is believed that the Widmanstätten colonies are formed through twinning or recrystallization and forms from present α grains that has different orientation compared to the surrounding material. The driving force for the formation of Widmanstätten colonies is believed to be the supercooling occurring at the applied cooling rate. It is also believed that Widmanstätten is formed to relieve thermal stresses or to reduce the stresses caused by retained α phase as cooling progress below the solvus line. Below the solvus line the α phase is not stable and transforms to γ+$\alpha_2$ lamellas (43). In Widmanstätten formation some long range diffusion can still take place, but it is not sufficient to create fully lamella structure (46).

#### *5.2.1.3 Lamellar formation*

If cooling rates lower than those discussed above (i.e. furnace cooling) are applied as the material is in the α phase lamellas is formed as the resulting microstructure seen in Figure 9.

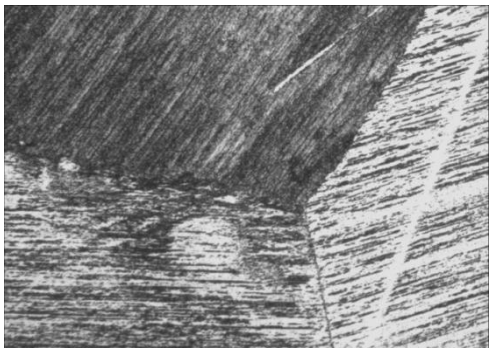

**Figure 9** *Optical micrograph of fully lamellar microstructure*

The lamellar formation is by the sequence (33):

$$\alpha \rightarrow \alpha+\gamma \rightarrow \alpha_2+\gamma$$

When the formation of lamellas starts the first step is the formation of the tetragonal fcc γ needles within the hcp α grains. This is followed by nucleation of γ phase through short range diffusion at, or near, the α grain boundaries (48), (49). By long range diffusion the γ needles continues to grow. Finally the remaining α is ordered into $\alpha_2$ (49).The formation of γ lamellas from α is believed to transform through movement of the Shockley partial dislocations (2). The movement of three Shockley partials is seen in Figure 10 as the $\frac{1}{3}$<1010> partials dislocate and passes the $(0001)_{hcp}$ planes from hcp to fcc structure (33).

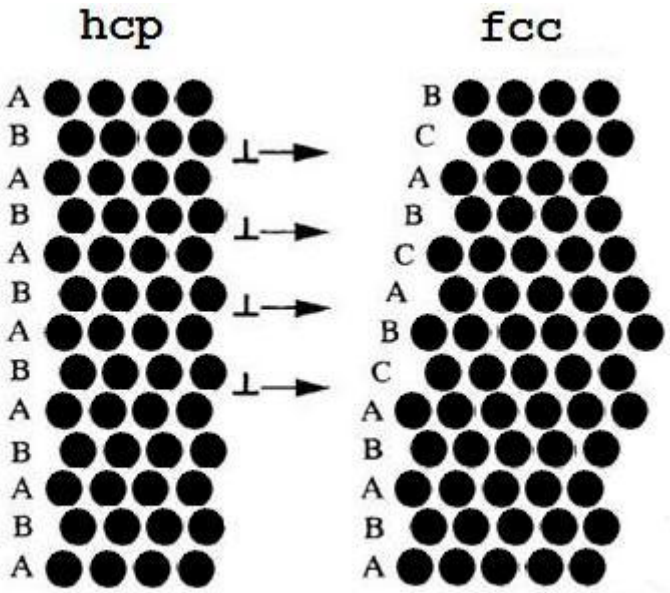


**Figure 10** *Movement of the Shockley parts transferring from hcp to fcc. Picture based on* **(33)**

The lamellas formed will have the Blackburn Orientation Relationship as follows (46):

$$\{111\}_{\gamma}//(0001)_{\alpha 2} \text{ and } <110]_{\gamma}//<1120>_{\alpha 2}$$

This means that the close packed $<110]_{\gamma}$ and $<1120>_{\alpha 2}$ directions will be parallel (46) causing fully coherent interfaces with low internal energy (28). Meanwhile the {111}γ will not be precisely parallel with plane $(0001)\alpha_2$ causing incoherent phase boundaries with twinning and intervariant boundaries (46), (28), (29). The non parallelism comes from the tetragonality in the γ structure compared to the hexagonal $\alpha_2$. As these γ/γ interfaces occur they will cause intervariant boundaries using, twinning, pseudo-twin and 120°rotations between the different crystal orientations (29). This interaction comes from the slightly difference in the $L1_0$ c/a ratio, which cause the γ/γ interaction described (2). It has however been reported that the c axis of the tetragonal γ is sometimes shifted by 90 ° and aligned parallel to the a and b axis of the surrounding crystals to avoid increasing the interface free energy (48).

The formation of lamellas is reported to be diffusion controlled (45), (43). As soon as the γ start to nucleate it will grow through the diffusion mechanism (46), (43). From literature it is reported that at least 80°C of undercooling is needed to trigger the formation of lamellas (49). Due to diffusion cooling rate will be a determining factor for the formation of lamellas. As cooling rate increases the supercooling will increase and release more free energy available for diffusion (43). However with high cooling rate the diffusion becomes slower as the mobility of the atoms decreases (28), (43). When the diffusion becomes slow the growth of the lamellas will decline causing lamellas with fine spacing (43). If, on the other hand, the cooling rate is slow the γ nucleation will be sparser but due to the higher diffusion available the lamellas will have time to grow thicker (43). For micrographs of different lamellar microstructures resulting from different cooling rates see (43).

All of the different microstructures that can be created by using different cooling rates when cooling from the α phase fields are summarized in Table 2, where the different appearing microstructures is ordered by their amount present.

**Table 2** *Summary of the transformed microstructures from the α single phase* **(33)**.

| Cooling rate | Resulting Microstructure |
|---|---|
| **Ice Water Cooling** | $\gamma_m + \gamma_W + L_f$ |
| **Water Cooling** | $\gamma_W + \gamma_m + L_f$ |
| **Air Cooling** | $\gamma_W + L_f$ |
| **Furnace Cooling** | $L_{eq}$+ DCL + CCL |

$L_{eq}$ = Equilibrium lamellas, DCL = Discontinuous Coarsened Lamella, CCL = Continuous Coarsened Lamella, $\gamma_W$ = Widmanstätten morphology, $\gamma_m$ = Massive Transformed γ morphology

### 5.2.2 Transformation of γ Titanium Aluminide

The γ material can be heat treated in the α+γ phase field of the phase diagram. As the material is quenched into γ and subsequently heat treated the phase transformation reactions can be compared to the reactions during ordinary cooling (10):

$$\alpha \rightarrow \alpha + \gamma \rightarrow \alpha_2 + \gamma$$

become:

$$\gamma \rightarrow \alpha + \gamma \rightarrow \alpha_2 + \gamma$$

In the first of these two reactions the γ will start to precipitate at the (0001) planes of the α grains created as the material is cooled through the α + γ phase field. The lamellas created with the same reaction will have the size of the pre-existing α grains created in the α region (10).

In the second reaction γ phase is already present and it is the α phase that start to precipitate during cooling. The α grains precipitate at the {111} plane of the tetragonal gamma structure. The nucleation mainly takes part at vacancies formed by dislocations in the γ stacking. The size of the lamellas created by this reaction is dependent on the size of the plates the α is nucleated on and by the amount of growth space that is available before a non parallel {111} γ stacking is obstructing the growth (10).

By heat treatment of a fine grained γ microstructure material just above the eutectic line in the α+γ region of the phase diagram in Figure 8 a so called near gamma or equiaxed microstructure is achieved (2), (29). Some $\alpha_2$ will be present in the triple points as the α transfers into $\alpha_2$ during cooling and in the grain boundaries between the γ grains as some α will be retained during cooling and transform to $\alpha_2$ (2), (48). The amount of each phase is determined by the lever rule (2). By raising the heat treatment temperature into the upper α+γ region a duplex microstructure will be obtained (2).

The volume fraction of lamellas within the duplex structure is dependent on the Al content and the cooling rate applied (29), (2). Some γ grains transform into α according to the lever rule and the duplex lamellas will follow the same formation route as the lamellas obtained from the single α phase (33), (46). As the heating temperature is raised in the α+γ phase field towards the α transus

temperature the amount of lamellas in the duplex structure will increase (2). Just around the α transus temperature the resulting in a near lamellar microstructure as the majority of the resulting structure is lamellar (2) and can be seen in Figure 11.

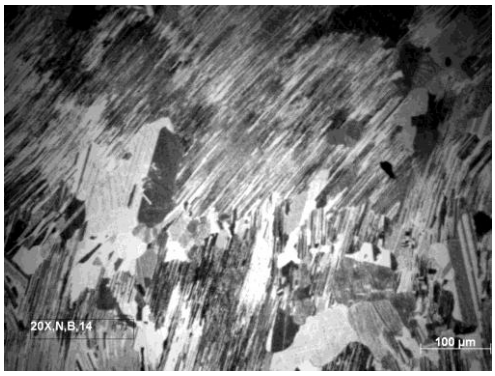


**Figure 11** *Optical micrograph of a nearly lamellar microstructure*

### 5.2.3 Discontinuous Coarsening

During annealing in the $\alpha_2$+γ phase field the microstructure will start to coarsen through discontinuous coarsening in the case of a microstructure containing both γ grains and γ+$\alpha_2$ lamellas. However, the coarsening progress is slow as diffusion in this phase field is slow due to the low temperature (33), (35). It has been reported that the coarsening is induced by nucleation and growth of macrodefects (33). If the structure only contains γ grains it will start to form γ+$\alpha_2$ lamellas according to the lever rule (33), (46).

# 6 Mechanical Properties of γ-TiAl alloys

In general TiAl experience good mechanical properties and are especially appropriate for automotive and aerospace applications (6). Many of the properties are depending on the microstructure that is achieved in the different metallurgical processes. However, a microstructure that benefits one property could limit another, which imply that it is always a trade-off when designing and choosing microstructure for a specific application (8).

## 6.1 Deformation

As mentioned in section 4.1, intermetallics are very brittle due to their lack of mobile dislocation or low dislocation density. The same attribute can be applied to TiAl (2). In section 4.1.1 and 4.1.2 the different dislocation mechanisms of the TiAl intermetallic compounds are described.

How mobile the dislocations are and how the material acts under mechanical load are important for the strength and fracture behavior of γ-TiAl (8). The brittleness of the material, which persists up to relatively high temperatures, severely affects some properties of the material. The multiplication and mobility of the dislocations are governed by micromechanisms and are often important to understand in order to predict the material properties (2).

Most of the deformation in two phase γ-TiAl alloys is concentrated to the γ phase and has a close relationship with the slip planes in the $L1_0$ structure. The most important deformation modes in the γ phase are ordinary dislocations, ordered twinning and superdislocations. The difference between the dislocations is the amount of energy required to initiate them and the stress they cause (2). Research has also shown that the Al content together with a third alloying element, deformation temperature and purity of the material have a large impact on active deformation mode (21). The Al concentration affects the amount of $\alpha_2$ present in the structure and this in turn affects the ductility.

The difference in ductility is based on differences in deformation mode. The two phase alloy have high propensity to deform by the low energy ordered twinning of the {111}<112]-type and ½<110] unit dislocations. Contrary, the single phase alloy, with a higher Al concentration, has a high density of sessile superdislocations and is not likely to deform through twinning (29).

Twinning deformation is nucleated on the grain boundaries, both γ/γ and $\gamma/\alpha_2$ interfaces. Twins nucleated at the γ/γ grain boundaries are parallel to the lamellae and are formed on the (111) plane of γ. Twins nucleated at the $\gamma/\alpha_2$ interface are created at an angle of about 70° to the lamellas on the $(\bar{1}11)_\gamma$ plane. The second twinning dislocation requires high stresses and can even fracture the $\alpha_2$ lamellas (23).

Two-phase alloys exhibit plastic anisotropy and the anisotropy originates from $\alpha_2$-lamellas being extremely difficult to deform (29), especially when the c-axis is parallel to the tensile axis. Additionally, motion of superdislocations in the γ-phase affects the γ/γ lamella interfaces and introduces coherency stresses and dense networks of interface dislocations in the boundaries, which also creates anisotropy (2). The anisotropy between the two lamella interphases (γ/γ and $\gamma/\alpha_2$) lowers the deformation ability of the alloy and severely limits the room temperature ductility. The ductility is better in polycrystalline two-phase alloys due to that constraint stresses, created by the anisotropy, create anti-twinning operations that enhance the deformation. This reduces the anisotropy of the material and improves the ductility (2).

The deformation behavior of TiAl is also dependent on the temperature. With increasing temperature more slip planes become activated and dislocations with higher energy can also move. Investigation made on Polysynthetically Twinned (PST) crystals , a single-crystal-like specimen composed of the lamellar structure, shows that the material exhibit a slip-mode transition between 600°C and 800°C, a so called brittle-to-ductile transformation (BDT) (25). By one definition, the BDT temperature is where the ductility reaches 7.5% (50). The transformation occurs earlier for the single phase γ-grains than for the lamellar grains, leading to the large temperature range (25). The transition temperature is also affected by the strain rate, increasing strain rate gives increasing transition temperature (2).The dislocations that were active at ambient temperature are still active at higher temperatures, but the propensity for ordered twinning decreases at even higher temperatures. At the same time, superdislocations are activated at temperatures over 800°C (29). In general, below this temperature the twinning density increases with increasing temperature (2), leading to an increase in ductility over the temperature range (25). As the temperature increases and more dislocations are activated they are becoming curly and entangled, which leads to strain hardening of the material. This applies for single crystals up to 600°C and up to 800°C for polycrystals (21). This increase in yield strength with increasing temperature is seen in other intermetallics as well and depends on thermally activated jogs and kinks, which inhibits the motion of low energy ½[110] dislocations. At elevated temperatures the deformation behavior becomes more dependent of the rate the material is deformed. This is an important feature that severely limits the creep resistance of TiAl and is a major design issue when it comes to replacing nickel-based superalloys with TiAl (2).

Different deformation mechanisms are active in different deformation processes, not only due to temperature, but also due to load orientation. Experiments on PST crystals show that when the orientation of the lamellae is perpendicular to the load axis the yield strength increases. However, the elongation of the specimen is strongly decreased comparing to when the load axis is parallel to the lamellae, see Figure 12 and Figure 13 (51). Angles in between shows a decrease of yield strength but an increase in elongation compared to the perpendicular orientation (25). This orientation dependency is due to the shear deformations active in different orientations. When the lamellas are parallel or perpendicular to the load axis a hard type of deformation occur, a shear deformation process on the {111} plane (shear deformation across the lamellar boundaries (51)). The deformation intersects the lamellar boundaries, which makes them hard. A more easy type of shear deformation occurs in the intermediate orientation, a shear deformation within the γ-lamellae boundaries (shear deformation parallel to the boundaries (51)). The $\alpha_2$ and the lamella boundaries are no obstacles to the deformation, implying that it is easier. This shear deformation can also occur in the parallel orientation, leading to a large elongation as well (25), (29).

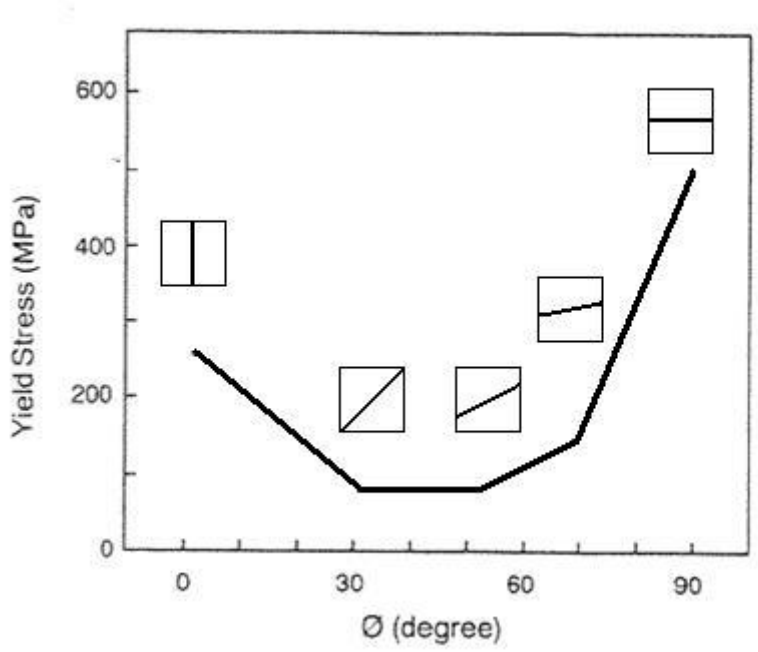


**Figure 12** *Yield stress as a function of orientation, the angle Φ between the lamellar boundaries and the loading axis, for PST γ-TiAl. Figure based on* **(51)**

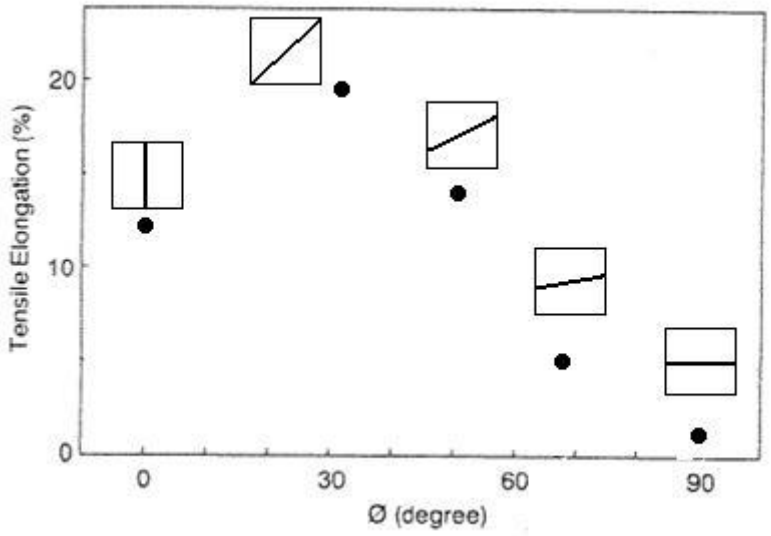


**Figure 13** *Elongation as a function of orientation, the angle Φ between the lamellar boundaries and the loading axis, for PST γ-TiAl. Figure based on* **(51)**

The low room temperature ductility depends, as shown above, on the low number of available slip systems (25) and the low room temperature ductility diminishes the suitability for the material to be used as a structural material (16).

### 6.1.1 Fracture mode

As stated above, TiAl suffers from lack of ductility at ambient temperatures, due to the lack of mobile dislocations or their low dislocation density. However, the low ductility is also based on the high likeliness for the material to fracture trough cleavage fracture. As for other properties, the fracture mode is dependent on the microstructure (2). The deformation transition from one grain to another is difficult and that enhances the possibility for the γ-grains to fracture through transgranular cleavage fracture or through intergranular fracture (25). The brittle fracture behavior of the material is not affected by differences in deformation orientation (29).

Microcracks form at the boundaries of the lamellas, along grain boundaries or at equiaxed gamma grains due to the hard transition of dislocations, which enhances the intergranular cleavage fracture. Two phase alloys fractures through transgranular cleavage fracture or grain boundary cracks (29). The $\alpha_2$ grains in two phase alloys act as reinforcement making the boundaries brittle, since the dislocation activity is low. As the slip transformation is hard between the grains the dislocations are piled-up and causes brittle fracture on the grain boundaries (25). Research has shown that planar cleavage fracture occur at room temperature, whereas when the temperature increases the grain boundary fracture are more likely to occur (50). Especially duplex structures fracture in transgranular mode at ambient temperatures and intergranular mode at elevated temperatures. Lamella structures fracture through transgranular fracture, however decreasing grain size favor intergranular fracture (21).

Orientation also affects how the samples fracture. Load orientation parallel to the lamella boundaries makes the sample fracture through a macroscopic crack that is initiated and propagates zigzag across the lamella boundaries. Orientation perpendicular or inclined results in fracture through a cleavage fracture mode parallel to the lamellas and most often through γ/γ interfaces (51).

Even though the slip and twinning formation becomes easier with increased temperature, the deformation transition across grain boundaries remains difficult and the amount of grain boundary decohesion and brittle intergranular failure increases up to the brittle-to-ductile-transition temperature (BDTT) (25). However, since the amount of twinning increases the grains are more easily deformed and the propensity for microcracks to form decreases, which leads to a decreased amount of transgranular cleavage fracture (25). Above BDTT the brittleness decreases and the fracture mode are changed from inter- or transgranular fracture to a ductile dimple-like fracture mode (2).

## 6.2 Thermal properties

γ-TiAl alloys has some appropriate and suitable thermal properties for aerospace applications and especially jet engines. The properties are a combination of low thermal expansion and high thermal conductivity (25).

The thermal expansion of TiAl is lower than for Ni-based superalloys and that gives TiAl some advantages compared to traditionally used superalloys for applications as turbine blades. The lower thermal expansion makes the control of the expansion of the blade easier and the clearance between the blade tip and the shroud is not as critical (25). The low thermal expansion coefficient is due to high bonding strength between the atoms and long-range order (52), which for TiAl is sustained also

high temperatures (8). A nickel-based super alloy has a thermal expansion coefficient at 538°C of around $14.2*10^{-6}$ /K (53) and a γ-based TiAl alloy has a coefficient at 538°C of around $11.8*10^{-6}$ /K (2).

Even though the thermal expansion is small in TiAl still some anisotropy occurs. The anisotropy causes internal stresses at the interfaces of different orientated γ-lamellas. These internal stresses can, under mechanical load, affect deformation mechanisms and fracture behavior of the alloy. Misfit dislocations are introduced, which causes stress-induced structural changes that in turn affect the deformation process (2).

Another important material constant for materials used for high-temperature applications is the thermal conductivity, a value of the heat transport properties (16). The thermal conductivity varies significantly for different TiAl alloys. The most important source for the variation is the stoichiometric composition. Alloys with a long-range order and a stoichiometric composition, as γ-TiAl and $\alpha_2$-$Ti_3Al$, can have up to five times higher thermal conductivity than off-stoichiometric alloys (23). At the same time, γ-alloys have about three times higher conductivity than $\alpha_2$ alloys. This is one explanation for thermal conductivity variation among alloys of different composition. However, the most important property that affect the thermal conductivity is shown to be microstructure; if the material is duplex or lamellar, the volume fraction of single-phase γ-grains and also the orientation of the grains. As high values as 22 W/m*K down to 12.3 W/m*K have been reported for different alloys, and microstructures. The reported values are somewhat higher than for superalloys (23). As an example, nickel-based superalloys has values around 11.4 W/m*K at room temperature (53).

The anisotropy of the material can be observed for thermal conductivity as well, varying in longitudinal and radial direction. The anisotropy is due to the difference in thermal conductivity for the different phases present in TiAl alloys; $\lambda_\gamma$=7 W/(mK) and $\lambda_{\alpha 2}$=22 W/(mK) (17). The amount of variation is dependent on the microstructure, being the fraction of the different phases, of the tested samples and has been shown, for the specific investigated microstructures, to vary between 13-16%. The microstructure throughout the sample determines if the radial or the longitudinal thermal conductivity is the largest. As observed for the investigated samples, material with duplex microstructure had a larger radial conductivity, contrary to the nearly lamellar samples (17). The thermal conductivity increases with as much as 50-60% as the temperature increase, and the increase is roughly linear (23).

## 6.3 Tensile and ductility properties

As been mentioned, γ-TiAl with some fraction of $\alpha_2$ has the most promising ductile properties (9). Therefore most of the research is made on these types of alloys and during the last decades progress has been made in understanding and development of alloys of engineering importance (7). It has also been shown that many other features influence the tensile and ductility properties, some of them being; production methods, heat treatment, microstructure and grain size (25). Both tensile strength and ductility are also dependent on the composition of the alloy, especially the Al content (7) and third alloying elements (21). Research has also shown that the orientation of the lamellas is of great importance for the ductility and strength (51), as mentioned in 6.1.1.

### 6.3.1 Effect of microstructure and grain size

Alloys with Al content between 45-50 at.% and a two phase ($\gamma+\alpha_2$) structure have better ductility than single-phase alloys (8). Duplex microstructure has also been shown to exhibit a larger room temperature tensile elongation and strength than fully lamellar structures (25). However, lamellar structure is better when high-temperature properties, such as creep resistance, and toughness are considered (8). The ductility and strength of the lamellar structure can also be tailored by control of the lamellae structures (25). Parameters that affect these properties are the lamella spacing, the volume fraction of the $\alpha_2$ phase and the lamellar colony size (7).

A polycrystalline alloy with the composition of Ti-47Al-2Cr-2Nb has been investigated thoroughly by Liu et al. (54) and it has been showed that the tensile ductility increases as the colony spacing decreases. An elongation, as high as, 4.7% was reported for a hot extruded and subsequent heat treated fully-lamellar material, with a colony size of 22µm. A coarser colony structure, with colony size of 258µm, reduced the elongation down to 1.9% (54).

The tensile strength is, in contrast to the ductility, not as dependent on the grain size. It has been shown to be dependent of the interlamellar spacing instead. As the interlamellar spacing decreases, the strength increases (54). It has further been shown by Umeda et al. that reduction of the lamellar spacing decreases the ductility as the yield stress increases (7). Figure 14 shows how the γ-lamella thickness influences the stress and the strain.

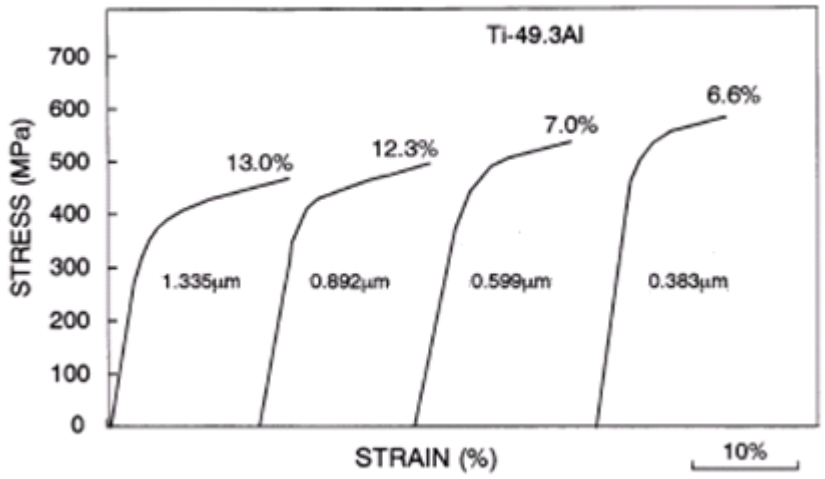


**Figure 14** *Influence of the γ-lamellae thickness on the stress-strain curve. Figure based on* **(7)**

Tönnes et al. (55) have also conducted tensile investigation on different microstructures and concluded that the tensile strength is influenced by the fraction of lamellas in the samples. The yield strength reaches highest levels when the fraction is below 10% of lamellas. Between 20% to 80% the yield strength is not affected by the fraction of lamellas. Above 80% of lamella content the yield strength stars to increase again. Further Tönnes et al. (55) concluded that the optimal lamella content for high ductility is between 30-50%, where the highest elongation value is achieved for 30% of lamellas. The ductility of TiAl is also determined by the volume fraction of the $\alpha_2$ phase, being shown to be optimal at a fraction of approximately 10%. When the fraction exceeds 20% the ductility

can be decreased (21). The $\alpha_2$ spacing, thickness and distribution in the microstructure also influence the ductility and strength of the material (25).

The yield strength can be related to grain size of the microstructure and can be estimated through the Hall-Patch equation, Equation 2 (2). The above described increase in strength with decrease in lamella spacing could also be related and estimated with the Hall-Patch equation (54). The Hall-Patch equation (Equation 2) estimates the required stress to transmit dislocations through the boundaries;

$$\boldsymbol{\sigma = \sigma_0 + k_y D^{-1/2}}$$

**Equation 2** *The Hall-Patch Equation* **(2)**

Where $k_y$ is a material constant, D is the structural length parameter of the microstructure and $\sigma_0$ is a constant stress contribution. Since the calculated stress is not affected by temperature the $\sigma_0$ constants can for example take thermal activated stresses into account (2), as a friction stress parameter (25). The equation has been applied to different classes of two-phase alloys. The parameters have been set for different microstructure; the lamella colony size influence of the yield strength can be described with $k_y$ ~ 5MPa√m, colony size of 290-2600µm (25). The duplex structure is more complex, as more than one length parameter is active (2), the $k_y$ constant varies between 0.8MPa√m and 3 MPa√m depending on the composition and ratio between lamellar colonies and single phase γ-grains (25).

### 6.3.2 Effect of increasing temperature

The anomalous increased yield stress at increasing temperature, see section 6.1 is not observed in all γ-TiAl alloys. Usually it is observed only in the single γ-phase alloys. Two phase alloys instead exhibit a broad plateau of the flow stress (23), usually consistent up to between 600° and 800°C (29). Grain boundary hardening (Hall-Petch) often occurs in two-phase alloys, which limits the increase in strength with increasing temperature (23).

Figure 15 shows two alloys with different Al content and thereby different microstructure; Ti-48Al has a duplex microstructure and Ti-54 has a single-phase gamma microstructure (29).

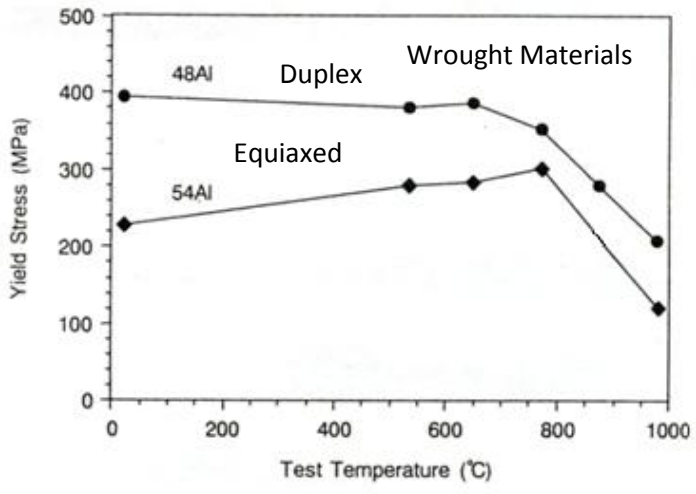


**Figure 15** *Microstructural effects on the yield stress vs temperature graph. Figure based on* **(29)**

The ductility increases with temperature when the strength rapidly decreases, in the temperature range of between 600°C and 800°C. Duplex structures exhibit good ductility over 600°-700°C and for lamellar structures the increase in ductility occurs at temperatures higher than 800°C (29).

The reduction in strength and increase in ductility is related to the brittle to ductile transition temperature, that occurs between 600° and 800°C (25) and is described in Section 6.1.

### 6.3.3 Effect of strain rate

It has been shown that the strain rate affects the tensile properties and with increasing strain rate both yield stress and ultimate tensile strength (UTS) increases. The yield stress and UTS increases with increasing strain rate up to a level of 10/s, then with further increase the yield stress and UTS remain on a constant level. The relationship can be estimated with the equation (Equation 3);

$$\sigma = C \cdot (\dot{\varepsilon})^m$$

**Equation 3** *Relationship between stress and strain rate* **(25)**

Where σ being the stress, $\dot{\varepsilon}$ being the strain rate, C a constant and m the strain rate sensitivity exponent. Reported values for the exponent is between 0.015 and 0.027, applicable for both yield stress and ultimate tensile strength and for a strain rate up to 10/s. The exponent is insensitive to temperature up to the brittle to ductile transition (25).

How the strain rate affect the ductility have not been clearly investigated yet, diverse result of the relationship has been seen and therefore no confirmed explanation can be drawn (25). However, research has showing that also the tensile elongation increases with increasing strain rate (50) (56).

The strain rate affects the beginning of the deformation, the transition from elastic to plastic deformation which thereby affects both the yield stress and ultimate tensile strength. The increase in flow stress with strain rate is dependent on the dislocation movement. The early plastic deformation occurs by dislocation movement that depends on thermal activation and thereby is more easily activated by increased strain rate. As the plastic deformation increases the deformation mode changes to twinning, which is not affected by strain rate. At strain rate over 10/s the dislocation moves entirely by twinning formation and therefore strain rates over 10/s does not affect the yield stress and UTS (25).

### 6.3.4 Effect of composition

The composition of the microstructure is also of importance for the mechanical properties, as it decides the achievable microstructure to some extent. There is a reverse relationship between the ductility and yield strength regarding the Al content. It has been shown that the yield strength increases with decreasing Al content (37). However the ductility increases with increasing Al content up to around 48 at.% Al, which can be seen in Figure 16. As the ductility is a main concern for structural applications, alloys that have a Al content of between 45-50 at.% is the most common to use as a base for further alloying (8).

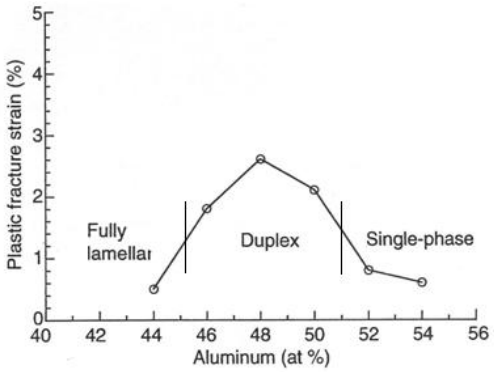


**Figure 16** *Aluminum content vs Plastic Fracture strain. Figure based on* **(8)**

On the other hand, Umeda et al. (7) have done research on PST crystals and shows that the ductility increases for decreasing Al content when the loading orientation is parallel to the lamellas. The elongation is not affected by the Al content (content between 46-49.3 at.% Al) in perpendicular or intermediate orientations. The reason for the increase in ductility with decreasing Al content is said to be the increase in volume fraction of the $\alpha_2$ phase. When the Al content is 47 at.% or less, the $\alpha_2$ lamellas acts as barriers and hinders the propagating microcracks. However, when the Al content is above 47 at.% the microcrack is not hindering the propagation, leading to lower ductility. Research on PST crystals shows that the yield strength increases with decreasing Al content for all directions (7).

As stated above the yield stress increases as the Al content decreases and that is due to the effect Al has on the lamella thickness. As the content decreases the number of thick $\alpha_2$ lamellas decreases, but the average thickness of the lamellas is fairly constant. Contrary the average thickness of the γ-lamellas decreases, leading to a finer lamella microstructure (7). As stated above, a fine lamellar structure increases the yield strength (54).

The tensile properties of TiAl can be improved by other alloying elements. Some small amounts, between 1-3%, of Cr, V or Mn can increase the ductility and addition of Nb or Ta can improve the strength (21). The amounts are kept at a low level to avoid formation of precipitates, which lowers the ductility (23). Even with these alloying elements the microstructure and the Al content is of great importance. For achieving ductilization with these elements the Al content must be between 45-50 at.% and the results are obtained for duplex microstructures (8).

Oxygen can severely limit the ductility of the material. Research has shown that oxygen level exceeding 1050 ppm is associated with a drop in ductility from around 2.1% to 0.5% in duplex structures. A decrease in ductility is seen in lamellar structures as well, but not as steep. The tensile strength is only slightly affected by the oxygen level (55).

## 6.4 Fracture toughness

As for tensile properties, the fracture toughness depends on the microstructure. The same alloy, heat treated differently can have $K_{IC}$ values altering between 10-35 MPa $m^{½}$ (25). Duplex microstructure has a low toughness of between 12-20 MPa $m^{½}$ (8) whereas lamellar structures have a much higher value of around 20-35 MPa $m^{½}$ (25). The fracture toughness of duplex structure is mainly determined

by the amount of γ-grains, as single γ-phase structures have a low $K_{IC}$ of ~ 10 MPa $m^{½}$ (29). All the fracture toughness values are fairly independent of temperature up to the BDTT (25).

The higher fracture toughness value of the lamellar structure, up to 35 MPa $m^{½}$ (25), is believed to be due to the $\alpha_2$ lamellas (23), which acts as a composite reinforcement and hinder crack front growth. The mechanism is most effective when the crack front is perpendicular to the $\alpha_2$+γ lamellas (8), which implies an anisotropic behavior of the material depending on the lamellae orientation. The reinforcement of the $\alpha_2$ lamellas is made through crack-tip blunting, if the lamellas are perpendicular to the crack front, through interphase cracking if the lamellas are parallel and through crack deflection if the lamellas are oriented at some angle to the crack front. The different mechanisms consumes different amount of energy from the crack growth, implying different fracture toughness values (25). The interphase cracking, or delamination, occur mostly in the γ/γ interface at ambient temperature and between γ/$\alpha_2$ interfaces at elevated temperatures. The crack deflection results in large plastic energy dissipation by fracture of the lamella ligaments and shear ligaments. The shear ligaments are strong as they induce mismatched crack planes (29).

In contrast to most metallic materials, TiAl exhibit an inverse relationship between ductility and toughness, see Figure 17 (25). This implies also that there is an inverse relationship between grain size of the two different properties as well (8), due to the relationship between grain size and critical microcrack size (25).

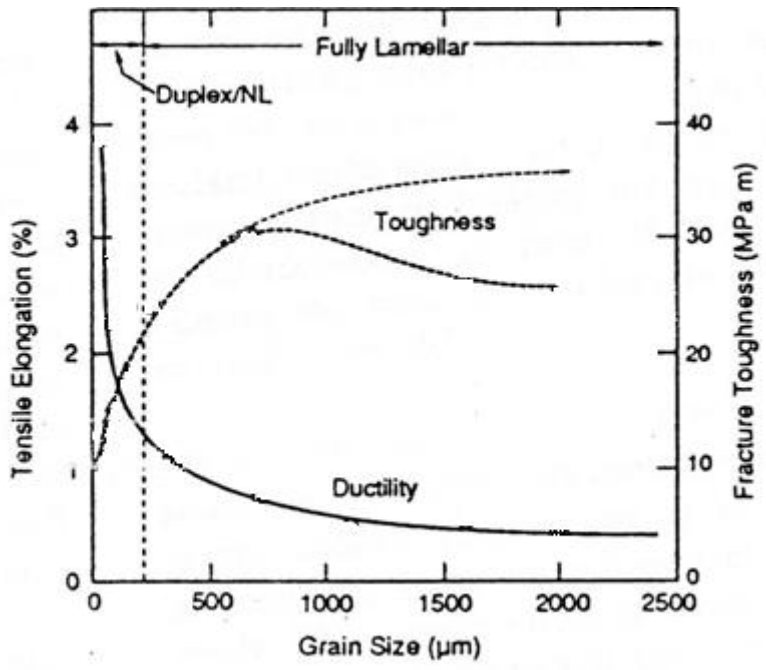


**Figure 17** *Reverse relationship between Ductility and Fracture Toughness. Figure based on* **(25)**

## 6.5 Fatigue properties

Lamellar structures exhibit the best crack growth resistance compared to duplex and equiaxed. Lamellar colony size, lamellar spacing and volume fraction of equiaxed γ-grains are microstructural factors that influence the fatigue growth rate. As for fracture toughness, there is an inverse relationship between strength, ductility and fatigue properties. By refining the lamellar colony size

and $\alpha_2$ spacing, higher ductility and strength can be obtained. However, for best fatigue growth rate a coarser structure is the best (25).

TiAl exhibit a high ratio of fatigue strength to ultimate tensile strength, between 70-80% at $10^7$ cycles (2). The high ratio can be explained by low tensile ductility, high cyclic work hardening rate and difficulty in the formation of strain localization (29).

The crack growth rate for both duplex and lamellar structures are dependent on the temperature, with lower growth rate at ambient temperature than at intermediate temperatures of 540-600°C. Just below the brittle to ductile transition temperature the crack growth rate decreases again and becomes slightly lower than for ambient temperatures. Above this temperature the fatigue life of TiAl seems to be limited by oxidation (2).

TiAl exhibit some differences in performance between high cycle fatigue and low cycle fatigue. Both duplex and lamellar structures show good high cycle fatigue properties and they are maintained to rather high temperatures. At 700°C the properties are exceeding the ones for Ni-based superalloy, even before the reduction in density is considered. For both lamellar and duplex structures, no fatigue limit below $10^8$ cycles has been identified (25). At temperatures lower than BDTT the duplex structure exhibit better fatigue life because of the finer grain size than lamellar structures. At temperatures above BDTT the material loses some of its strength, but the lamellar retains its strength better, leading to better fatigue properties than duplex in temperatures above BDTT (25).

In low cycle fatigue the strains are high and the fatigue life of the material can be related to the yield strength and ductility of the material. Therefore duplex materials often exhibit longer low cycle fatigue life in comparison to lamellar structures. As the strength and ductility is fairly constant up to the BDTT the low cycle fatigue properties are not dependent on the temperature up to the transition temperature (25).

## 6.6 Creep properties

Creep properties are not the most favorable for TiAl, however they are important as many of the applications involve excessive temperature stresses (25). In many ways the creep resistance is much inferior to the nickel-based superalloys (2). As for other properties, the microstructure is important, but also the morphology of each phase is important (23). The lamellar structure has enhanced creep properties compared to duplex structures, especially if the lamella boundaries are serrated or interlocked (29). The time to 0.2% creep strain are increased two orders for lamellar compared to duplex structures (8). It has been shown that TiAl-alloys with fully lamellar structure have creep properties comparable to those of nickel-based superalloys, whereas duplex structures only have 70% of the specific creep strength (55).

The creep resistance in lamellar structures can be improved even more by reducing the lamellar spacing, either by heat treatment or by controlling the Al content (23). Large interface areas impedes dislocation glide and climb of dislocation segments can be trapped in boundaries and restrict dislocation movements, which improves the creep properties with decreasing lamellar spacing (25).

The difference in creep resistance between lamellar and duplex structures decreases when the stress is lower. The lamellar structure exhibits better creep resistance at higher stress due to stronger

hardening at initial loading. However, this is not a true hardening but a result of significant weakening of the single-phase material in the duplex structure (25).

## 6.7 Oxidation resistance

The oxidation resistance of TiAl is considered sufficient up to a temperature of about 800°C (25). However, at elevated temperature the oxidation resistance is decreased, due to the fact that non-protective $TiO_2$ is more prone to form than protective $Al_2O_3$ (9). Even at temperature below 800°C the less protective $TiO_2$ is formed, but the protective $Al_2O_3$ is formed in higher density. Below 800°C four different layer of oxide can be identified; first the outer layer of $TiO_2$ that grows outwards, then a mixture of $TiO_2$ and $\alpha$- $Al_2O_3$, next a rich $Al_2O_3$ layer and adjacent to the matrix a thin layer of $Ti_3Al$ can be observed (25).

# 7 Ti-48Al-2Cr-2Nb

As earlier stated γ TiAl have been found to offer great potential to replace existing materials used today for high temperature applications. The Ti-48Al-2Cr-2Nb (48-2-2) alloy has had a lot of attention in research throughout the years. This alloy consists of a Ti base alloyed with 48 at.% Al, 2 at.% Cr and 2 at.% Nb (57). The alloy was developed by General Electric Corporate Research Center in the late 1980's (19). Since the discovery of the desirable properties of the alloy it has been patented and licensed to other manufacturer by GE (19). What the 48-2-2 alloy offers compared to other gamma TiAl is increased toughness and ductility at lower temperatures together with the desired creep properties (57). These properties make the 48-2-2 easier to process at ambient temperatures (25).

Addition of chromium (Cr) and niobium (Nb) into the alloy changes the properties of the material (57). The addition of Cr is reported to increase the ductility and thereby increase the workability of the material (58). At higher concentration than added into 48-2-2 Cr has been reported to improve the oxidation resistance (58). The major reason for addition of Nb is to enhance the oxidation resistance (58). Nb has also been reported to enhance the creep resistance in the material. This is primary due to the fact that Nb slows down diffusion in TiAl alloys (59), (8). The addition of these two elements has also been reported to decrease the number of stacking faults in the resulting microstructure (23). By the addition of these elements the binary phase diagram will be changed compared to pure Ti-Al phase diagram. Suggested changes in the phase diagram are marked by dotted lines in Figure 18for the example of Nb.

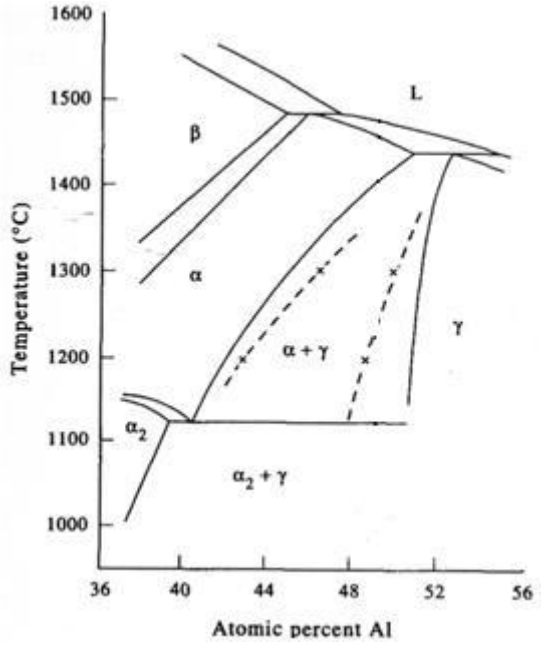


**Figure 18** *Ti-Al binary phase diagram with the dotted lines showing the phase lines changes if Nb is added. Picture based on* **(45)**

The typical grains size for cast and wrought TiAl is 1200 µm ± 645 µm (44) and 250 µm respectively (8). Some physical properties have been measured for components of 48-2-2 manufactured through wrought processing or by casting. These properties are summarized in Table 3 and Table 4 respectively.

**Table 3** *Mechanical Properties of Wrought Ti-48Al-2Cr-2Nb* **(8)**

| Mechanical properties | Test temperature | Duplex Structure | Fully Lamellar Structure |
|---|---|---|---|
| **Ductility (%)** | Room temp.<br>760°C | 3.1<br>50 | 0.4<br>2.8 |
| **Yield Strength (MPa)** | Room temp.<br>760°C | 480<br>406 | 455<br>403 |

**Table 4** *Mechanical Properties of Cast Ti-48Al-2Cr-2Nb* **(19), (60)**

| Mechanical Properties | Test Temperature | Duplex Structure |
|---|---|---|
| **Ductility (%)** | Room temp.<br>760°C | 1-3<br>9 |
| **Yield Strength (MPa)** | Room temp.<br>760°C | 275-380 |

# 8 Manufacturing

Different manufacturing methods are investigated and applied to TiAl in order to make it commercial. Due to the material's low ductility and fracture toughness processing of the material is hard and conventional manufacturing methods are difficult to apply (6). Conventional manufacturing methods have been applied, like casting, forging or powder processing, but they are all accompanied with difficulties that must be overcome. The difficulties in producing the material are said to be one reason for the limited use of TiAl today. Especially the automotive industry is sensitive to the end cost of the material and for TiAl, being so hard to process; the main cost of the product is the manufacturing cost (10).

Industrial scale processing routes that have been tried include ingot casting, powder processing and ingot forging, sheet production by hot-rolling, powder metallurgy processing (3) and investment and permanent mould casting (25). Conventional methods for alloying and creation of ingot include induction scull melting, vacuum arc remelting and plasma melting (25). One type of manufacturing method that has drawn attention recently is near net shape technologies. Different laser methods (6), together with Electron Beam Melting (EBM) have been investigated (61). Novel research shows that dense TiAl parts can be produced by EBM technology (3), (61), (12) with tensile properties that are comparable to literature data on cast alloys over a large temperature range (11)

As stated, conventional manufacturing methods can be challenging to use and some of the features in TiAl that has to be considered includes:

- Careful control of resulting the microstructure, regarding for example duplex or lamellas, grain size and interlamellar spacing, as it affects the ductility and the propensity for cleavage fracture
- Limited ductility and susceptibility to cleavage fracture limits the workability, even at high temperatures
- Significant plastic anisotropy
- Low recoverability due to low dislocation mobility
- Relatively low diffusivity
- Slow recrystallization due to low grain boundary mobility

The industrial-scale processing routes used today are in most aspect the same as those applied to nickel-based and conventional Ti alloys (2).

Different problems must be handled when casting TiAl, the firsts being the reactivity of the molten material. TiAl reacts with all ceramics and is therefore extremely hard to contain. The problem is solved by using a cold-wall furnace; however that creates problem when the mold is being filled. With cold-wall furnace the superheating of TiAl can only be 600°C, which makes it hard to fill the mold properly. Further problem is that Al is easily vaporized from the melt when molten in vacuum. To solve that problem the melting is done in argon, which can in turn be trapped in the melt due to the low superheating and thereby the fast mold filling. The high reactivity of TiAl also causes trouble finding a good and cost efficient material for the mold. Another problem involves the microstructure that can be rough, with large grains and coarse lamellar structure. This problem can be inhibited by

the use of grain refinement alloying (10). Segregation of Al and other alloying elements and creation of non-equilibrium and non-homogenized structures are also problems with casting (8).

Despite all the problems stated above, TiAl parts such as turbine airfoils and helicopter engines, have been successfully manufactured by investment casting. However, one problem with investment casting is that it is too expensive to use for parts used in the automotive industry. To lower the costs permanent mold casting has been investigated. Permanent molds have been seen to increase the cooling speed, which leads to fine grained near-γ or duplex structures (25). Cast γ-based materials are generally found weaker and less ductile than wrought materials. This is due to the coarse structure usually obtained in cast alloys, which is often left even after heat treatment (8).

The advantages with wrought methods are that the structure from the ingot is broken and recrystallization takes place. The workability of the material is strongly dependent on the Al content and it is increased with increasing Al content. This is due to the fact that increasing Al content decreases the volume fraction of $\alpha_2$-lamellas and $\alpha_2$-lamellas tents to resists deformation, which causes cracks in the material (8). With other alloying elements, as for example Cr, the workability can be increased even more (25). It could be demanding in wrought processing to form fine lamellar structures, which exhibit good properties (8).

The coarse microstructure and segregation obtained in casting could be avoided by using powder metallurgy with rapid solidification. The solidification microstructure can be refined and homogenous and comparable to wrought material (8). Investigation made on γ-TiAl produced by Electron Beam Melting shows that an ordered microstructure with extremely fine grains is obtained. The fine grains are expected since the melt pool is small and the cooling rate is high. By appropriate subsequent HIP and heat treatment a fine-grained duplex microstructure can be obtained (11). The manufacturing technique is built on additive manufacturing, adding layer by layer of material; despite that complete interlayer fusion is achieved (12).

# 9 Experimental Procedure

The experimental methods used in the study are chosen in order to perform an investigation to realize the aim of the study. The manufacturing of specimens are performed at Arcam AB and analyzed at either Oak Ridge National Laboratory or by companies contracted by Arcam.

## 9.1 Manufacturing of specimen

The samples used in the study are produced by an additive manufacturing process, Electron Beam Melting (EBM). The process builds up the material layer by layer out of powder to create a fully dense density near net shape component (62). The EBM system used is a laboratory modified Arcam A1 machine produced by the Swedish company Arcam AB. A schematic sketch of the machine can be seen in Figure 19. The powder are melted by an electron beam [3, in Figure 19], using an accelerating potential of 60 kV (3). The electrons are emitted from a tungsten filament [1] and the current can be varied between 1-50 mA. The beam is being directed and focused by two magnetic coils [2]. The diameter of the beam is regulated by the first magnetic coil and can be as small as ~0.1 mm. The second magnetic coil deflects the beam to the desired point of the powder bed (11).

The powder is held in powder cassettes [3] and the rake lays out the powder on the build table [6]. The beam melts the powder according to a predetermined shape, controlled according to a 3D model designed by computer aided system (3). When a layer is finished the build table is lowered and a new layer of powder is raked out, which is melted and the process is repeated. A typical layer thickness is 0.1 mm and the build speed is typical around 3-6 mm build height per hour, depending on the geometry of the part. To maintain high quality of the beam and to protect molten metal the process is conducted in a vacuum chamber [5] (11).

After a complete build the part cools down inside the machine, in a helium atmosphere in order to increase the cooling rate. All the powder that surrounds the molten material can be reused, leading to a minimum material waste (11).

Not standardized process parameters were used to produce material for this study in order to investigate the difference in microstructure. The samples were produced by melting the material in circular patterns from the outside towards the center. The thickness of each layer was 200 µm and the process temperature was 1050°C. For this project a powder material of the Ti-48Al-2Cr-2Nb alloy was used. The powder was produced by gas-atomization from a pre-alloyed melt, with a particle size of 45-150 µm. The powder was melted in the EBM machine to cylindrical bars with the diameter of 15 mm and a length of 100 mm.

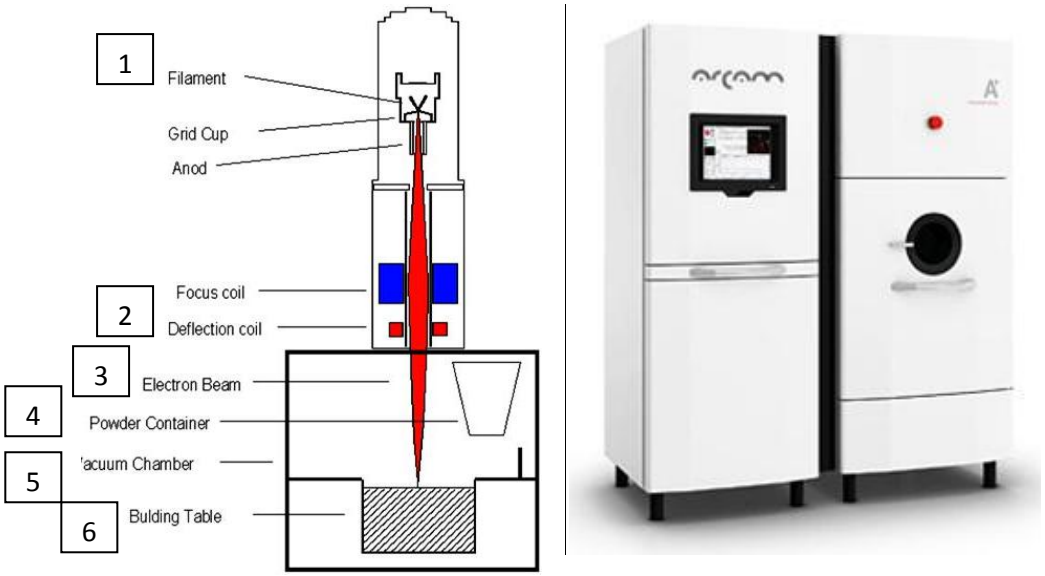


**Figure 19 Left:** *Schematic picture of the EBM system (numbers discussed in the text)* **(3) Right:** *The Arcam A1 Machine* **(63)**

## 9.2 Post manufacturing treatments

The EBM processed samples were post-processed through HIP and heat treatments.

### 9.2.1 HIP

To remove spherical and non-spherical pores within the as machined specimens the specimens were run through a HIP cycle. To evaluate the elimination behavior of pores, without excessive grain growth or microstructural changes, two different HIP cycles were executed.

The samples were sent to Bodycote in Belgium where they were run in two sheared cycles; one operating at 1155°C, 100MPa for 3 hours and the other at 1200°C, 100MPa for 4 hours.

After investigation of the two HIP cycles it was found that 1200°C, 100MPa for 4 hours gave the best result in pore reduction. Therefore all heat treated samples were pre-HIPed using this cycle.

### 9.2.2 Heat treatment

After HIP the samples were heat treated at Oak Ridge National Laboratory by the Materials Processing Group (ORNL) at different temperatures to alter the as-built microstructure. The different heat treatments were the following (see Table 5), in total 13 different cycles.

**Table 5** *Heat treatment cycles*

| Number | 1st Heat treatment Temperature [°C] | Holding time [hour] | Cooling rate | 2nd Heat treatment Temperature [°C] | Holding time [hour] | Cooling rate |
|---|---|---|---|---|---|---|
| **1** | 1150 | 5 | AC | | | |
| **2** | 1250 | 1 | AC | | | |
| **3** | 1300 | 1 | AC | | | |
| **4** | 1380 | 1 | FC | | | |
| **5** | 1380 | 1 | AC | | | |
| **6** | 1380 | 1 | WQ | | | |
| **7** | 1380 | 2 | WQ | | | |
| **8** | 1380 | 1 | AC | 1250 | 0.5 | AC |
| **9** | 1380 | 1 | AC | 1250 | 1 | AC |
| **10** | 1380 | 1 | AC | 1250 | 1.5 | AC |
| **11** | 1380 | 1 | WQ | 1250 | 0.5 | AC |
| **12** | 1380 | 1 | WQ | 1250 | 1 | AC |
| **13** | 1380 | 1 | WQ | 1250 | 1.5 | AC |

AC= Air cooling, FC= Furnace cooling, WQ=Water quenching

## 9.3 Chemical analysis

In order to investigate the full content of the starting powder and to see if the EBM process and the HIP affect the chemical content of the produced material a chemical analysis was performed. Powder, as-built and HIPed material was investigated. The chemical content of the material has a great influence of the achievable microstructure in TiAl and were therefore considered important to investigate.

The chemical analysis performed by Exova, United Kingdom, was made through the ICP-OES method, with combustion of carbon and sulfur, fusion of nitrogen and oxygen and fusion of hydrogen.

## 9.4 Sample preparation

All samples were cut transverse using an abrasive cutting saw with water as cooling lubricant at ORNL. Due to the brittleness of the material some cuts chipped off creating a spall on the ending edge of the cut surface. These spalls were carefully grinded away. As a flat cut surface was created the samples were cold mounted into Struers ClaroCit quick cure. All samples were flat ground after mounting using a Struers RotoPol-22 fitted with RotoForce-4 machine and 320 grit SiC paper, 25 N, 300rpm and water cooling. After flat grinding the samples were polished using Wendt Dunnungton 9 µm diamond solution that was sprayed on the Struers MD Largo wheel revving at 150 rpm, 30 N, without water. In the final polishing step the samples were polished using a Struers UP-U solution together with a MD Chem disc, 35 N, 150 rpm counter rotating plates. After chemical polishing the samples were rinsed using alcohol and cotton balls, carefully swabbing the chemical solution away.

The samples for microstructural evaluation were etched in a modified Kroll's agent. The etch was of 3 vol.% HF, 12 vol.% $HNO_3$ and 85 vol.% $H_2O$. As some samples were hard to etch a stronger solution, containing 10 vol.% HF, was used. During the etching the etchant was swabbed onto the surface

using a cotton tip. The etchant was held for 2-10 seconds before dropping the sample in water and finally rinsed with alcohol.

## 9.5 Microscopy

The microstructure obtained from as-built, as-HIPed and heat treated samples were investigated and characterized using both optical and SEM microscopes.

### 9.5.1 Light Optical microscopy

A light optical microscope is built up of a series of lenses together with a light source. As the light illuminates the sample the light will deflect differently depending on the surface. The reflected light is collected through the lenses and altered for good imaging. The disadvantage with optical microscope is its low depth of field. Therefore the samples have to be ground and polished for best view. To be able to see the morphology the samples can be etched.

The optical microscope used in this study was Nikon Epiphot Type 108, together with ScopePhoto 3.0 software to take pictures.

#### *9.5.1.1 Grain size measurement*

Grain size measurements were made on as-built, HIPed and the four most promising heat treatment conditions; being 1250°C, 1300˚C, 1380˚C AC and 1380˚C AC + 1250˚C.

Through optical microscopy the grain size was reorganized not to be a log-normal distribution and ASTM standard E 1181-02, standard test methods for characterizing duplex grain size, was first used to characterize the sample. The classification was determined by optical microscopy on a low magnification and comparison with characteristic pictures presented in the standard. The area fraction of each homogeneously distributed grain size was determined by point counting procedures or measuring of the area depending on the identified class.

The grain size of the individual grains in each determined class was measured according to ASTM standard E 112-96 by planimetric procedure. The grains inside a determined area was calculated and repeated for three different, randomly chosen fields to ensure a reasonable average. The number of grains inside the box was calculated as one and the intercepted ones as a half, Equation 4 where $N_A$ is the number of grains per mm$^2$. To encounter for the magnification the Jefferies' factor, f, is used.

$$N_A = f\left(N_A + \frac{N_{intercepted}}{2}\right)$$

**Equation 4** *Calculation of grains per square millimeter*

The ASTM grain size, G, was calculated from Equation 5, $\overline{N}_A$ being the average grain per mm$^2$.

$$G = (3.321928\, log_{10}\overline{N}_A) - 2.954$$

**Equation 5** *Calculation of ASTM grain size*

The average grain size diameter is calculated with the approximation that the grain is equiaxed in the two dimensional plane, using:

$$\bar{d} = \sqrt{\left(\frac{\frac{1}{\overline{N_A}} * 4}{\pi}\right)}$$

**Equation 6** *The average grain size diameter*

### 9.5.2 Scanning Electron Microscopy

During analysis in Scanning Electron Microscope (SEM) the sample is scanned by an electron beam. The beam is generated from a field emission tip and normally has an energy intensity of between 0.5 and 40 keV. The beam is focused on the sample via a series of condenser lenses. As the electron reaches the sample it interacts with the atoms in the sample and signals such as secondary electrons, backscattered electrons and X-rays are generated. Back scattered electrons (BSE) are electrons from the original beam that are reflected from the sample surface and is thereby related to the atomic number of the atoms in the sample. Due to the atomic number the micrographs created with BSE will show the phase with highest atomic number as the brightest in the micrographs. As the electron beam excites an inner shell electron of the sample, X-rays are emitted when the electron releases the energy to return to its unexcited position. Secondary electrons are emitted from the outer orbital of the atom.

The investigations were made on a Hitachi, S-3400N scanning electron microscope. The microscope has secondary electron and backscattered electron collector and an X-ray detector. The BSE was detected through 5 different detectors located in the focus perimeter. The accelerating voltage was 15.0 kV for the pictures and was lowered to 10.0 kV for the mapping. The max resolution of the used SEM is 50-60 Å.

#### *9.5.2.1 EDX analysis*

The X-rays emitted from the atoms in the sample is analyzed by Energy Dispersive X-rays spectroscopy (EDX). The X-rays emitted from the sample are dependent on the atomic electron configuration and will be different for different atomic elements. Therefore chemical composition measurements can be obtained by this method.

The EDX analysis was made through the same SEM used above, with EDAX Genesis as the analyzing software. The EDX was made through spectrum measurements. A mapping was made through measuring a spectrum of elements in each pixel of the pictures. In the mapping the brightest areas are the ones with highest concentration.

## 9.6 FIB-SEM

A Focused Ion Beam – Scanning Electron Microscope (FIB-SEM) is a combined instrument that uses a focused ion beam (FIB) as well as a SEM to analyze materials. A FIB uses ions instead of electron to analyze the sample. Normally a Ga source is used to create $Ga^+$ ions which are projected onto the sample. The projected atoms will scatter atoms of the sample away from the sample surface. The

back scattered ions can be analyzed using the same principal as BSE in SEM. The FIB technique can also be used to remove material from the sample to polish or etch the sample.

The FIB-SEM equipment used at Oak Ridge National Laboratory within the SHaRe program has a setup as seen in Figure 20. The FIB column is directed right on the sample with the SEM at an angle of 58° vertically and 32° horizontally.

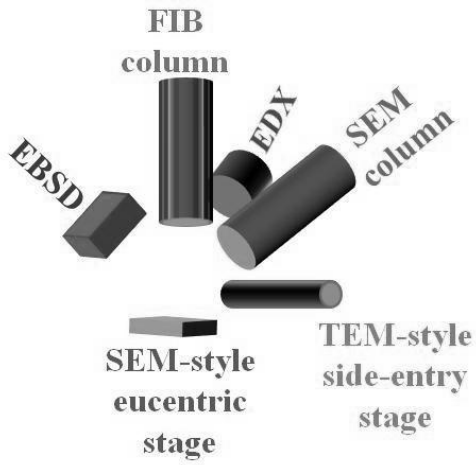


**Figure 20** *FIB-SEM setup at Oak Ridge National Laboratory*

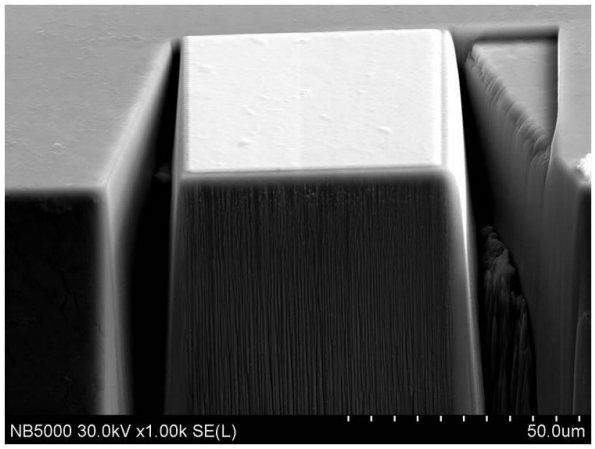


**Figure 21** *Cut out of TiAl using FIB*

For testing of TiAl pre-cuts were made by the FIB. An area of about 50 µm was laid bare and polished for analysis, which can be seen in Figure 21. The area was analyzed using ESBD and EDS imaging. Phase ID (PI), image quality (IQ), confidence index (CI) and inverse pole figures (IPF) were used to analyze the sample using OIM Analysis 5.31 software.

## 9.7 Micro hardness

To evaluate how the hardness of the microstructure changes according to differences in treatments micro hardness was measured. The measurement was made in a Buehler Micromet 2100 Series Micro hardness Tester. 20 indents across the sample were taken, in a total of 12 mm, with 500 g of load.

The analysis of the indents was made by the software Omnimet MHT and the results were presented graphically.

## 9.8 Tensile testing

Tensile testing is a fairly inexpensive and fully standardized test method used on every kind of materials. The test provides a good knowledge of how the material behaves under mechanical tension load.

The tensile testing made in this study was performed by the Metals and Ceramics Division, Mechanical properties group at Oak Ridge National Laboratory. The testing was made in an Instron 4507 machine and the force was applied until the specimen broke. The strain rate used was 0.001/s.

The geometry of the specimen was cylindrical with a diameter of 6.35 mm, specimen gage length of 31.974 mm and the gage length between the extensometer was 25.273 mm.

In total 19 tensile tests were performed. Three different heat treatment conditions were tested; 1250˚C, 1300˚C, 1380˚C Air cooled + 1250˚C, together with as-built and as-HIPed material. The three specific heat treatments were chosen due to their unique microstructure. All different conditions were tested in room temperature, two bars of each. In addition two bars of the HIPed condition was tested in 500˚C, 600˚C, 760˚C and 850˚C.

## 9.9 Relevance

In the different analyzing methods used some sources of error or faults may be present. These sources are important to consider since the result may be misleading if completely trusted.

Since some of the elements chemically analyzed are present in very small amounts the method for chemical analysis of the material may not give reliable results. The chemical analysis can be a source for error since the result from the chemical analysis shows a higher amount of Al in the as-HIPed material compared to the as-built. Since the HIP do not add any material the increase of Al during HIP is unlikely.

To be able to analyze the material in optical microscope and SEM the sample has to be etched. It has been reported from several studies that TiAl is complicated to etch. The recipe used to etch the samples in this study contains a large amount of especially HF acid and it may be a possibility that the samples are over etched and lamellas are etched into the γ-phase.

The ASTM standards used to measure the grain size are a subjective method since the grains are measured manually. For the samples in this study the grain boundaries was sometimes hard to determine due to issues while etched which is a source of error.

Analysis of the samples in microscope gives a good look at the microstructure. However by using for example SEM only a small fraction of the sample will be analyzed. The microstructure in the analyzed fraction may not be representative for the entire sample and multiple fractions should be analyzed. Due to lack of time and resources the samples in this study is only evaluated in one fraction, which must be considered.

The planimetric method was used in the ASTM E112-96 standard. This method presumes that equiaxed grains are obtained throughout the entire sample. As the TiAl samples does not have a completely equiaxed structure this may be a source of error. The sample was only measured in two dimensions which also may be a source of error since the microstructure may vary in all dimensions. Due to lack of time and geometry of specimen other measuring methods was not applied to measure the grains size.

The FIB-SEM used at ORNL is a prototype unit where all parameters are not yet fully established which does not make it an optimal method. In the software used to analyze the ESBD data $Ti_3Al$ structure is not yet implied which will cause the analysis of data invalid for the $Ti_3Al$ parts of the specimen. Despite these disadvantages the FIB/EBSD method is still a unique method to analyze the microstructure in a 3D perspective.

The micro hardness test is only run one time on each sample as it was used as a comparative method. As the standard deviation is large for the samples the actual values from the test is not to be

trusted. For internal comparison the test result may be used as the test is conducted similar in all samples. From literature it has been reported that the hardness is dependent of what kind of microstructure is present. As the duplex structure, which is present in this study, contains both equiaxed and lamellar grains it can be a source of error for the standard deviation.

# 10 Results

The results from the experimentally performed investigations are presented to give a context for the upcoming analysis. The results are based on theory and experimental methods chosen to realize the aim. To give comprehensive picture of how the post manufacturing treatments affects the material the results for the as-built material are first shown followed by the results for as-HIPed and heat treated materials.

## 10.1 The EBM as-built material

The full content of the powder before built can be seen in Table 6, together with the chemical content of as-built and as-HIPed solid material. For comparison the chemical specification for the alloy is also provided in the table.

**Table 6** *The chemical content of the material; as powder, as-built and as-HIPed together with the alloy specification*

| Element [weight] | Ti [%] | Al [%] | Cr [%] | Nb [%] | C [%] | Fe [%] | N [%] | O [%] |
|---|---|---|---|---|---|---|---|---|
| **Alloy Spec.** | Base | 33.0-34.0 | 2.2-2.6 | 4.5-5.1 | Max 0.015 | Max 0.04 | Max 0.02 | Max 0.08 |
| **Powder** | Base | 33.1 | 2.43 | 4.64 | 0.011 | <0.01 | 0.005 | 0.10 |
| **As-Built** | Base | 32.6 | 2.40 | 4.70 | 0.015 | <0.01 | 0.011 | 0.16 |
| **As-HIP** | base | 33.5 | 2.40 | 4.75 | 0.017 | 0.04 | 0.019 | 0.15 |

In Figure 22 and Figure 23 optical micrographs of the center of the EBM-produced bars can be seen. Some areas with enlarged grain structure can be seen, however the microstructure is fairly homogeneous in the center of the bar. The microstructure consists of fine lamellas distributed in alternating directions and a low amount of equiaxed γ-grains distributed in between.

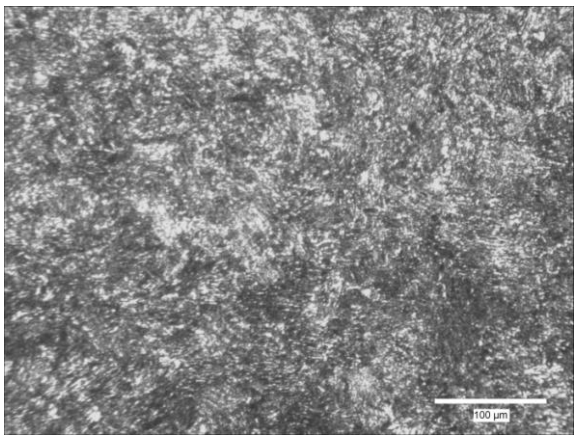


**Figure 22** *The center of the as-built material, optical micrograph*

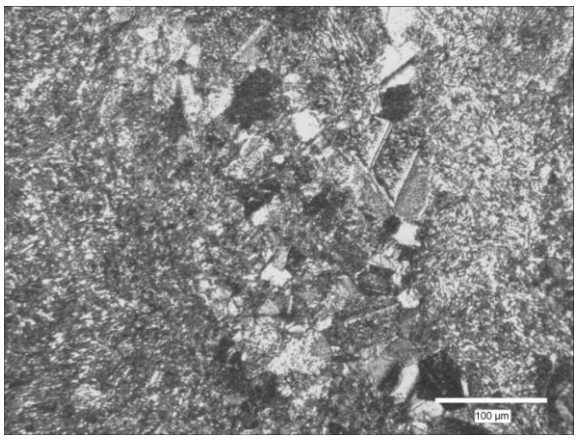


**Figure 23** *The center of the as-built material, with some areas with enlarged grains, optical micrograph*

Investigation shows changes in microstructure towards the edges of the samples. The as-built microstructure at the edges can be seen in Figure 24. A lower amount of lamellas are seen at the edge. The amount of equiaxed γ-grains is increased and areas of segregated elements are spotted at the grain boundaries and triple points of the γ-grains.

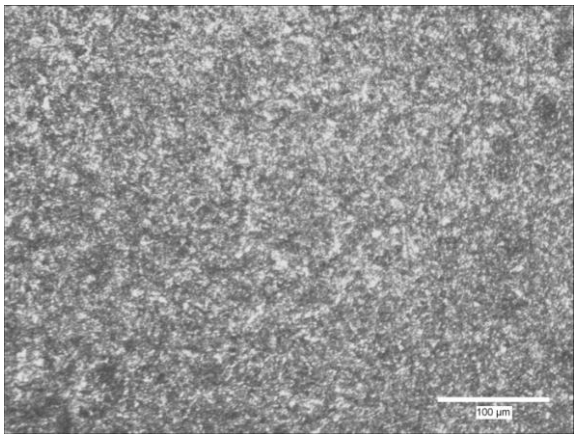


**Figure 24** *The edges of the as-built material, optical micrograph*

SEM micrograph, Figure 25, of the as-built material reveals a heterogeneous structure of the sample as a large fraction of the sample is analyzed.

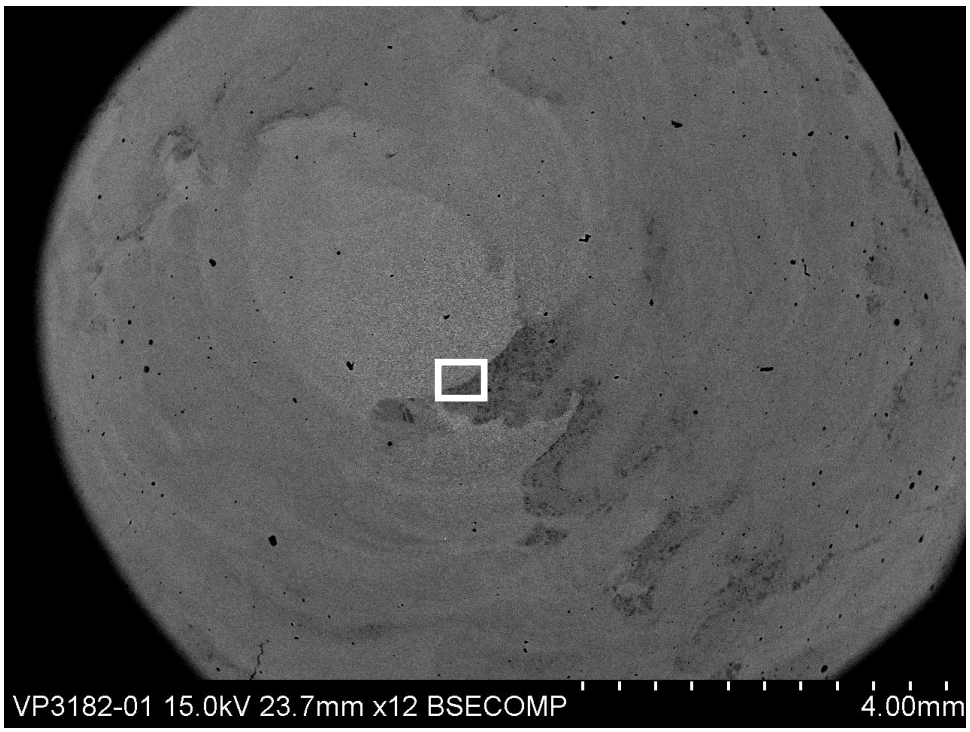


**Figure 25** *Backscattered electron micrograph of the as-built sample. The marked area is further studied*

As the magnification is raised in the marked area of Figure 25 it reveals an area of duplex structure neighboring an area of single phase structure, seen in Figure 26.

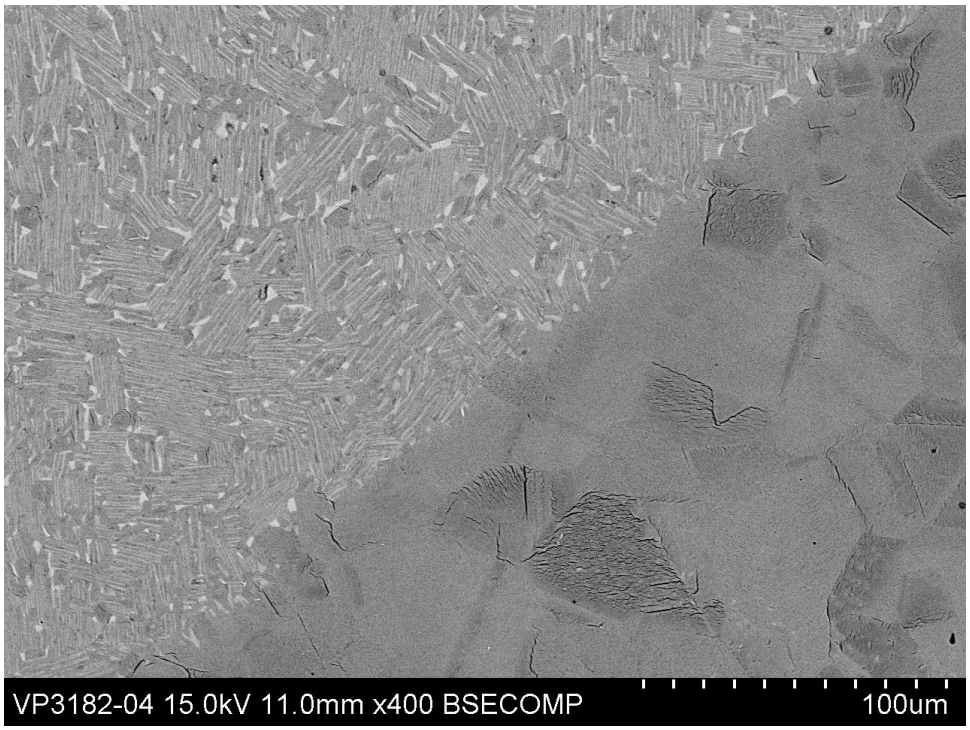


**Figure 26** *Backscattered electron micrograph of the as-built sample, 400X*

The area shown in Figure 26 is analyzed through EDX mapping with background scatter removed. A higher concentration of the analyzed elements is revealed with lighter print. The pictures from the mapping are seen in Figure 27.

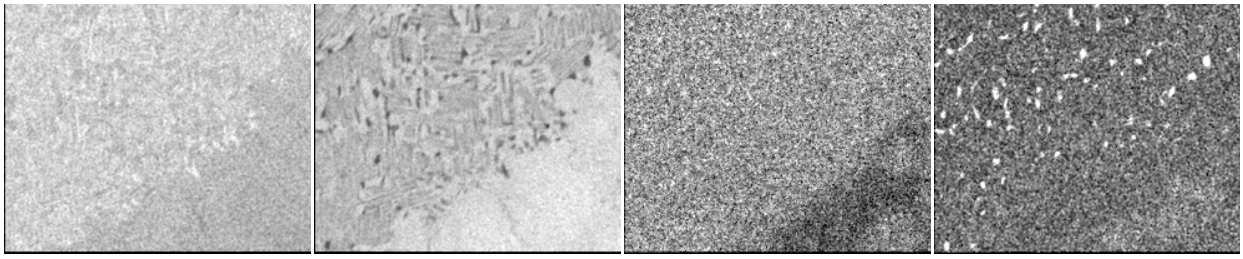

**a** **b** **c** **d**

**Figure 27** *EDX mapping of* **a)** *Ti,* **b)** *Al,* **c)** *Nb,* **d)** *Cr*

From the EDX mapping it is seen that the Ti concentration is high in the duplex phase whereas the Al is concentrated in the single phase field. The Nb concentration is quite uniform throughout the section. It is clearly seen that the Cr is concentrated into local spots, recognized as β phase. These spots are observed to be lean in Al concentration.

## 10.2 The EBM as-HIP material

Resulting microstructure from both 155°C, 100 MPa, 3 hours and 1200°C, 100 MPa, 4 hours HIP cycles was evaluated to find a suitable HIP treatment.

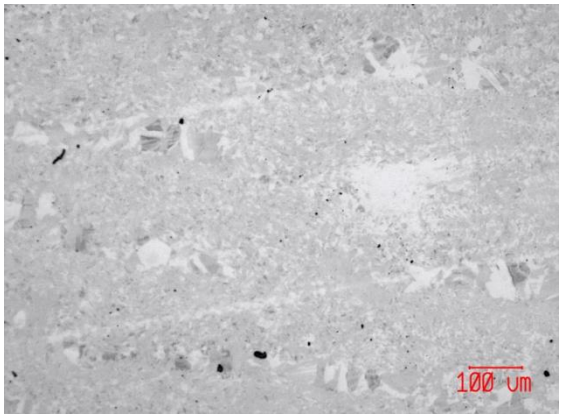


**Figure 29** *Micrograph from HIP cycle at 1155°C, 100 MPa, 3 hours*

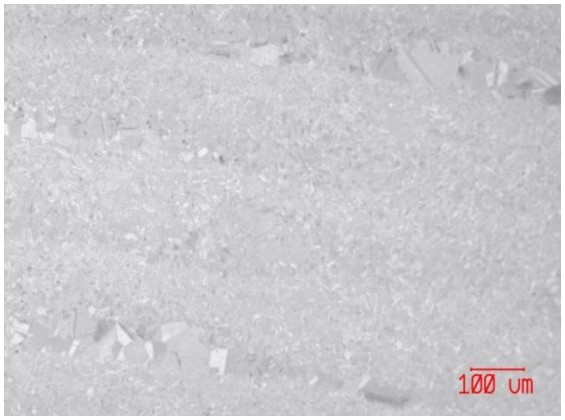


**Figure 28** *Micrograph from HIP cycle at 1250°C, 100 MPa, 4 hours*

To the left, Figure 29, a micrograph from the 1155°C cycle is shown. In this micrograph some pores can be seen as black areas. Some of the pores have a diameter of more than 10 µm. In the micrograph on the right in Figure 28, which is the cycle run at 1200°C, pores are not observed. Some small pores are observed in remote areas of the sample but are small enough not to be considered.

The resulting SEM micrographs for material HIPed at 1200°C, 100 MPa, 4 hours are seen in Figure 30 and Figure 31.

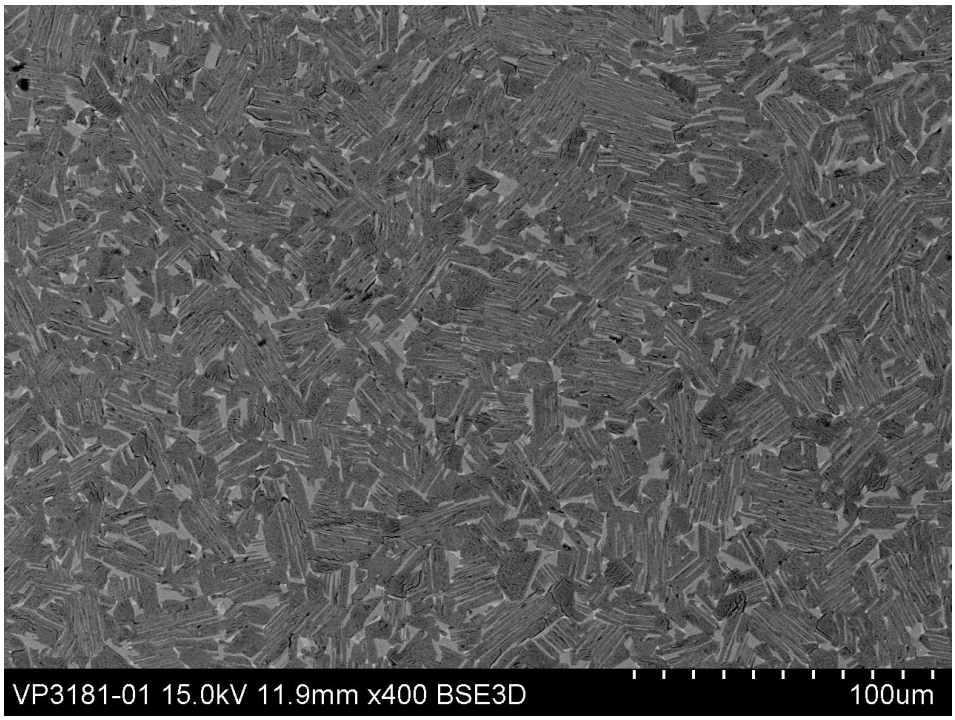


**Figure 30** *Backscattered electron micrograph of as-HIPed material in 400X*

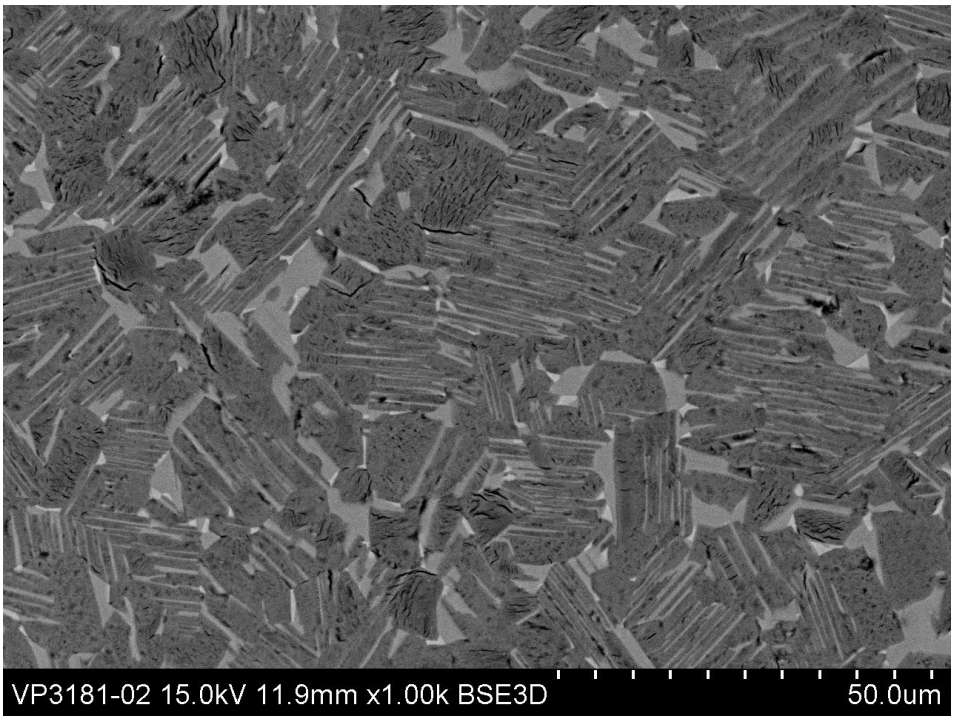


**Figure 31** *Backscattered electron micrograph of as-HIPed material in 1,000X*

The as-HIPed material shows a homogenous duplex microstructure with fine grains. The fraction of lamellas is observed to be high together with equiaxed γ grains and some retained β phase. From EDX, Table 7, analysis it is revealed that the white phase is β since it is rich in Cr together with high amounts of Ti. The large intermediate gray phase is revealed to be $\alpha_2$ phase and the dark phase is believed to be γ phase.

**Table 7** *EDX analysis of as-HIPed material*

| Element/Phase | Ti | Al | Nb | Cr |
|---|---|---|---|---|
| **White phase** | 53.5 | 35.7 | 2.9 | 7.9 |
| **Intermediate gray** | 56.1 | 38.7 | 2.5 | 2.7 |
| **Dark gray** | 48.5 | 47.6 | 2.4 | 1.5 |

### 10.2.1 FIB-SEM and EBSD analysis

The bare laid and polished area was scanned by SEM and EBSD detectors and analyzed for image quality in the OIM software. From this analysis a god view of the grain boundaries is obtained, Figure 32, with comparison to the BSE image in Figure 33.

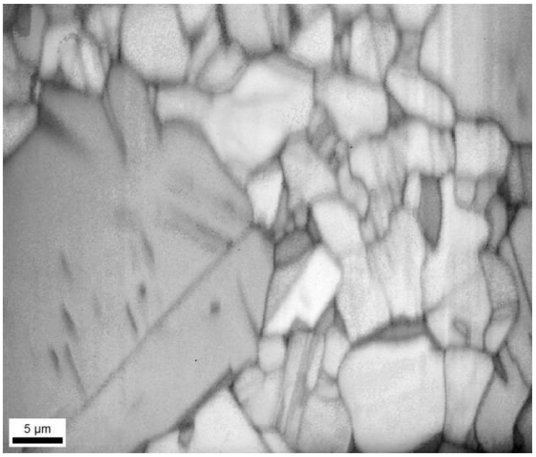


**Figure 32** *Image Quality map showing grain boundaries*

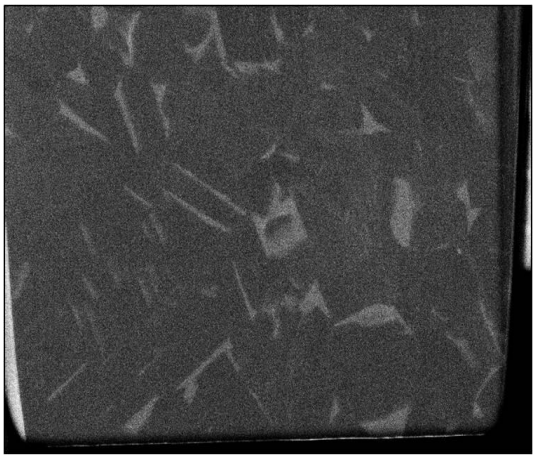

**Figure 33** *BSE image of the FIB polished HIPed TiAl sample*

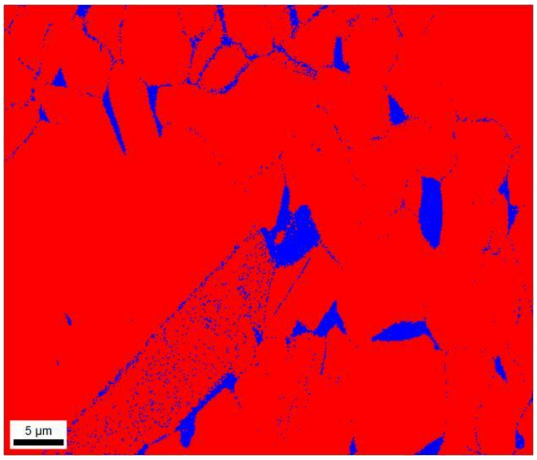


**Figure 34** *Phase ID figure where FCT/BCC systems are indexed red and HCP indexed in blue*

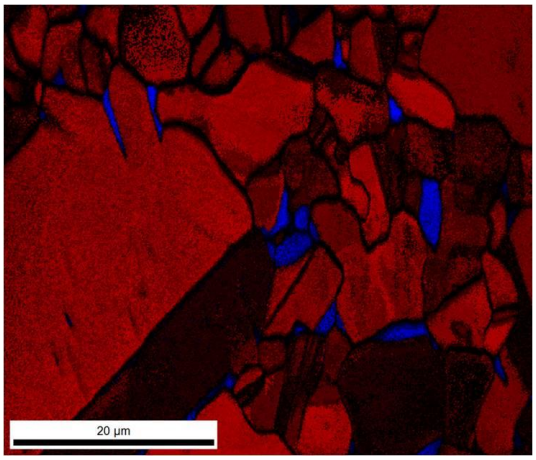


**Figure 35** *Confidence Index of the Phase ID mapping*

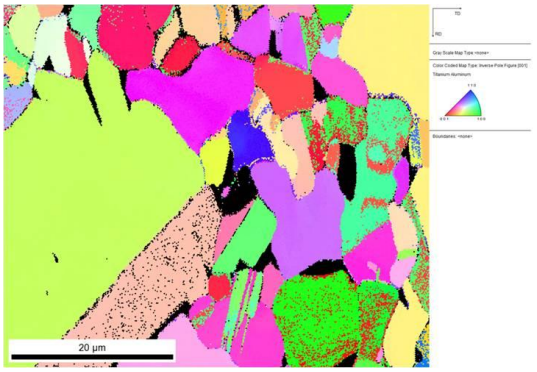


**Figure 36** *IPF map showing the orientation of the BCT/BCC phases*

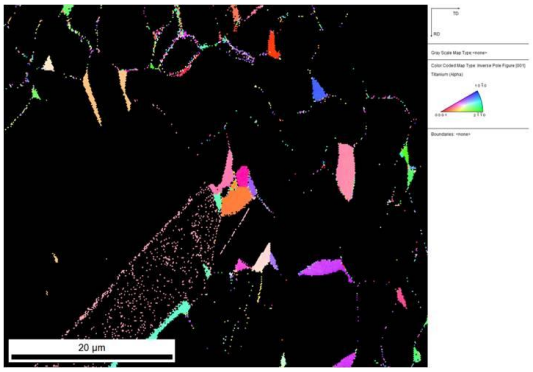


**Figure 37** *IPFmap showing the orientation of the HCP phases*

It is observed form Figure 32 that the grain size is differing between small grains of less than 2 μm up to larger grains larger than 4 μm.

The same area was also evaluated with the OIM software to find the different phases for the different grains. In the OIM software the γ-TiAl is analyzed as a FCT system as the c/a ratio is almost 1 and the software cannot tell the difference from BCC. In the OIM software the β phase is analyzed as a BCC phase and difference is not seen between β and γ. The α-phase together with $\alpha_2$ is indexed as HCP phase due to software limitations.

In Figure 34 the γ and β phases are indexed in red and the α and $\alpha_2$ phases are indexed in blue. As can be seen from the figure the α and $\alpha_2$ phases are mostly oriented in the grain boundaries, compared to Figure 32. If compared to Figure 33 no clearly lamellas can be seen in the phase ID figure. The confidence index for the phase ID mapping is seen in Figure 35.

To further analyze the polished area an inverse pole figure was analyzed to find the orientation of the different grains and phases. In Figure 36 and Figure 37 IPF maps are seen where the (001) is projected outwards from the paper.

The different grains in the FCT/BCC systems are seen to order themselves randomly. The grains oriented in the (100) direction is although seen to be harder to analyze as they are not homogenously colored. It can be observed that the hexagonal α phases are distributed in the grain boundaries. However, some individual α grains can be found in the microstructure. In the larger grain in the lower left that has the dotted structure in both Figure 36 and Figure 37 is believed to be of a lamellar structure with the lamellas pointing out from the picture.

## 10.3 Microstructural characterization of Heat Treated Materials

Different heat treatment procedures were performed in order to investigate the heat treatment temperature and the cooling rate dependency of the material. All the investigated samples reveal a different resulting microstructure in the center compared to the edge. The difference in microstructure is expected since the starting microstructure of the as-HIPed material is heterogeneous.

### 10.3.1 Temperature dependence of heat treatment in the α+γ phase field

Figure 38 and Figure 39 shows optical micrographs from sample heat treated for five hours at 1150˚C.

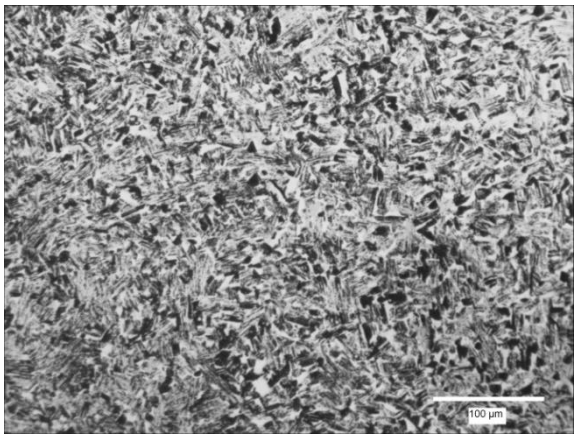


**Figure 38** *The center of the bar, optical micrograph*

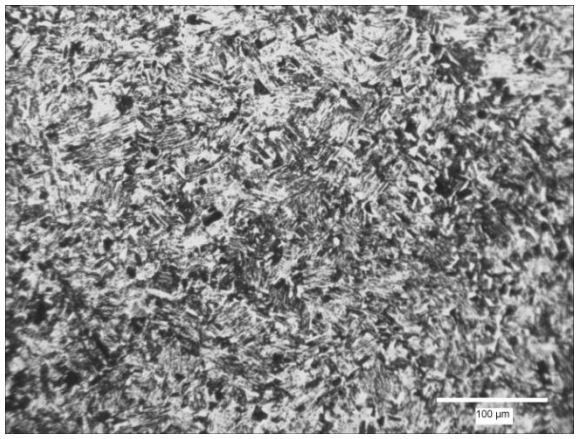


**Figure 39** *The edge of the bar, optical micrograph*

Figure 40 and Figure 41 shows optical micrographs from sample heat treated for one hour at 1250˚C,

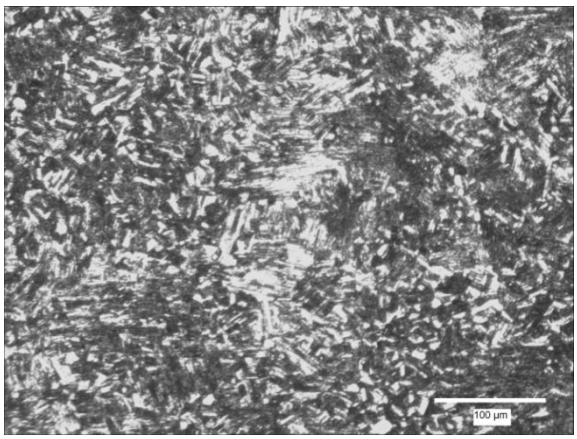


**Figure 40** *The center of the bar, optical micrograph*

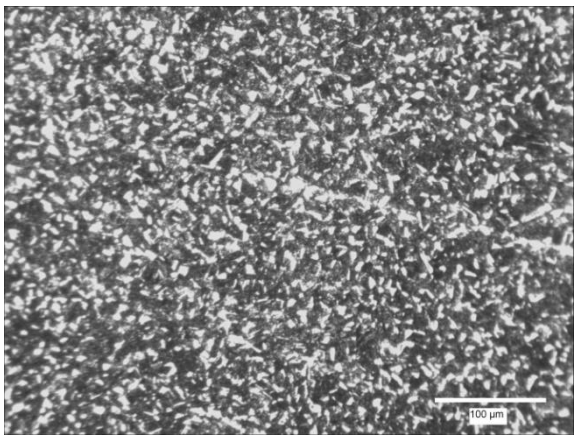


**Figure 41** *The edge of the bar, optical micrograph*

Figure 42 and Figure 43 shows optical micrographs from sample heat treated for one hour at 1300˚C.

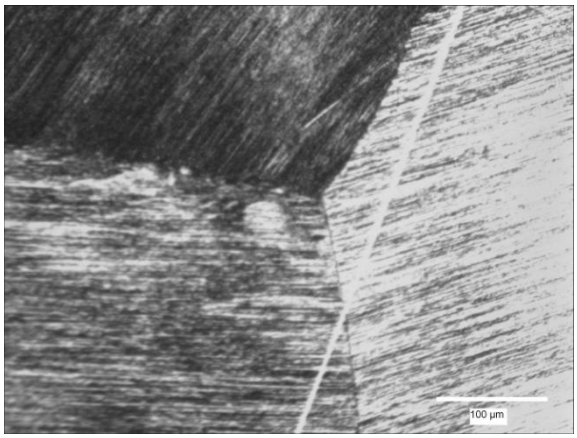


**Figure 42** *The center of the bar, optical micrograph*

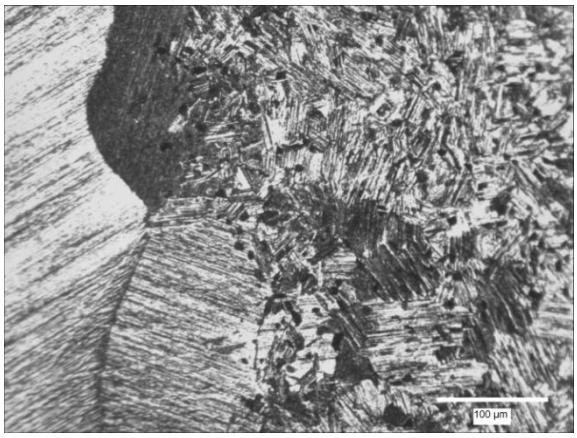


**Figure 43** *The edge of the bar, optical micrograph*

The center and the edge of the sample heat treated at 1150°C have no significant difference in microstructure. The microstructure in both pictures both contains γ grains, seen as the darker areas, as well as lamellas, seen as zebra shaped colonies.

From the picture showing the edge of the sample heat treated at 1250°C a similar microstructure as the one for 1150°C is observed. For the microstructure of the center of the material a coarser microstructure is revealed. It is also observed that the microstructure obtained from 1250°C contains larger amount of lamellas in the center.

In the center of the sample heat treated in 1300°C distinct lamellas are observed. It is also observed that the grain size of these lamellas has grown compared to the as-built material. Around the edge a rim of fine grained lamellas with fine equiaxed γ grains are observed. The amount of γ grains is observed to be low, as only small fractions of equiaxed areas are found.

Figure 44 and Figure 45 shows backscattered electron micrographs from the center of the bar heat treated at 1150°C and 1250°C respectively.

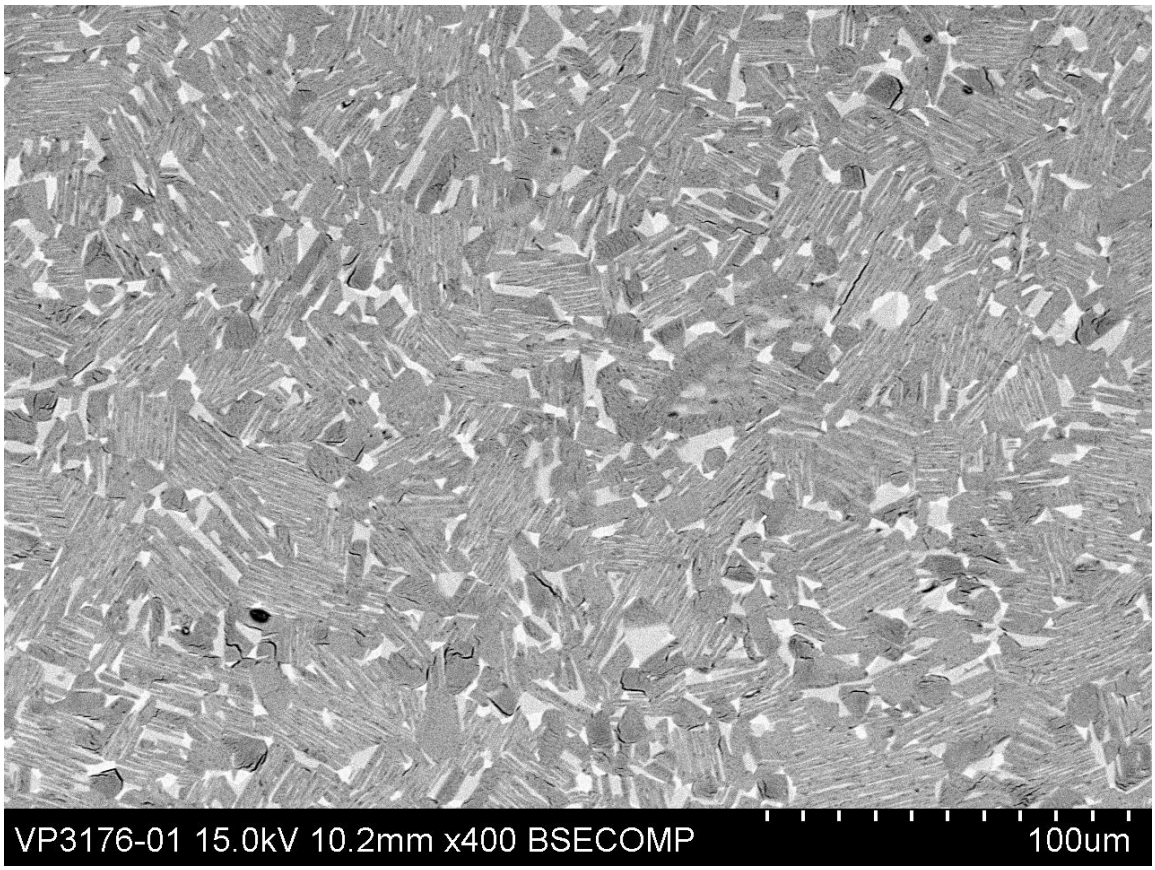


**Figure 44** *Backscattered electron micrograph 1150°C, 5 hours, air cooling*

In the backscattered electron micrograph, Figure 44, it is clearly seen that the sample heat treated at 1150°C have a larger amount of lamellas compared to the amount of lamellas observed in the optical micrograph. Although some β and a significant amount of γ is also observed. From EDX analysis, Table 8, it is determined that the white phase is β phase due to high amount of Cr and low amount of

Al. The darkest phase is determined to be γ as the amount of Ti and Al is equal. The intermediate phase is believed to be $\alpha_2$.

**Table 8** *EDX analysis of material heat treated at 1150°C*

| Element/Phase | Ti | Al | Nb | Cr |
|---|---|---|---|---|
| **White phase** | 56.0 | 35.6 | 2.9 | 5.4 |
| **Intermediate gray** | 55.2 | 40.2 | 2.3 | 2.2 |
| **Dark gray** | 49.0 | 47.4 | 2.3 | 1.2 |

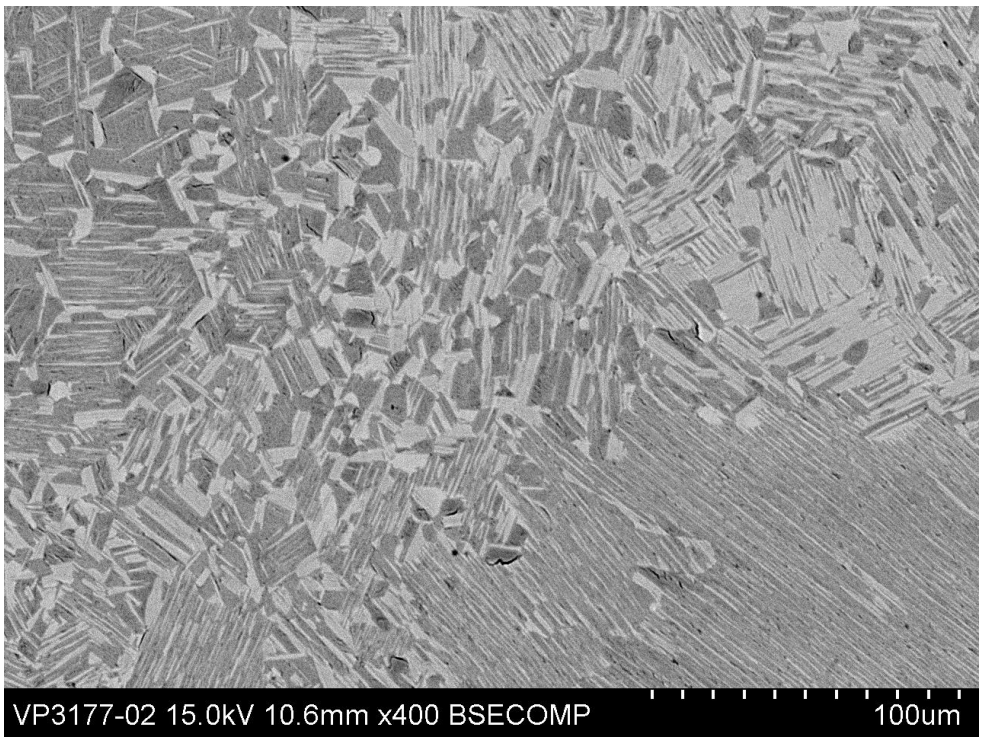


**Figure 45** *Backscattered electron micrograph 1250°C, 5 hours, air cooling*

From the SEM micrograph, Figure 45, it is clearly seen that the 1250°C material is not homogenous as some large lamellas are observed within the small grained duplex. In this picture no white β phase is observed. The different phases are analyzed via EDX, Table 9.

**Table 9** *EDX analysis of material heat treated at 1250°C*

| Element/Phase | Ti | Al | Nb | Cr |
|---|---|---|---|---|
| **Intermediate gray** | 51.9 | 43.6 | 2.4 | 2.1 |
| **Dark gray** | 46.9 | 49.5 | 2.4 | 1.2 |

### 10.3.2 Cooling rate dependence of heat treatment in single α phase field

Figure 46 and Figure 47 shows optical micrographs from sample heat treated at 1380˚C with subsequent furnace cooling.

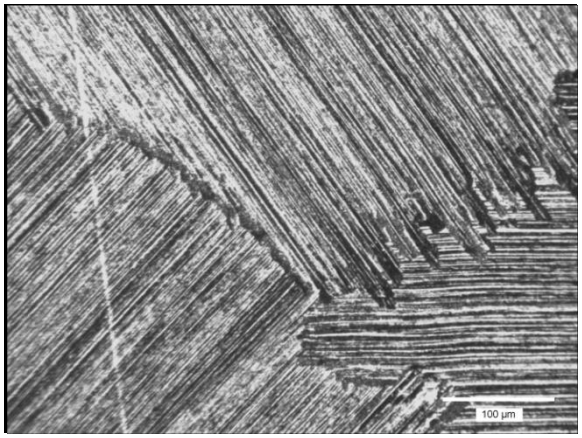


**Figure 46** *Center of the furnace cooled bar, optical micrograph*

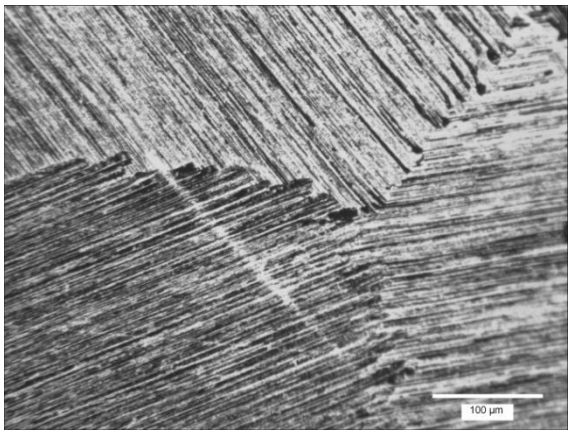


**Figure 47** *Edge of the furnace cooled bar, optical micrograph*

Figure 48 and Figure 49 shows optical micrographs from sample heat treated at 1380˚C with subsequent air cooling.

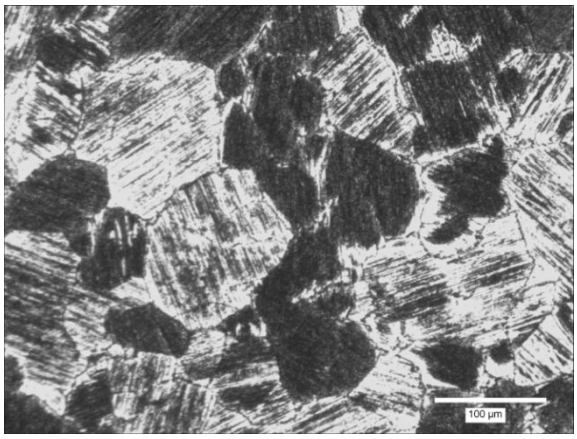


**Figure 48** *Center of the air cooled bar, optical micrograph*

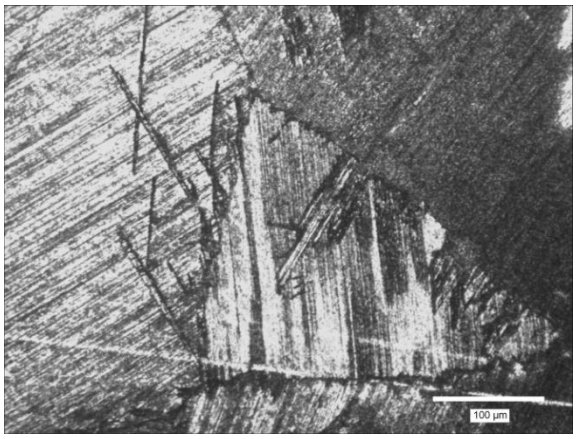


**Figure 49** *Edge of the air cooled bar, optical micrograph*

Figure 50 and Figure 51 shows optical micrographs from sample heat treated at 1380˚C, with subsequent water quenching.

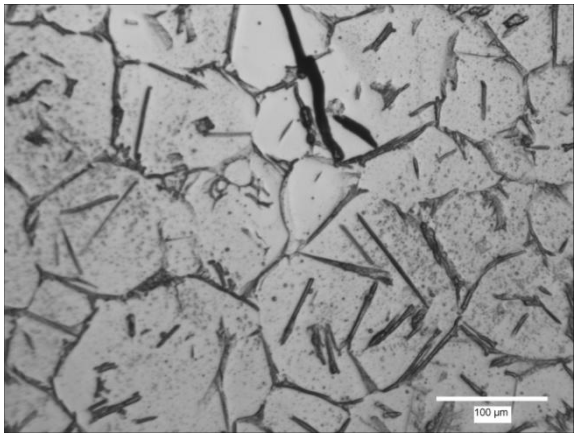


**Figure 50** *Center of the water quenched bar, optical micrograph*

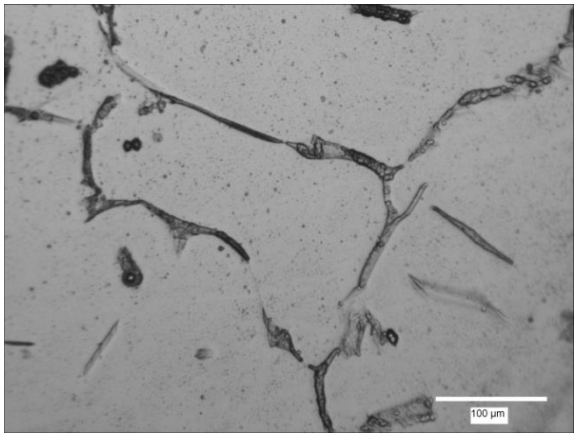


**Figure 51** *Edge of the water quenched bar, optical micrograph*

The effect of different cooling rates can clearly be seen in the figures above. With furnace cooling after heat treating in the α field a fully lamellar structure is obtained. No clear differences, such as grain growth or coarsening of interlamellar spacing, between the center and the edge of the bar can be seen by looking at the pictures.

After air cooling a difference between the center and the edge can be seen. At the edge a fully lamellar structure with some Widmanstätten needles present can be observed, which is not the case for the center of the bar. The center consists of more irregular shaped grains with a structure that appears to contain lamellas.

A different structure, only revealing the grain boundaries, is seen after water quenching. The microstructure consists of massively transformed single phased γ. As there is no difference in microstructure the only difference that can be observed between the center and the edge is the difference in grain size.

When the time at 1380˚C is increased to two hours with subsequent water quenched no significant change in structure is observed, Figure 52. However, growth of the grain size can be spotted both at the center and edges of the sample.

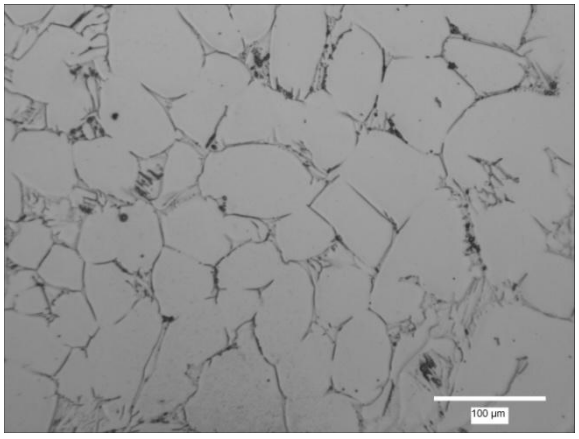


**Figure 52** *Center of the water quenched bar, held in 1380℃ for 2h, optical micrograph*

Investigation of air cooled and water quenched material with the aid of SEM reveals more details and other features of the structures. In Figure 53 the center of the air cooled bar is seen, revealing no clear lamella structure. A similar structure is seen in water quenched material, a single phased γ-structure.

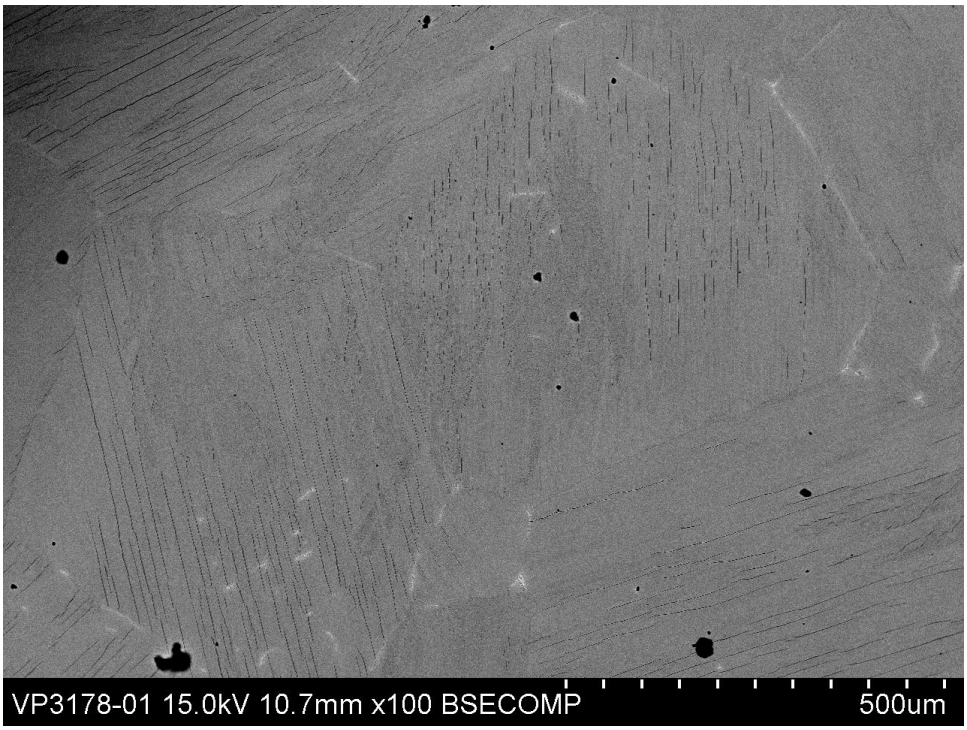


**Figure 53** *The center of air cooled bar, SEM picture*

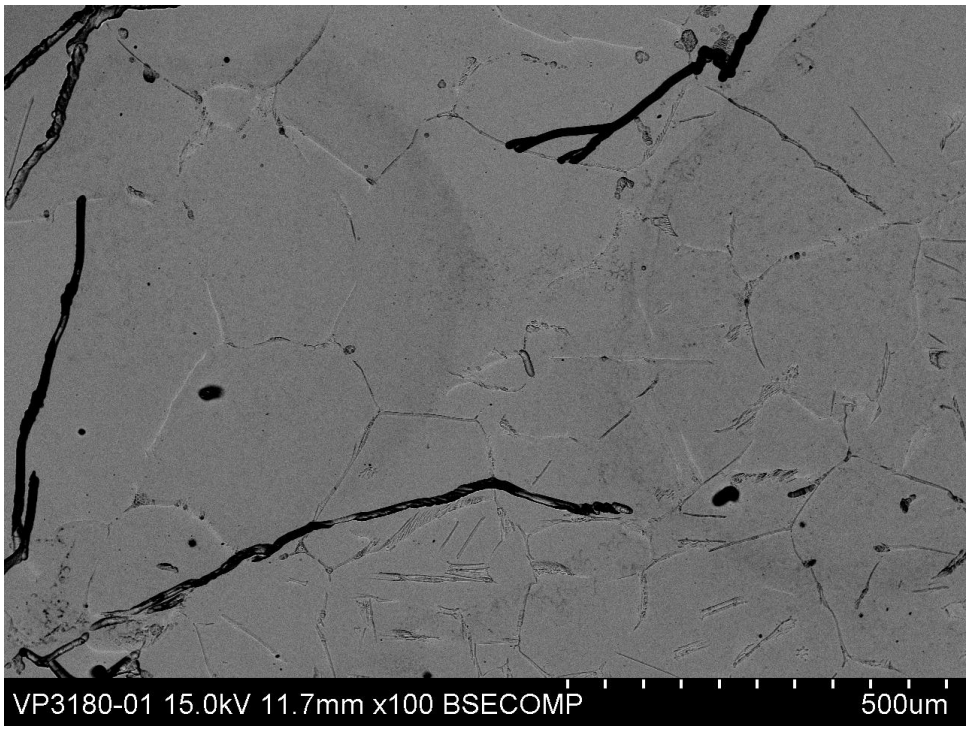


**Figure 54** *The center of water quenched bar, SEM picture*

EDX analysis, Table 10, made on an area of both air cooled and water quenched material shows similarities in chemical composition. From the EDX it can be seen that the phase created in the center of the bar in both air cooled and water quenched material is single phase γ.

**Table 10** *EDX analyze of air cooled and water quenched material*

| Elements [at.%] | Ti | Al | Nb | Cr |
|---|---|---|---|---|
| **Water quenched** | 49.8 | 46.1 | 2.3 | 1.7 |
| **Air cooled** | 49.7 | 46.4 | 2.2 | 1.7 |

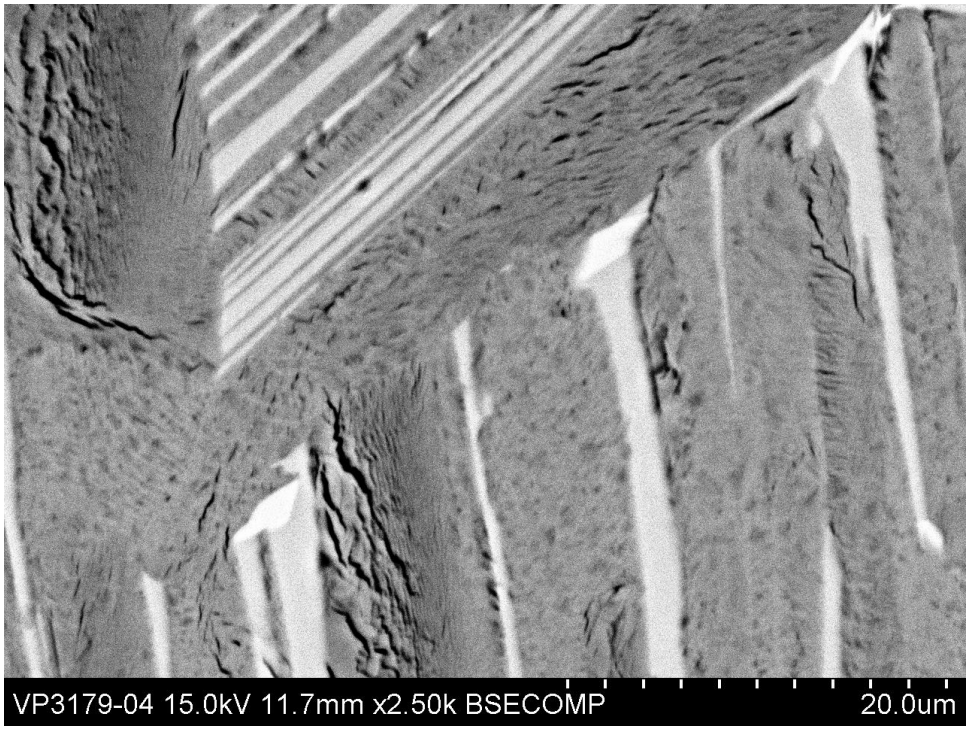


**Figure 55** *The center of the furnace cooled bar, SEM picture*

Study of the furnace cooled material in SEM, Figure 55, reveals a similar lamellar structure, as observed from the optical micrographs. EDX analysis, Table 11, shows that retained β-phase, with segregation of Cr, can be seen as white segregation in the grain boundaries. The light gray phase is $\alpha_2$ and the dark phase is γ in the lamellar structure.

**Table 11** *EDX analyze of furnace cooled material*

| Elements [at.%] | Ti | Al | Nb | Cr |
|---|---|---|---|---|
| **White** | 52.7 | 34.7 | 2.8 | 9.8 |
| **Intermediate gray** | 57.2 | 37.5 | 2.3 | 2.9 |
| **Dark gray** | 47.9 | 48.1 | 2.6 | 1.4 |

### 10.3.3 Creation of duplex structure

Figure 56 shows an optical micrograph of sample heat treated at 1380°C, water quenched followed by a second heat treatment at 1250°C for 0.5 h with subsequent air cooling.

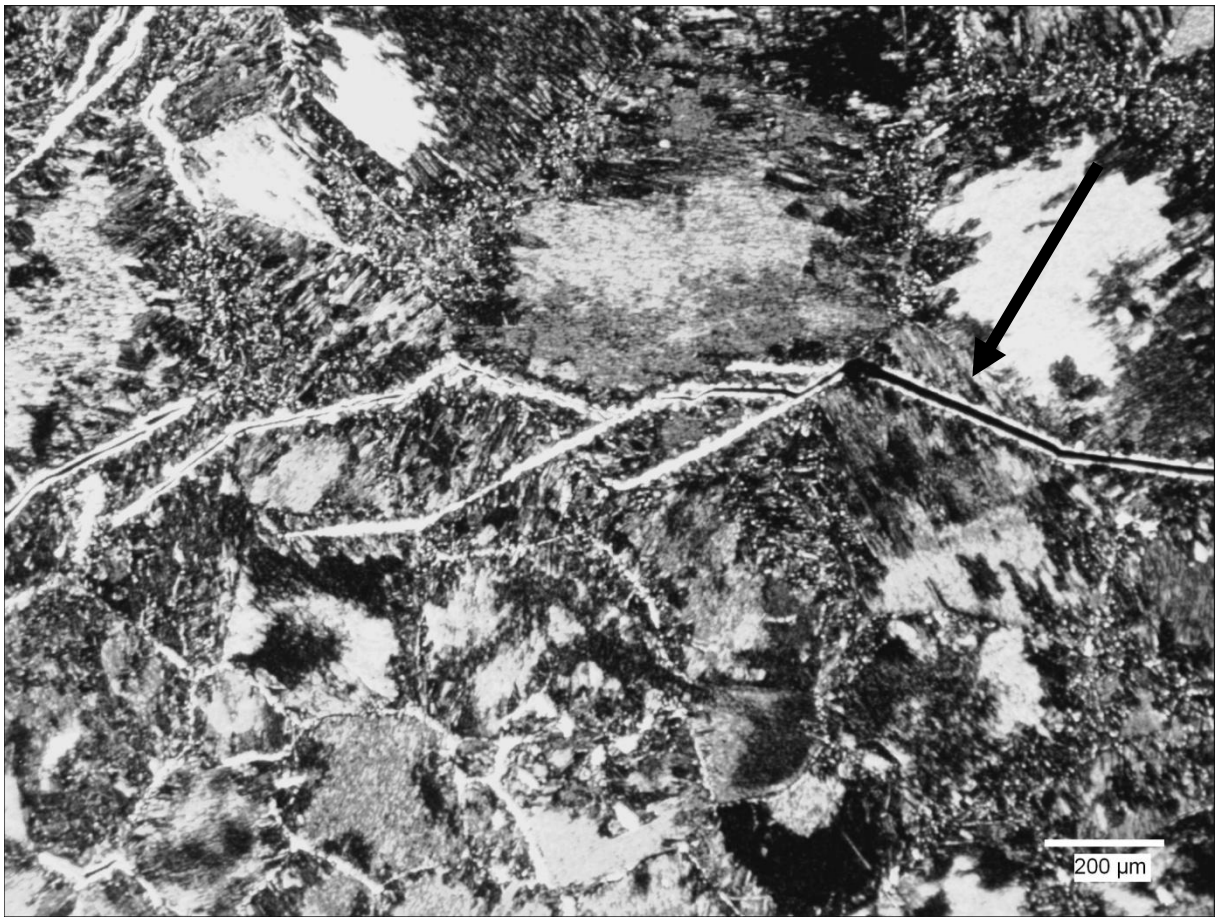


**Figure 56** *Crack in water quenched material*

In Figure 56 a large crack across the picture can be observed, marked with an arrow. As the material was further investigated multiple cracks in the same size was found. Therefore no further investigation was made on the sample heat treated at 1380°C followed by water quenching and second heat treatment at 1250°C.

Figure 57 through Figure 62 shows optical micrographs of samples heat treated at 1380°C, air cooled followed by a second heat treatment at 1250°C for 0.5, 1 and 1.5 h with subsequent air cooling.

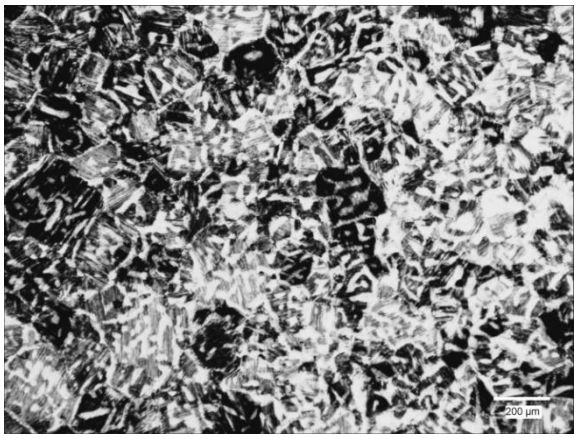


**Figure 57** *Center of bar air cooled from 1380℃ with subsequent treatment at 1250℃ for 0.5 h, optical micrograph*


**Figure 58** *Edge of bar air cooled from 1380°C with subsequent treatment at 1250°C for 0.5 h, optical micrograph*

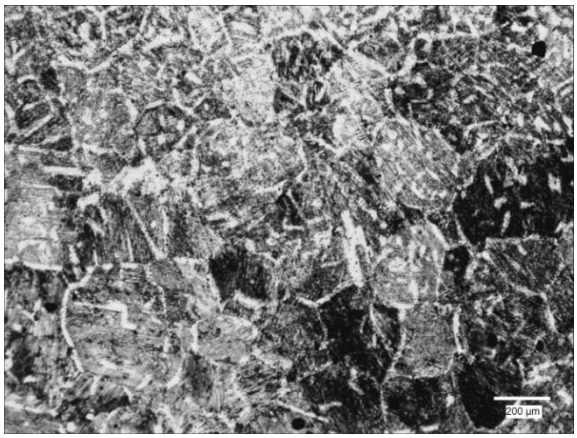


**Figure 59** *Center of bar air cooled from 1380°C with subsequent treatment at 1250°C for 1 h, optical micrograph*

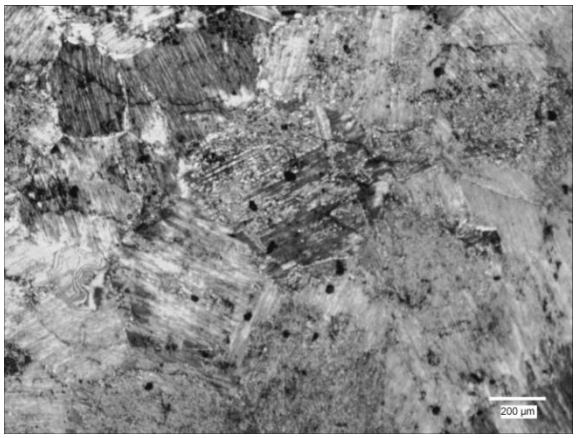


**Figure 60** *Edge of bar air cooled from 1380°C with subsequent treatment at 1250°C for 1 h, optical micrograph*

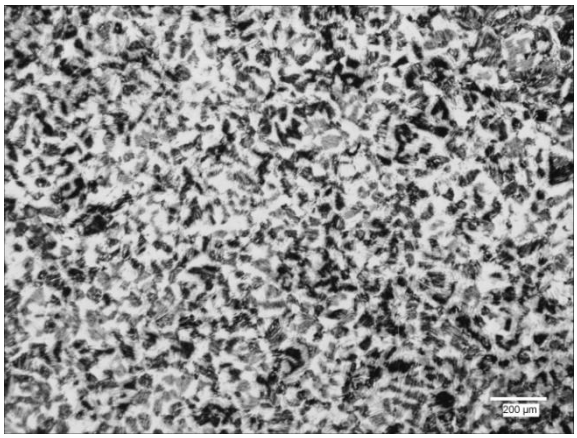


**Figure 61** *Center of bar air cooled from 1380°C with subsequent treatment at 1250°C for 1.5 h, optical micrograph*

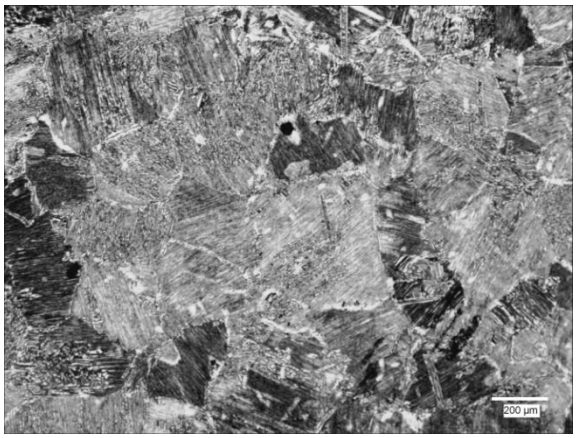


**Figure 62** *Edge of bar air cooled from 1380°C with subsequent treatment at 1250°C for 1.5 h, optical micrograph*

In all of the three samples the center is observed to be of a pseudo-duplex structure as can be seen in Figure 57, 65 and 67. The pseudo-duplex is recognized by the lack of clear grain boundaries which can be observed in all samples. For the sample treated at 1.5 h the amount of the bright phase is increased.

At the edges of all the samples, Figure 58, 66 and 68, lamella grains with a larger size is observed. For the sample held at 1250°C for 0.5 h a large amount of, what must be, retained α or β phase is observed within the grain boundaries. The black dots in Figure 60 are considered to be dirt.

## 10.4 Micro hardness

Micro hardness was used as a comparative method between the different heat treatments investigated, and thereby the different microstructures. From the hardness values across the sample the mean value of each sample was calculated for comparison. The graphs showing the micro hardness across the sample is seen in Figure 63.

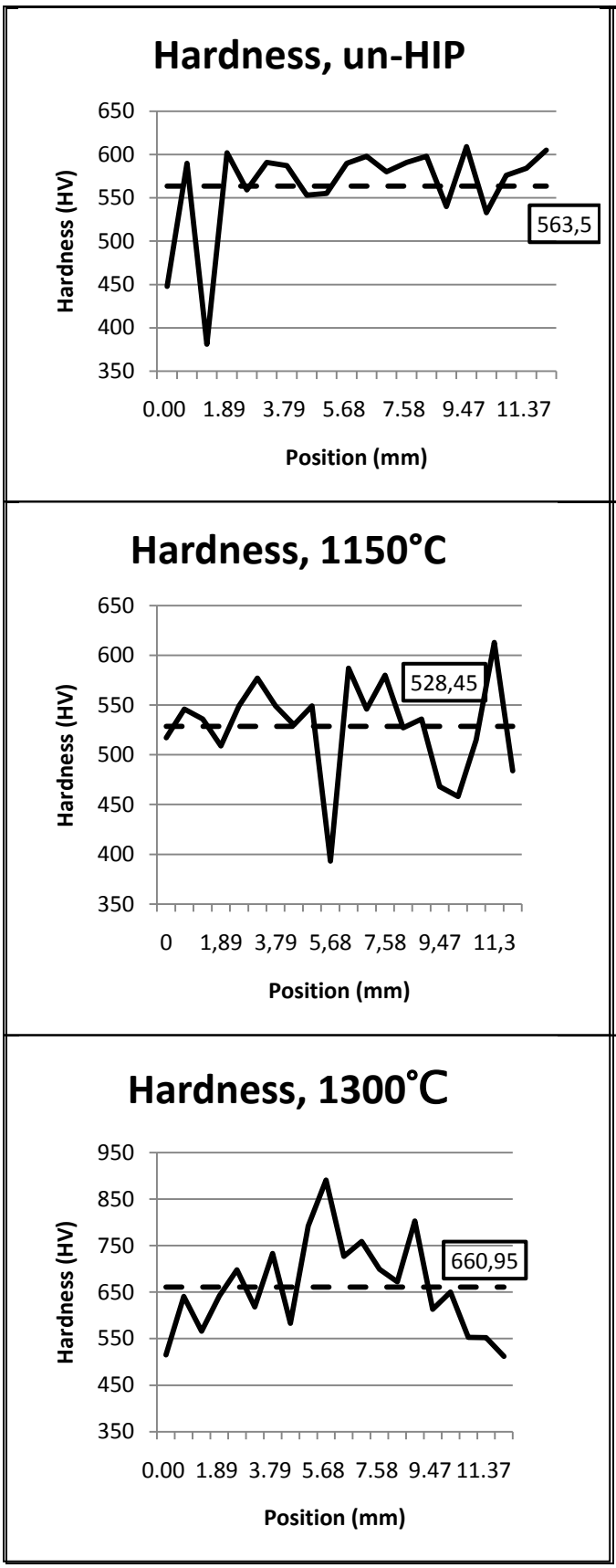
Hardness, un-HIP
Hardness (HV)
650
600
550
500
450
400
350
563,5
0.00 1.89 3.79 5.68 7.58 9.47 11.37
Position (mm)
Hardness, HIP
Hardness (HV)
600
550
500
450
400
350
527,1
0.00 1.89 3.79 5.68 7.58 9.47 11.37
Position (mm)
Hardness, 1150°C
Hardness (HV)
650
600
550
500
450
400
350
528,45
0 1,89 3,79 5,68 7,58 9,47 11,3
Position (mm)
Hardness, 1250°C
Hardness (HV)
750
700
650
600
550
500
450
400
350
564,7
0.00 1.89 3.79 5.68 7.58 9.47 11.37
Position (mm)
Hardness, 1300°C
Hardness (HV)
950
850
750
650
550
450
350
660,95
0.00 1.89 3.79 5.68 7.58 9.47 11.37
Position (mm)

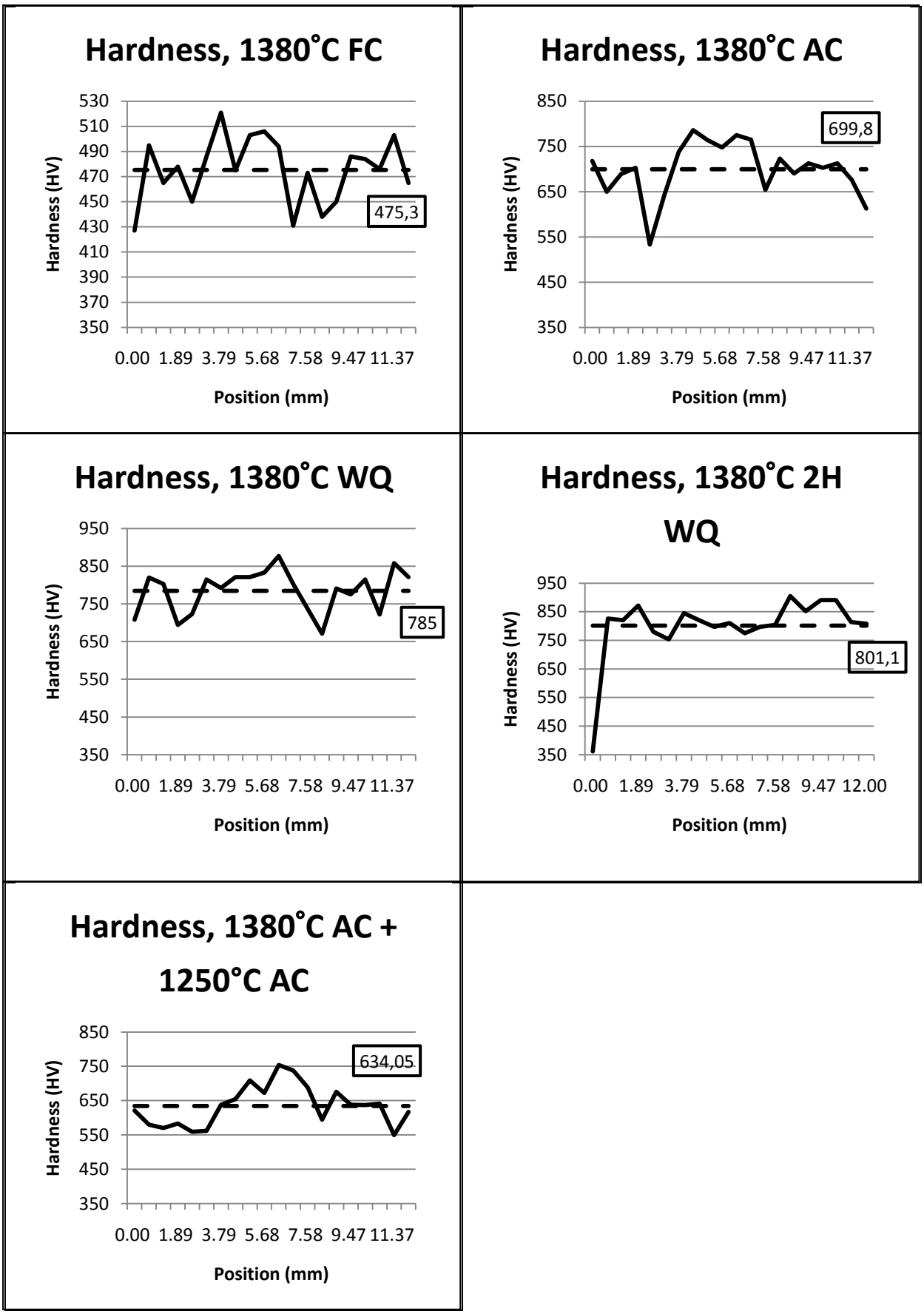


**Figure 63** *Hardness value for different heat treatments across the samples, mean value printed in the graph and as a dotted line*

## 10.5 Grain size measurement

The grain size distribution was done according to ASTM E 1181-02 and the grain size measurements of homogeneous areas were done according to ASTM E 112-96. The result of the measurement is seen in Table 12.

**Table 12** *Grain size measurement on un-HIPed, HIPed and heat treated material*

| Heat Treatment | ASTM Condition | Average grain size diameter (μm) |
|---|---|---|
| **As-built** | Duplex, Biomodal, 11.1% ASTM No 6.7, 88.9% ASTM No 11.3 | Larger grain: 39.1<br>Smaller grain: 8.0 |
| **As-HIP** | Duplex, Biomodal, 6.7% ASTM No 6.2, 93.3% ASTM No 10.6 | Larger grain: 49.7<br>Smaller grain: 10.5 |
| **HIP+ HT 1250°C** | Duplex, Biomodal, 9.9% ASTM No 7.9, 90.1% ASTM No 10.4 | Larger grain: 27.8<br>Smaller grain: 11.1 |
| **HIP+ HT 1300°C** | Duplex, Cross-Section, ASTM No 9.0 at center, ASTM No 0.5 1.34 mm deep from surface | Larger grain: 336.7<br>Smaller grain: 18.0 |
| **HIP+ HT 1380°C** | Duplex, Cross-Section, ASTM No 5.3 at center, ASTM No 0.2 5.7 mm deep from surface | Larger grain: 380.4<br>Smaller grain: 65.5 |
| **HIP+ HT 1380°C+ 1250°C** | Duplex, Cross-Section, ASTM No 6.6 at center, ASTM No 0.2 4.14 mm deep from surface | Larger grain: 384.8<br>Smaller grain: 41.2 |

The rapid increase of grain size measured and shown in Table 12 after heat treatment at 1300˚C and further heat treatment can be closely related to microstructural changes. For the Biomodal case of duplex grain size the large grains are observed as local areas randomly distributed in the microstructure. These larger grains are shown in Figure 23 and appear to be different, in structure, from the matrix with smaller grains. These areas of randomly larger grain are not observed in material heat treated over 1300°C. They have been dissolved and the larger grains measured constitute of grains with similar microstructure as the small ones, distributed at a homogeneous band at the circumference of the sample.

## 10.6 Tensile tests

The table and graphs below shows the result from the performed tensile tests. The mean value of the tests performed in room temperature is presented in Table 13. In Figure 64 and Figure 65 the stress-strain curves of the different conditions are shown, each test are shown separately. Figure 64 shows the as-built and as-HIPed conditions and Figure 65 shows the results for the heat treated sample.

**Table 13** *Tensile test of as-built, as-HIPed and three heat treated material*

| Specimen condition | Stress at peak [MPa] | Young's Modulus [GPa] | Plastic Elongation at Break [%] |
|---|---|---|---|
| **As-built** | 337.843 | 261.518 | 0.182 |
| **As-HIP** | 639.742 | 152.213 | 1.246 |
| **HIP+ HT 1250°C** | 616.874 | 173.575 | 1.117 |
| **HIP+ HT 1300°C** | 346.324 | 116.659 | 0.306 |
| **HIP+ HT 1380°C+ 1250°C** | 497.353 | 128.415 | 0.722 |

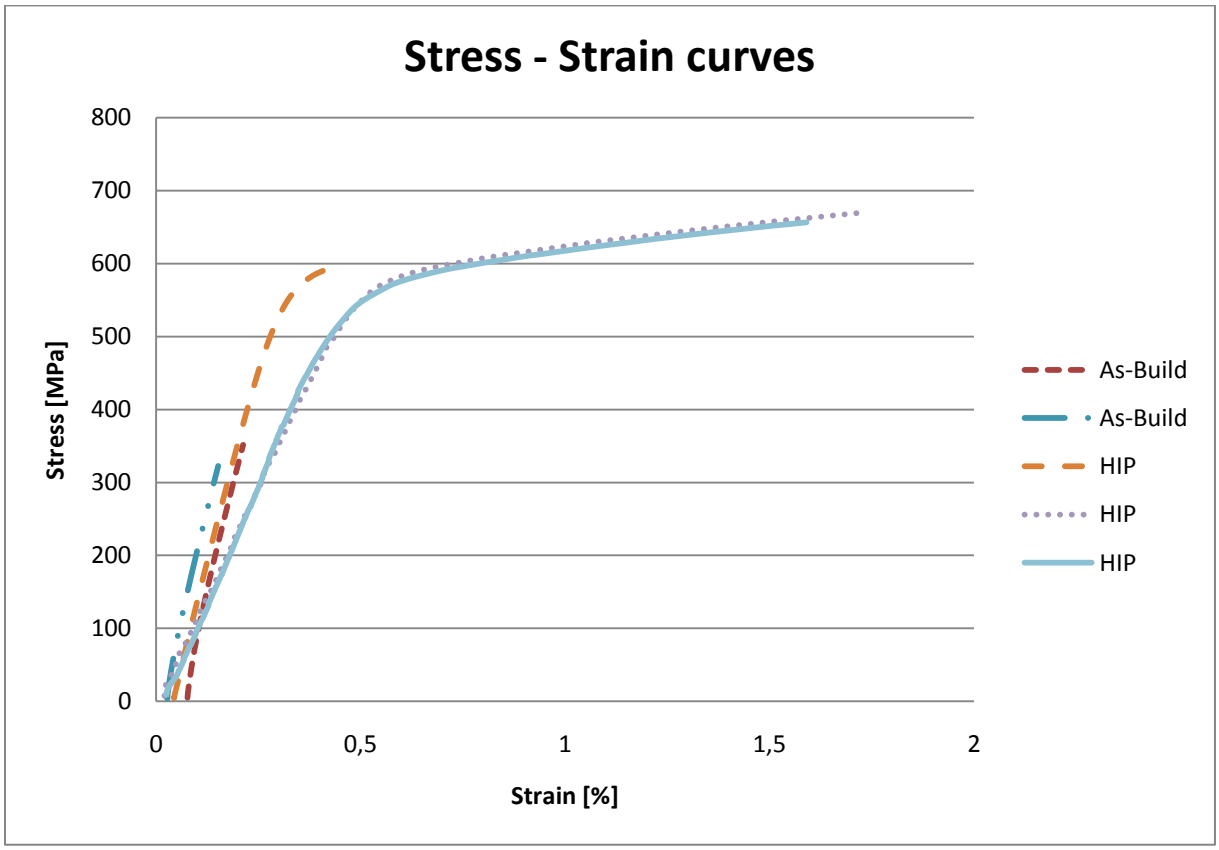


**Figure 64** *Stress – Strain curves for As-built and As-HIPed conditions*

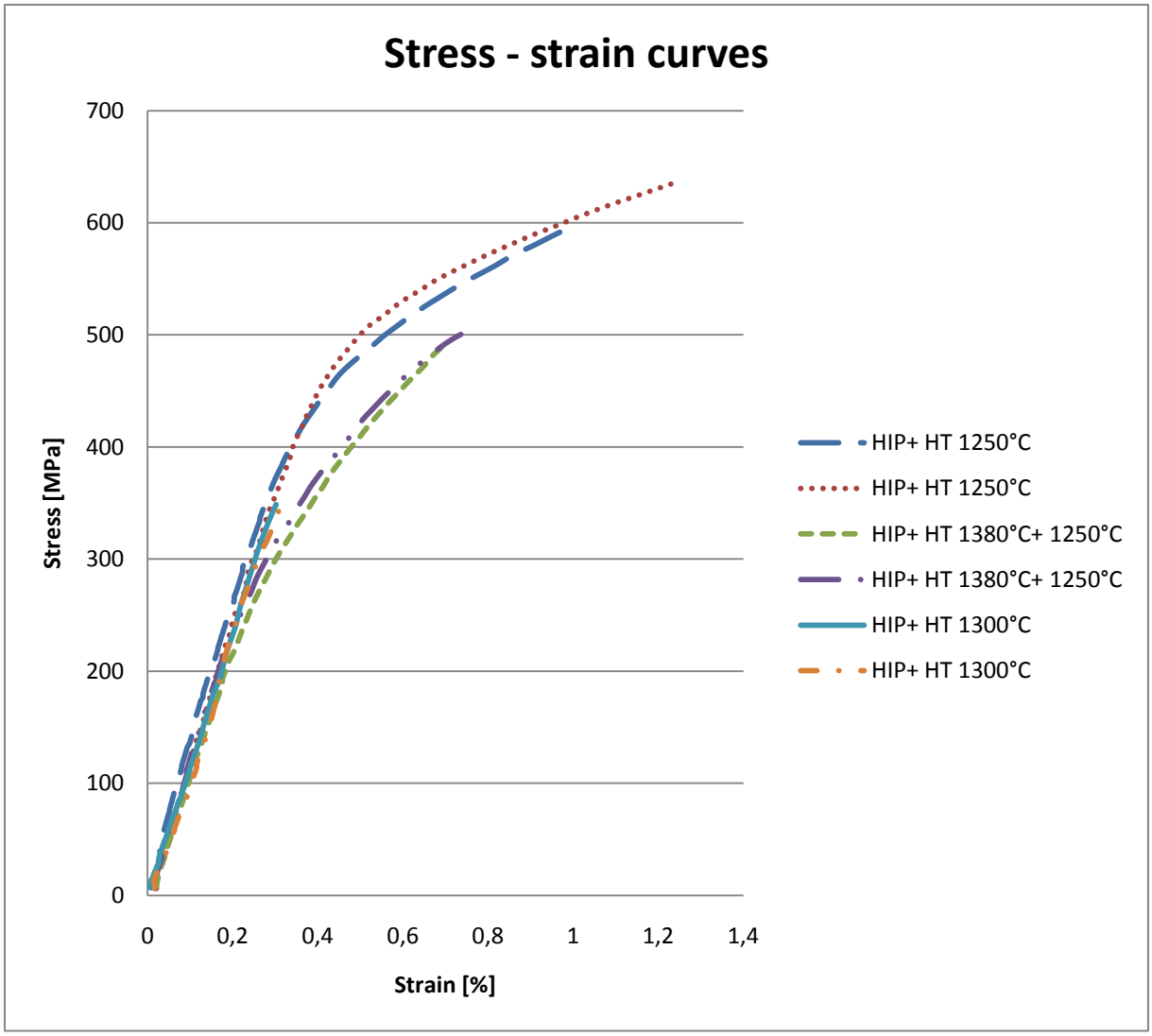


**Figure 65** *Stress – Strain curves for heat treated conditions*

From the results from the tensile tests above it is clearly seen that the ductility in each sample is quite limited, however some treatments result in certain microstructure reveals better ductility than others. From Table 13 it can be seen that the best ductility is achieved by the as-HIPed sample, without any subsequent heat treatment. The as-HIPed sample also experiences the highest UTS. The highest Young's modulus is seen for the as-built sample, however, as expected, it suffers from severe brittleness. The as-HIPed sample has ductility values of 1.73%, as a maximum, however, as can be seen in Figure 64, one result is slighter lower than the other ones, which lowers the mean value.

In Figure 65 the different heat treatments could be compared, it is seen that the variation between the two samples tested for each treatment is small. The best result is achieved for the sample heat treated in 1250°C, which has the duplex microstructure and is most similar to the as-HIPed microstructure. The sample heat treated two times, containing the pseudo-duplex microstructure, also experience some ductility.

In Figure 66 the increase of the ductility as the temperature increases for as-HIPed sample is shown. The variation of the UTS with the temperature is seen in Figure 67.

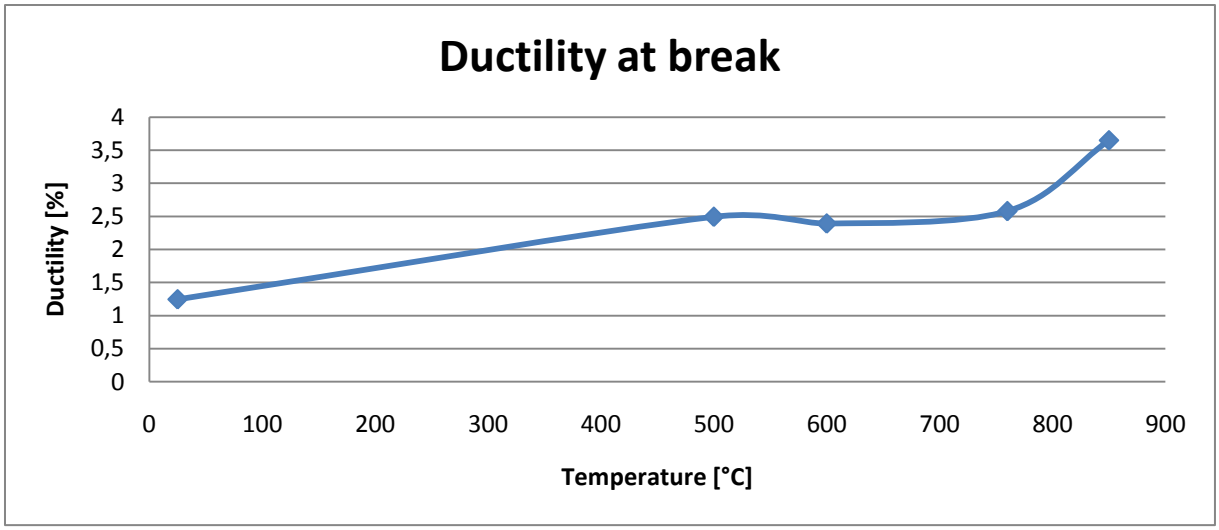


**Figure 66** *Ductility at break vs temperature*

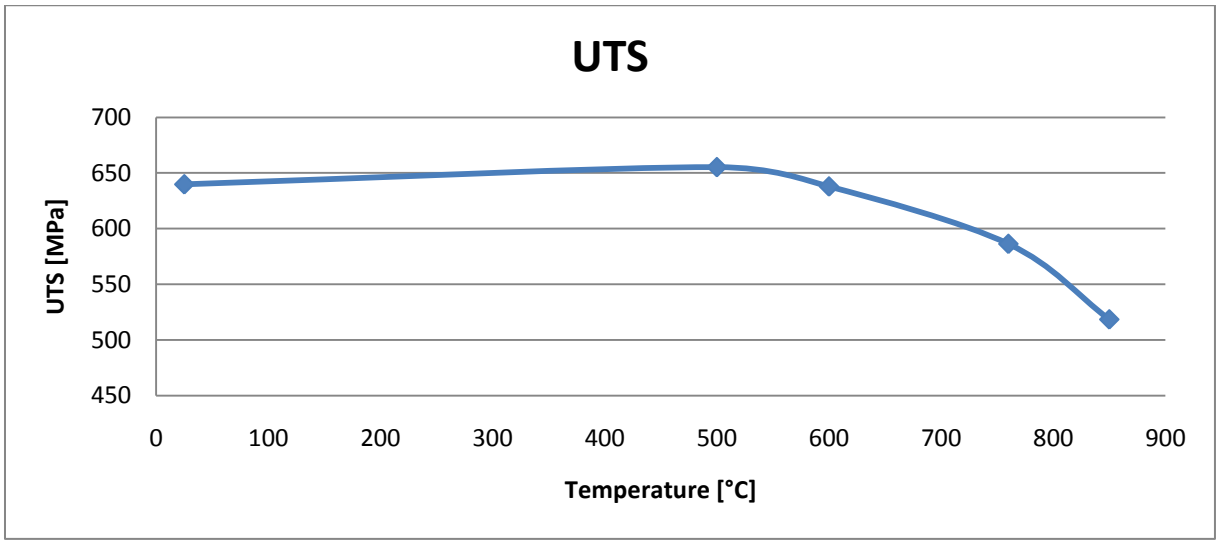


**Figure 67** *UTS vs temperature*

From the figures it is clearly seen that the ductility increases with the temperature as the UTS goes down. The UTS experience a drop after around 500°C. This drop in UTS and the increase in ductility are related to the brittle-to-ductile transformation temperature, where the slip mode system is changed, allowing for more movement inside the crystal structure.

# 11 Discussion

The grains in the EBM manufactured material are very small due to the special feature of the EBM process. The area of the melt pool is small, down to ~0.1 mm in diameter, and the nucleation of new grains is high as the powder is melted. As the beam moves away fast from the melted material the time for diffusion and grain growth is small. The cooling rate applied in the area is fast enough to prevent grain growth in the solidifying material due to the small melt pool.

The heterogeneity seen in the as-built specimen, Figure 25, is closely related to the process parameters used in the EBM machine. The surface is melted using smaller and smaller circles, starting from the outside towards the center, with the same energy input. The beam is coming back to an adjacent area faster compared to when the scanning line is longer, implying a buildup of heat in the inner circles. The heat built up in the center creates a lower cooling rate in the center compared to the fringe of the bar. The slower cooling rate increase the propensity to create lamellas in the center and a higher density of lamellas can be observed in the center of the bar. At the edges of the as-built bar the cooling rate is faster, since the time is longer before the melting spot returns to adjacent areas. Faster cooling rate implies for more equiaxed γ-grains, however it is observed that the cooling rate is not fast enough to completely avoid formation of lamellar grains.

Inhomogeneities on a microscale can also be associated with compositional differences. Studies show (39), (8) that the microstructure in TiAl is sensible to composition, especially the Al concentration. From the chemical analysis performed it can be seen that some Al is evaporated during the process and if this is done heterogeneously this can lead to microstructural differences. Research done previously by Cormier et al (61), (12) also report evaporation of Al from the material manufactured by EBM. However Cormier et al experiences a higher level of evaporation, between 6.1% and 7.5%, compared with evaporation level of this study. The evaporation level can to some extent be associated with process parameters used in the machine.

The as-built material was HIPed to reduce the pores and homogenize the microstructure. It is considered that pores with a size larger than 10 µm is too large to be used in aerospace applications due to the concentrated stress fields created around the pore. Comparison of the two pictures showing the porosity after the two HIP cycles, Figure 28 and Figure 29, clearly shows that the HIP cycle at 1200°C will remove the pores as no considerable amount of pores can be seen. The HIP cycle at 1200°C is therefore considered to be sufficient to remove the pores in TiAl samples manufactured by EBM. From the results it can also be seen that the material will become more homogeneous compared to the as-built. This is because the pressure and temperature will help to alter the microstructure. However, the time is not sufficient to create a fully homogeneous material. Even though the HIP process is done in order to remove porosity and in some way homogenizes the microstructure, it is important to avoid excessive grain growth. At 1200°C no excessive grain growth can be seen and the grains after HIP are still very small. . This is a temperature lower than reported by GE (57) and is due to the small grain size in the EBM as-built material.

As shown in the Phase ID picture, Figure 34, it is clear that the material is constructed by two phases. As the OIM software can identify both FCT/BCC and HCP phases and both are seen it can clearly be stated that the material consists of two different phases.

From Figure 36 the different orientation of the areas shown in the BSE image, Figure 33, can be seen. As the software cannot index the information as $Ti_3Al$, only TiAl, the picture does not show the structure inside the grains. However, it is believed that the needle like structures with different orientation (color) are γ-lamellas. As lamellas are observed from the optical microscope and SEM as well, this should be a right presumption. The FIB-SEM/EBSD analysis is consequently a proof that the grain size after the HIP is small and consists of equiaxed grains with some lamellas.

From theory it is found that a duplex structure of Ti-48Al-2Cr-2Nb will contain γ grains and $\alpha_2/\gamma$ lamellas with some $\alpha_2$ and β present at grain boundaries and triple points. The SEM micrograph of the as-HIPed material, Figure 31, however shows large amounts of $\alpha_2$ within the material. This is confirmed by the EDX analysis where the Al content is seen to be low. The reason for the excessive formation of $\alpha_2$ is believed to be local variation in composition from the original 48-2-2 composition. When the composition is altered with leaner composition of Al the formation of $\alpha_2$ is more likely as the composition moves towards the single $\alpha/\alpha_2$ phase in the phase diagram.

The formation of β is clearly observed from the EDX-mapping, Figure 27, where the Cr is seen to be enriched in some small areas. As Cr stabilizes the β phase it can be concluded that these areas are β phase. Due to compositional variations, as discussed above, and differences in cooling rate β will only form in areas containing the right amount of Cr and with a sufficient cooling rate. The β phase can in adequate amounts be favorable as it is a high temperature phase pinning the grain boundaries and hinders grain growth in both ambient and high temperatures. However it can lower some mechanical properties as the β phase will hinder slip plane movements.

Previously studies from Stoloff et al. (21) and others have shown that an optimal trade-off between ductility and strength is obtained if the material has a lamellar amount of around 30%. In the EBM as-built and as-HIPed material it is observed that the material holds a larger amount of lamellas than the desired 30%. By heat treatment in the single phase region it is possible to reset the microstructure and rebuild the desired amount of lamellas. However it has also been reported by Wang et al. (26) that a small sized fully lamellar structure will give excellent mechanical properties. By heat treating in the α+γ it is possible to receive a lamellar structure. To create a fully lamellar structure the material was heat treated through different cycles.

At 1150°C the diffusion rate is slower compared to the rate at 1250°C, which will cause differences in resulting microstructure. In the material heat treated in 1150°C some thickening of the interlamella spacing is observed. This is believed to arise from the long holding time of 5 hours where discontinuous coarsening appearing as slow diffusion enables single atoms to attach the broad side of the lamellas making them thicker. The high amount of γ and $\alpha_2$ grains hinders the lamellas to grow longer in the sample heat treated in 1150°C. For the sample treated at 1250°C the lamella colonies are able to grow longer as the diffusion rate is higher. The γ and $\alpha_2$ grain boundaries are dissolved as the lamellas grow longer. This is due to the so called terrace-ledge-kink mechanism, where the lamellas grow longer, as the diffusion of the atoms to the lamella edge is faster compared to the sample treated at 1150°C.

In the material heat treated in 1300°C for 1 hour a fully lamellar structure is obtained. At this high temperature the diffusion rate is higher and the possibility for terrace-ledge-kink mechanism (64) where the atoms grow on the moving ledge of the lamella is more likely. Due to the high

temperature the grains will grow where the larger grains will survive according to the Gibbs-Thomson effect. For the sample heat treated at this temperature smaller grains are observed around the perimeter of the bar. This is due to the diffusion of oxygen during heat treatment as the oxygen will stabilize the α phase and hinder further growth (65).

In SEM pictures presented in the result microcracks are observed in the γ-phase. They are believed to rise from the chemical polishing performed during preparation of the sample. Ahlström (66) has also reported that chemical polishing introduces such micro cracks in TiAl.

The samples heat treated at 1380°C is within the single α phase at this temperature. With the different cooling rates applied the resulting microstructure did turn out according to theory. For the sample air cooled from 1380°C some stripes is observed within the SEM micrographs, Figure 53. According to literature the resulting microstructure is supposed to be single phased with Widmanstätten needles. The lamellar-like structure is believed to be lamellas fully dissolved with compositional differences in the single phase material and the remains are seen as stripes in the microstructure. As the same sample is etched and analyzed with optical microscope, Figure 48, the same lamellar like structure is observed. Here it is concluded that the etchant definitely etch the compositional differences creating a lamellar like structure. From Baselack III et al (67) it is reported that highly aggressive etchant can etch non-existing lamellas within a single phase structure which is believed to be the case for the air cooled sample.

The microstructure observed after heat treatment first at 1380°C air cooling, followed by subsequent heat treatment at 1250°C is of a so called pseudo duplex microstructure which is reported by Lundström (23) and Lapin et al (68) for different alloys. Due to the compositional differences remaining after air cooling from 1380°C, lamellas will easily be formed according to the previous compositional difference where long range diffusion is not necessary. With the compositional differences spread over grain boundaries lamellas are created over the grain boundaries in a randomly pattern. As lamellas grow over the grain boundaries they will create diffuse boundaries as they will start and stop within equiaxed grains.

For the microstructure obtained from the water cooled sample from 1380°C large cracks are observed at a macro structural level. These cracks arise due to the high cooling rate as the sample is cooled fast. Due to the high ordering taking place during the phase transformation as the sample cools, cracks will develop as internal stresses are built up as the sufficient ordering cannot take place.

From the different heat treatment cycles it can be seen that when the heat treatment temperature is increased the fraction of lamellas increases. However, it can be seen that there is a change in diffusion and creation rate of the lamellas between 1250°C and 1300°C since the obtained microstructure after 1 h is different. Comparing 1150°C and 1250°C it can be seen that the time at these temperatures do not affect the out coming microstructure more than coarsening. The cooling rate applied to the material is proven to be important for the designing of the heat treatment path as it is shown to severely affect the resulting microstructure.

In the EBM process, the cooling rate is also shown to be important in the process as it alters the as-built microstructure. The cooling rate in the machine can to some extent be tailored by changing the process parameters. As the as-built microstructure is more optimal regarding lamella content in the

edges of the bar than in the center it is shown that a desired microstructure can be optioned directly from the machine, without need for post-heat treatments. The most important change is believed to be to alter the melting strategy to make the cooling rate more constant over the whole cross section. All through, by more investigation of how the process parameters affect the nucleation- and cooling rate of the material and thereby the microstructure. There is potential for the process to be tailored to create optimal microstructure directly from the machine, needing only HIP as post-manufacturing treatment. As the best result of the ductility is achieved for the as-HIPed, with no subsequent heat treatment, it should be proven to be possible to enhance the process parameters to achieve the desired microstructure directly after HIP.

Together with the process parameters the chemical content of the powder is also important for the resulting microstructure and especially the Al concentration. A material with Al concentration in the lower regime of the limit for the alloy will be closer to the single phase $\alpha_2$-area and more $\alpha_2$ is created as can be seen in the studied material. The transition in the two-phase field when the Al concentration is lower is stated by Murr et al (3) as well. As an equiaxed γ-material is desired, the starting powder of the EBM-process would preferable has Al-concentration in the higher regime of the alloy specification.

Liu et al. (54) show an increase in tensile ductility when the grain size decreases. EBM manufactured material shows a very small grain size, magnitudes lower compared to conventional manufacturing methods. Kóscielna (44) states that cast material have an average distribution of grain size between 1200±625 µm and Westbrook & Fleischer (8) present a grain size of ~250 µm for wrought material. These larger grain sizes can be compared to 8 µm of as-built EBM material and 10.5 µm of as-HIPed. This small grain size implies that the ductility of EBM TiAl should be superior to parts made by other manufacturing techniques. However, this superior ductility is not really shown in the results from the tensile test. The ductility for the as-HIPed material is in the lower range of the ductility for cast material, which has a ductility of 1-3 % (19), (60). At high temperature (760°C) the ductility of the EBM-manufactures material has a ductility of 2.6 %, compared to 9% for cast material (19), (60). The EBM-manufactured material has a modulus and UTS slightly in the higher range compared to TiAl material produced with conventional manufacturing methods.

It is hard to give a comprehensive explanation over why the sample does not show the expected improvement of ductility compared to samples with larger grains. It is possible that there is some defect or pore in the sample that acts as a crack initiation point and lowers the ductility. As the ductility is quite low in general the material is more sensitive for these kinds of inclusions. Especially for the case of the HIPed sample that shows lower ductility compared to the other two. Analyzing of the fractured surface of the sample has to be performed in further studies in order to reveal the reason for crack. As the yield strength is more closely related to interlamellar spacing (54), this is also something that should be investigated more closely in further studies to be able to increase the UTS and Young's modulus of the EBM-manufactured material.

The low ductility obtained, despite of the small grain size, can also be explained by the enhanced oxygen level. From the chemical analysis it is shown that the oxygen level is higher than the limit for the alloy. Embrittlement of the material by oxygen is also proven by Tönnes et al (55), which show that oxygen level over 1050 ppm severely limits the ductility. In general Ti is sensitive to oxygen and

picks up oxygen easy, which is shown also for conventional Ti alloys (69). The lower ductility can also be explained by the low Al concentration and thereby the high concentration of $\alpha_2$ grains seen in some areas, which stated above could be lowered by close control of the used powder.

Newly made research shows that fully lamella structure with fine grain size can obtain higher ductility and thoughness at ambient temperature than duplex structure (26). This is a contrast to what is previously believed being the microstructural dependency of TiAl, for example what is stated by Westbrock & Fleischer (8) and Recina (25). However, in order to achieve this increase in ductility with fully lamella structure the grain size must be in the magnitude of 10-30 µm, which is very hard to obtain. The small grain size is obtained by complex methods, not appropriate for production purpose. Wang et at. (26) show that it is possible to obtain fully lamella structure with small grain size from cast material by five or more subsequent heat treatments, hot extrusion or hot forging plus heat treatments. Liu et al has reported as high value as 4.7 % of the room-temperature ductility for fully lamellar structures with a grain size of 22 µm. Further Liu et al states that the ductility drops to less than 1% if the grain size is increased to ~600 µm (54). As some grain growth occurs during heat treatment to achieve the lamellar structure in this study the ductility is not so superior. However, the small grain size achieved by EBM machine and the possibility to tailor the process parameters could make EBM attractive for this kind of microstructure, as it makes it possible to process for productional reason, possible to avoid lots of different subsequent processing steps.

As a summary, even though the EBM manufacturing material does not produce the superior ductility or yield strength in this study that is expected, the study still shows that EBM is a feasible way to manufacturing TiAl, and in some case the best alternative. It is shown that the EBM process can be tailored to produce usable parts direct from fabrication with unique properties, as for example the small grain size. The process avoids the negative characteristics of the TiAl material and could in that way make TiAl a feasible material and a material suitable for serial production. The process will be especially feasible for the aerospace industrial market since the product series are small and the variation is big.

# 12 Conclusion

The as-built EBM material, with the process parameters used in this study, will not have an optimal microstructure as it contains too much lamellas. Although by further study of the process parameters it is possible to obtain an optimal microstructure for the desired application. One possible feature, if the process parameters are developed, is to obtain a sufficient duplex structure of the as-built that will have the optimal structure after HIP. HIP is important in the aerospace applications to remove all voids and homogenize the material.

From the results of the two HIP cycles it can be concluded that the HIP cycle at 1200°C, 100 MPa, 4 hours are sufficient to reduce the pores within the EBM built material. The HIP also proved to homogenize the material to some extent.

In this study it is shown that different heat treatments will alter the microstructure of Ti-48Al-2Cr-2Nb. The microstructure is proven to change according to theory for the actual composition as the temperature is raised through the different phases in the phase diagram. By design of a sufficient heat treatment cycle it is possible to obtain any desired microstructure from the EBM-built material.

An advantage with the EBM built material is the small grain size. Compared to other commercial manufacturing processes the grain size is magnitudes smaller in the EBM system. For cast materials the normal grain size is 1200 ± 625 µm and wrought materials have a normal grain size of 250 µm. For the EBM as-built material in this study the average grain size is only 8 µm and 10.5 µm after HIP.

The small grain size in the EBM built material is closely linked to the mechanical properties obtained. Due to the small grain size the ductility is enhanced in both ambient and high temperatures. The small grain size will also enhance the tensile strength of the material both at ambient and high temperatures.

Tensile strength of the EBM built material is concluded to be high compared to conventional manufacturing techniques of TiAl. The UTS for the as-HIPed material is about 100 MPa higher compared to cast TiAl at room temperature. The ductility is however lower than expected and can be concluded to be a result from the higher amount of oxygen in the material used in this study. To further increase the knowledge of the mechanical properties the fracture surfaces has to be investigated.

The EBM system is an excellent way to manufacture different TiAl parts. As the application is manufactured in a near net shape it is possible to produce complex shapes of TiAl materials For example turbine blades for aircraft engines can be produced by EBM, something that is almost impossible with other techniques. When producing in near net shape it is possible to keep the waste from the production to a minimum. Producing in the Arcam EBM system there is a short way from drawing to the actual product is produced, something that will save both time and money as intermediate stages can be left out.

Producing in the Arcam EBM system will give unique microstructural and mechanical features that are superior compared to other techniques. With a small grain size and good mechanical properties the EBM built material will be very suitable for aerospace applications.

# 13 References


1. **ASM International.** ASM Handbook Online - Ordered Intermetallics. C Liu and J.O Stiegler. *Ordered Intermetallics.* 2002.

2. **Leyens, Christoph and Peters, Mafred.** *Titanium and Titanium Alloys.* Weinheim : WILLEY-VCH, 2003.

3. **Murr, L E, et al.** Characterization of titanium aluminide alloy components fabricated by additive manufacturing using electron beam melting. *Acta Materialia.* Mars 2010, pp. 1887-1894.

4. **Matthew, J and Donachie, Jr.** *Titanium - A Technical Guide.* United States of America : ASM International, 2000.

5. **Austin, C M and Kelly, T J.** Development and Implementation Status of Cast Gamma Titanium Aluminide. 1993, pp. 143-149.

6. **Srivastava, D.** Microstructural Characterization of the γ-TiAl alloy Samples Fabricated by Direct Laser Fabrication Rapid Prototype Technique. *Bull. Material Science.* 2002, Vol. 25, 7.

7. **Umeda, H, et al.** Efftects of Al-concentration and lamellar spacing on the room-temperature strength and ductility of PST crystals of TiAl. *Material Science and Engineering.* 1997, pp. 336-343.

8. **Westbrock, Jack Hall and Fleischer, Robert Louis.** *Intermetallic Compounds Principles and Practice - Volume 2 Practice.* West Sussex : John Wiley & Sons Ltd, 1995.

9. **ASM International.** ASM Handbook Online - Titanium Aluminides. C T Liu and J O Stiegler. *Titanium Aluminides.* 2002.

10. **Hu, D, et al.** Heat Treatment of Cast TiAl-based Alloys. *Materials Forum*. 2005, Vol 29

11. **Sabbadini, Salvia, et al.** *Additive Manufacturing of Gamma Titanium Aluminide Parts by Electron Beam Melting.* Seattle, Washington, USA : Washington State Convention Center, 2010. TMS 2010 139th Annual Meeting & Exhibition. February 14-18.

12. **Cormier, Denis, et al.** *Electron Beam Melting of γ-Titanium Aluminide.* Austin, USA : University of Texas, 2005. The 16th Solid Freeform Fabrication Symposium.

13. **Boeing.** Boeing Commercial Airplanes. *Boeing Commercial Airplanes.* [Online] 03 12, 2010. [Cited: 03 12, 2010.] http://www.boeing.com/commercial/.

14. **GE Aviation.** GE Aviation Engines. *GE Aviation Engines.* [Online] 03 12, 2010. [Cited: 03 12, 2010.] http://www.geae.com/engines/index.html.

15. **Nicholas, Cumpsty.** *Jet Propulsion - A Simple Guide to the Aerodynamic and Thermodynamic Design and Performance of Jet Engines .* Cambridge : Cambridge University Press, 2003.

16. **Ashby, Michael F.** *Materials Selection in Mechanical Design.* Amsterdam : Elsevier Butterworth-Heinemann, 2005.

17. **Lundström, D, Karlsson, B and Gustavsson, M.** Anisotropy in thermal transport properties of cast TiAl alloys. *Creep Behaviour of Titanium Aluminides and its Relation to Phase Distributions and Dislocation Structures.* Göteborg : Chalmers University of Technology, 2001.

18. **Elliott, J Richard and Lira, T Carl.** *Introductory Chemical Engineering Thermodynamics.* London : Prentice-Hall Inc., 2001.

19. **Bartolotta, P, et al.** The Use of Cast Ti-48Al-2Cr-2Nb in Jet Engines. *Journal of Material (JOM).* 1997, pp. 48-50, 76.

20. **Bartolotta, Paul A and Krause, David L.** *Titanium Aluminide Applications in the High Speed Civil Transport.* Cleveland, Ohio : Glenn Research Center, 1999.

21. **Stoloff, Norman S and Sikka, Vinod K.** *Physical Metallurgy and Processing of Intermetallic Compounds.* New York : Chapman & Hall, 1996.

22. **Mohammadi, Amirahmad.** *Thermal stability of γ-TiAl intermetallics for Industrial Turbines.* Göteborg : Diploma thesis, Chalmers University of Technology, 2009.

23. **Lundström, Dennis.** *Creep Behaviour of Titanium Aluminides and its Relation to Phase Distributions and Dislocation Structures.* Göteborg : Doctoral thesis, Chalmers University of Technology, 2001.

24. **Cupid, M Damian.** *Thermodynamic Assessment of the Ti-Al-Nb, Ti-Al-Cr and Ti-Al-Mo Systems.* Gainesville : University of Florida, 2009.

25. **Recina, Viktor.** *Mechanical Properties of Gamma Titanium Aluminides.* Göteborg : Chalmers University of Technology, 2000.

26. **Wang, J N, et al.** On the grain size refinement of TiAl alloys by cyclic heat treatment. *Materials Science and Engineering.* 2002, pp. 118-123.

27. **Lapin, J and Nazmy, M.** Microstructure and Creep Properties of a Cast Intermetallic Ti-46Al-2W-0.5Si Alloy for Gas Turbine Applications. *Materials Science and Engineering.* 2004, Vol. A 380, pp. 298-307.

28. **Porter, A David, Easterling, E Kenneth and Sherif, Y Mohamed.** *Phase Transformation In Metals and Alloys.* Boca Raton : CRC Press, Tayler & Francis Group, 2009.

29. **Yamaguchi, M and Inui, H.** *TiAl Compounds for Structural Applications.* Champion PA, USA : TMS, 1993. Proceedings of First International Symposium on Structural Intermetallics. pp. 127-142.

30. **Jeon, J H, et al.** Recrystallization in Cast 45-2-2 XD Titanium Aluminide During Hot Isostatic Pressing. *Materials Science Engineering.* 1999, Vol. A271, pp. 128-133.

31. **Mussman, Steven.** AzoMaterials, A to Z of Materials. *Hot Isostatic Pressing.* [Online] 09 28, 2001. [Cited: 04 07, 2010.] http://www.azom.com/Details.asp?ArticleID=924.

32. **Fuchs, E G.** Homogenization and Hot Working of Ti-48Al-2Nb-2Cr Alloys. R Darolia, et al. *Strucutal Intermetallics.* Champion, Pennsylvania : The Minerals, Metals Materials Society, 1993, pp. 195 - 203.

33. **Ramanujan, R V.** Phase Transformations in γ Based Titanium Aluminides. *Internationall Material Reviews.* 2000, Vol. 45, pp. 217-239.

34. **Schaeffer, R J and Janowski, G M.** Phase Transformation Effects During HIP of TiAl. *Acta Metall and Materials.* 1992, Vol. 40, 7, p. 1645.1651.

35. **Herzig, Chr, et al.** Titanium Tracer Diffusion in Grain Boundaries of α-Ti, α2-Ti3Al and.α2-TiAl and in α2/γ Interphase Boundaries. *Intermetallics.* 2001, Vol. 9, pp. 431-442.

36. **Choi, B W, et al.** Densification of Rapidly Solidified Titanium Aluminide Powders -I. Comparison of Experiments to HIPing Models. *Acta Metall Materials.* 1990, pp. 2225-2243.

37. **Habel, U, Yolton, C F and Moll, J H.** Gas atomized γ-Titanium Aluminide based alloys - Processing, microstructure and Mechanical Properties. *The Minerals, Metals & Materials Society.* 1999, pp. 301-308.

38. **Kakitsuji, Atsushi and Miyamoto, Hiroki.** *Synthesis of TiAl Intermetallic Compounds by HIP-Reaction Sintering.* Osaka, Japan : Elsevier Applied Science, 1991. Hot Isostatic Pressing, Theroy and Applications. pp. 293-300.

39. **Habel, Ulrike and McTiernan, Brian J.** HIP Temperature and Properties of a Gas-Atomized γ-Titanium Aluminide Alloy. *Intermetallics.* 2004, Vol. 12, pp. 63-68.

40. **Hu, D and Botten, R R.** Phase Transformations in some TiAl-based alloys. *Intermetallics.* 2002.

41. **A. Bartels, H. Clemens, R. Gerling, V. Güther, S. Kremmer, W.G. Smarsly.** Status of Alloy Development, Production Processes and Application. *MTU Aero Engines.* [Online] 09 10-13, 2007. [Cited: 02 10, 2010.] http://www.mtu.de/en/technologies/engineering_news/development/smarsly_alloy.pdf.

42. **Semiatin, S L, et al.** Phase Transformation Behavior of Gamma Titanium Aluminide Alloys during Supertransus Heat Treatment. *Metallurgical and Materials Transactions.* 1998, pp. 7-18.

43. **Takeyama, M, et al.** Cooling Rate Dependence of the α/γ Phase Transformation in Titanium Aluminides and Its Applications to Alloy Development. R Darolia, et al. *Structural Intermetallics.* Champion, Pennsylvania : The Minerals, Metals Minerals Society, 1993, pp. 167-176.

44. **Kóscielna, Agnieszka and Szkliniarz, Wojciech.** Effect of Cyclic Heat Treatment Parameters on the Grain Refinement of Ti-48Al-2Cr-2Nb Alloy. *Materials Characterization.* 2009, pp. 1158 - 1162.

45. **Li, Y G and Loretto, M H.** Microstructure Evolution of Ti-48Al-xNb γIntermetallics. *Acta Metall Materials.* 1994, pp. 2009-2017.

46. **Yamabe, Yoko, Takeyama, Masao and Kikuchi, Makoto.** Microstructure Evolution Through Solid-Solid Phase Transformation in Gamma Titanium Aluminides. Young-Won Kim, Richard Wagner and

Masahary Yamaguchi. *Gamma Titanium Aluminides.* Las Vegas, Nevada : The Minerals, Metals & Materials Society, 1995, pp. 111-129.

47. **Srivastava, D, et al.** The Influence of Thermal Processing Route of Some TiAl-based Alloys. *Intermetallics.* 1999, pp. 1107-1112.

48. **Kaufman, M J and Jones, S A.** Phase Equilibria and Transformations in Intermediate Titanium-Aluminum Alloys. *Acta-Metall Materials.* 1993, pp. 387-398.

49. **Charpentier, M, Hazotte, A and Daloz, D.** Lamellar Transformation in Near γ-TiAl Alloys - Quantitative Anylisis of Kinetics and Microstructure. *Materials Science and Engineering.* 2008, Vol. A491, pp. 321-330.

50. **Zan, Xiang, et al.** Strain rate effect on the tensile behaviour of Duplex Ti-46.5Al-2Nb-2Cr intermetallics as elevated temperatures. *Materials Science and Engineering A.* 2008, pp. 296-301.

51. **Inui, H, et al.** Room-temperature Tensile Deformation of Polysynthetically Twinned (PST) Crystals of TiAl. *Acta metall. mater.* Vol. 40 No. 11, 1992, pp. 3095-3104.

52. **ASM International.** ASM International Online - Types of Material Property Charts. M.F. Ashby. *Types of Material Property Charts.* 2002.

53. **Donachie, Mattew J and Donachie, Stephen J.** *Super Alloys - A Technical Guide.* United States of America : ASM INternational, 2002.

54. **Liu, C T, et al.** Tensile Properties and Fracture Toughness of TiAl alloys with Controlled Microstructures. *Intermetallics.* Vol 4 1996, pp. 429-440.

55. **Tönnes, C, et al.** Influence of Microstructure on the Tensile and Creep properties of Titanium Aluminides Processed by Powder Metalurgy. R Darolina, et al. *Structural Intermetallics.* Champion, Pennsylvania : The Minerals, Metals & Materials Society, 1993, pp. 241-245.

56. **Oh, M H, et al.** Environmental effects on the room temperature ductility of Polysynthetically Twinned (PST) crystals of TiAl. *Acta metal mater.* Vol 41 Nr 7, 1993, pp. 1939-1949.

57. **Austin, C M, et al.** Aircraft Engine Applications for Gamma Titanium Aluminide. M V Nathal, et al. *Structural Intermetallics 1997.* s.l. : TMS, 1997, pp. 413-425.

58. **Huang, Shyh-Chin.** Alloying Conciderations in Gamma Based Alloys. R Darolia, et al. *Structural Intermetallics.* Champion, Pennsylvania : The Minerals, Metals Minerals Society, 1993, pp. 299-307.

59. **Hu, D, Huang, A J and Wu, X.** On the Massive Phase Transformation Regime in TiAl Alloys: The Alloying Effect on Massive/Lamellar Competition. *Intermetallics.* 2007, Vol. 15, pp. 327-332.

60. **Weimer, Michael J and Kelly, Thomas J.** *TiAl Alloy 48Al-2Nb-2Cr, Materials Database and Application Status.*

61. **Cormier, Denis, et al.** Freeform Fabrication of Titanium Aluminide via Electron Beam Melting Using Prealloyed and Blended Powders. *Research Letters in Materials Science.* 2007, p. 4 pages.

62. **Cormier, Denis, et al.***Freeform Fabrication of Titanium Aluminide via Electron Beam Melting Using Prealloyed and Blended Powders.* 2007, Research Letters in Materials Science, p. 4 pages.

63. **Arcam AB,** Additive Manufacturing. [Online] 2009. [Cited: 05 03, 2010.] http://www.arcam.com/.

64. **Denquin, A and Naka, S.** Pase Transformation Mechanisms Involved In Two-Phase TiAl-based Alloys - I .Lamellar Structure Growth. *Acta Material.* 1996, Vol. 44, pp. 343-352.

65. **Rios, Orlando.** *Phd Oak Ridge National Laboroty.* Oak Ridge, Tennessee, USA, 05 24, 2010.

66. **Ahlström, Johan.** *Sample preparation and microstructure characterisation of gamma Titanium Aluminides.* Göteborg : Chalmers University of Technology, 1995.

67. **Baselack III, W A, et al.** Metallography of Gamma Titanium Aluminides. *Materials Characterization.* 1993, Vol. 31, pp. 197-207.

68. **Lapin, J and Nazmy, M.** Microstructure and Creep Properties of a Cast Intermetallic Ti-46Al-2W-0.5Si Alloy for Gas Turbine Applications. *Materials Science and Engineering.* 2004, Vol. A380, pp. 298-307.

69. **Kutz, Myer.** *Handbook of Materials Selection.* New York : John Wiley & Sons, Inc, 2002.